Université de Montréal

Zinc and Zirconium catalysts in *rac*-lactide polymerization

Par

Fatemeh Dordahan

Département de Chimie

Faculté des Arts et des Sciences

Mémoire présentée en vue de l'obtention du grade de maîtrise en chimie

Septembre, 2021

© Fatemeh Dordahan, 2021

Université de Montréal

Unité académique : chimie/ FAS

Ce mémoire intitulé

Zinc and Zirconium catalysts in *rac*-lactide polymerization

Présenté par

Fatemeh Dordahan

A été évalué(e) par un jury composé des personnes suivantes

Nikolay Kornienko
Président-rapporteur

Frank Schaper
Directeur de mémoire

Davit Zargarian
Membre du jury

Résumé

Le ligand phénoxy-imine était préparés par condensation de para-formaldéhyde, 4-(tert-butyl)- 2-tritylphénol et di-(2-picolyl)amine. LZnN(SiMe 3) 2 était préparé par la réaction de Zn(N(SiMe 3) 2) 2 avec le ligand. Le complexe était étudié par diffraction de rayons X et par RMN. L'utilisation de ce complexe dans la polymérisation du rac-lactide amène à un acide polylactique atactique parun mécanisme de contrôle par la fin de la chaine, transféré par le site catalytique.

Des ligands pyridyle -aminophénol étaient préparé à partir du phénol (2,4-di-tert-butylphénol, 2,4-di-chlorophénol, 2,4-di-méthylphénol), pyridine-2-ylméthylamine et formaldéhyde (LH 2 = (2,4-X 2 C 6 (OH)H 2 (5-CH 2) 2 N(CH 2 C 5 H 4 N), X = Me ou Cl). Réaction de Zr(OnPr) 4 avec 2 équiv de LH 2 a fourni L 2 Zr. L 2 Zr était un mélange des isomères avec une symétrie C 2 . Ceci était conformé par RMN, DFT et diffraction de rayons X. La seule isomère pour X=Me était l'isomère cis. Pour X=Cl, l'isomère majeur était l'isomère trans. Tous les complexes étaient actifs pour la polymérisation du rac-lactide à 140 °C et un acide polylactique atactique était obtenu. L 2 Zr a suivi un mécanisme du monomère activé avec l'alcool benzylique comme co-initiateur.

Mots-clés : Catalyse, Complexes de zinc, Complexes de Zirconium, Acide polylactique, Polymérisation du lactide, Mécanisme.

Abstract

The phenoxy-imine ligand bearing heteroatom-containing N and O were prepared from condensation of paraformaldehyde, 4-(*tert*-butyl)-2-tritylphenol with di-(2-picolyl)amine. $LZnN(SiMe_3)_2$ was prepared by reaction of $Zn(N(SiMe_3)_2)_2$ and the ligand. The complex has been studied by X-ray diffraction and NMR. Application of this complex in *rac*-lactide polymerization gave atactic PLA via a catalytic-site mediated chain-end control mechanism.

Pyridylaminophenol ligands were prepared from phenol (2,4-di-*tert*-butylphenol, 2,4-di-cholorolphenol, 2,4-di-methylphenol), pyridine-2-ylmethylamine and formaldehyde (LH_2 = $(2,4\text{-}X_2C_6(OH)H_2(5\text{-}CH_2)_2N(CH_2C_5H_4N)$, X = Me or Cl). Reaction of $Zr(O\textit{n}Pr)_4$ with 2 equiv of LH_2 gave L_2Zr. L_2Zr were mixtures of C_2-symmetric isomers, which was confirmed by NMR, DFT and X-ray diffraction studies. The only isomer for X=Me was the *cis*-isomer while the major isomer for X=Cl was the *trans*-isomer. All complex were active in *rac*-lactide polymerization at 140 °C and heterotactic PLA was obtained. L_2Zr followed an activated monomer mechanism with benzyl alcohol as co-initiator.

Keywords: Catalysis, Zinc complexes, Zirconium complexes, Polylactic acid, Lactide polymerization, Mechanism.

Table of Content

Scheme list

Table list

Figure list

Abreviation list

Ac	acetyl
Bn	benzyl
Ar	aryl
CIF	crystallographic information file
Et	ethyl
L	ligand
J	coupling constant (in NMR)
Me	methyl
m	*meso*
*P*m	probability for a *meso* diads insertion
*P*r	probability for a *racemic* diads insertion
MS	mass spectrometry
r	*racemic*
UV-vis	Ultraviolet-visible
ROP	Ring-Opening Polymerization
ppm	part per million
NMR	nuclear magnetic resonance
PLA	polylactic acid

Chapter 1. Introduction

1. Polymer

Polymers are macromolecules or very large molecules formed by repeating small units called monomers. Polymerization is the process of joining one by one these low mass monomer molecules and eventually forming polymers. Actually, the word "polymer" comes from Greek meaning "many members.". German Chemist Hermann Staudinger was the first scientist who called these molecules "macromolecules" (Nobel Prize in 1953).[1] Natural polymers like proteins, ribonucleic acid (RNA) and deoxyribonucleic acid (DNA) have existed on Earth since early Earth history. Some other examples of natural polymers are starch, cellulose and lignin. In the 1800s, scientists attempted to modify natural polymers to increase their physical properties. Over the past six decades, the production of synthetic polymers has increased significantly. Polylactones, especially those derived from lactic acid (PLA), glycolic acid (PGA), and their copolymers (PLGA), are considered suitable sustainable replacements of traditional polymers and have been used in a large variety of fields, such as packaging, food industry, medicinal and pharmaceutical applications.[2-4]

The term "biodegradable" is ill-defined in that it does not specify the speed or environmental requirements for degradation. PLA, for example, will degrade in two weeks in industrial compotation plants, it will degrade eventually in the soil, and it is unlikely to degrade at all in marine environments. In a medical context, "biodegradable" refers to polymers which are eventually absorbed by the body; typically, the absence of toxic effects is implied.

PLA belongs to a group referred to as "biopolymers", a term which is even more vague than "biodegradable". "Biopolymers" either imply that a polymer derives from nature or does not impact on nature. It is important to understand that the biodegradability as a characteristic is independent of to the polymer. Hence, there are some polymers that are produced from petroleum feedstock, but are biodegradable

(Mohanty et al., 2005). Plastics such as PLA, PHA, and starch are the most frequently used biopolymers and have the lowest impact on the rising environmental carbon footprint, since they are biodegradable (under the right conditions), as well as derived from renewable feedstocks.

2. Lactide

Polylactic acid (PLA) is an aliphatic polyester which is prepared from lactide (LA) (Scheme 1.1).[5] It has attracted considerable attention as a biocompatible, renewable and biodegradable polymer and is used in medical applications such as implants and sutures, as well as in industrial packaging of food and beverages.[6-8]

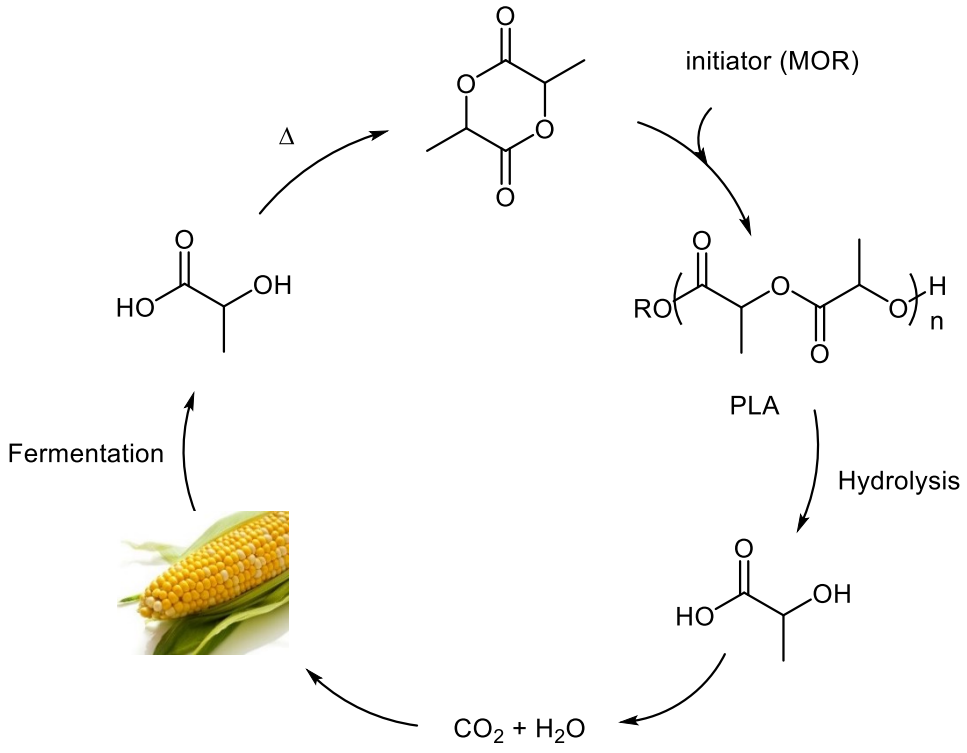

Scheme 1.1. The lifecycle of polylactide (PLA).

Lactic acid is obtained from the fermentation of carbohydrates, sugars and mostly corn starch. Lactic acid or 2-hydroxypropionic acid is the building block of PLA.[5] In

1780, the Swedish chemist Scheele isolated lactic acid for the first time from sour milk and in 1881 it was produced commercially.[9] It is the simplest hydroxy acid with an asymmetric carbon atom which results in two active optical configurations (Scheme 1.2).

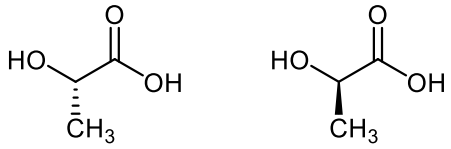

L-lactic acid D-lactic acid

Scheme 1.2. Stereochemistry of lactic acid.

Lactide is the cyclic dimer of lactic acid and used to produce PLA. The lactide monomer contains two stereocenters, therefore it has three distinct diastereomers: L-lactide, D-lactide and *meso*-lactide (Scheme 1.3).

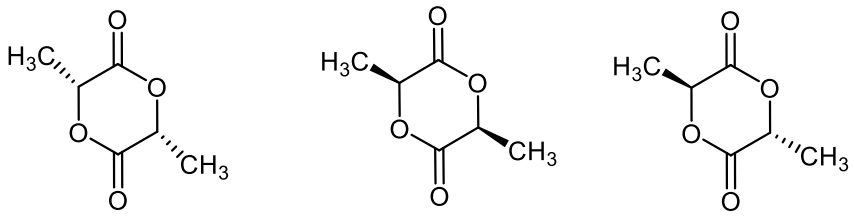

D-lactide L-lactide LD-lactide

rac-lactide *meso*-lactide

Scheme 1.3. Stereoisomers of lactide

The chiral isomers are commercially available as single enantiomers and as *rac*-lactide.

3. Polymerization of Lactide

PLA synthesis can be accomplished by lactic acid polycondensation as well as ring-opening polymerization (ROP) of lactide. ROP provides more control over the molecular parameters of the resulting polymer. In comparison to polycondensation reactions, this increase in control leads to higher molecular weight, lower polydispersities and a more end-group fidelity. Depending on whether *rac*- or *meso*-lactide is used, stereocontrolled ROP can lead to different polymer microstructures (Scheme 1.4).

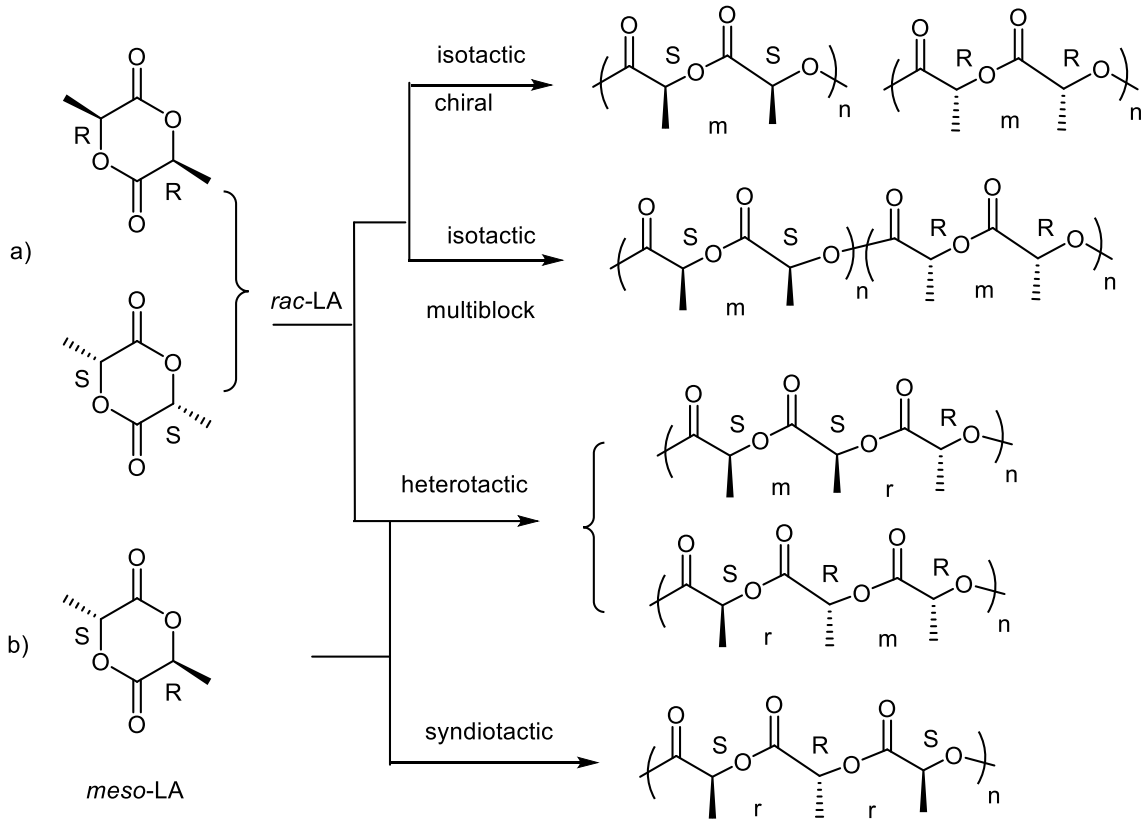

Scheme 1.4. PLA microstructures from the stereocontrolled ROP of lactide for (a) *rac*-lactide and (b) meso-lactide.

The stereochemistry of the chiral centers located along the polymer chain, is called tacticity. The same orientation of two chiral centers in the polymer chain is called meso, and the opposite orientation of each other is called racemic. Two nomenclatures are used for lactide: isotactic and syndiotactic diads (i and s), as well as *meso* and *racemic* diads (m and r).[10, 11]

The stereocontrolled ROP of *meso/rac*-lactide can potentially lead to three types of PLA:

a) heterotactic PLA, in which the stereocentres doubly alternate (-SSRRSSRR-), which alternating meso and racemic diads (-rmrmrm-).

b) syndiotactic PLA, in which the stereocentres alternate (-SRSRSR-), consisting only of *r*-diads.

c) isotactic PLA, in which all stereocentres are either S or R (-SSSSSS- or -RRRRRR-) consisting only of *m*-diads.

ROP of *rac*-lactide can lead to heterotactic PLA or isotactic polymers. ROP of *meso*-lactide can lead to heterotactic PLA or syndiotactic polymer.

Stereochemistry is one of the significant factors that determine the mechanical and physical properties, such as glass transition (T_g) and melting temperature (T_m) of a polymer. For instance, heterotactic PLA shows a T_m of 130 °C and no observable T_g, chiral isotactic PLA displays T_m of 180 °C and T_g = ~ 50 °C and a 50: 50 mixtures of multiblock isotactic PLA shows a comparable T_g to chiral isotactic polymer but a remarkably increased T_m of 230 °C.[12]

Munson et al. have shown that ^{13}C NMR and homonuclear decoupled ^{1}H NMR analysis can be used to determine the tacticity of the polymer.[13] In general, two parameters are used to express the degree of stereoregularity: P_m which is the probability of meso (isotactic) diads formation and P_r which indicates the probability of racemic (syndiotactic) diad formation. P_m and P_r can be calculated by decoupled

^{1}H NMR spectroscopy. For *rac*-lactide, P_r =1.00 (P_m = 0.00) describes completely heterotactic polymers and P_m =1.00 (P_r = 0.00) describes perfect isotactic polymers. For *meso*-lactide, P_r =1.00 (P_m = 0.00) describes completely syndiotactic polymers and P_m =1.00 (P_r = 0.00) describes completely heterotactic polymers. For both, *rac*- and *meso*-lactide, $P_r = P_m = 0.50$ shows a completely atactic polymer.[14]

4. General mechanisms for ROP

Several mechanisms have been proposed for the ROP of Lactide:

a) Anionic ROP mechanisms: This mechanism initiates by attack of an anion on the carbonyl carbon of lactide (Scheme 1.5).[7, 8] Although there is a wide range of initiators for anionic ROP[15], only lithium species were successfully used to give significant stereocontrol in polymerization of *rac*-lactide.[7, 8]

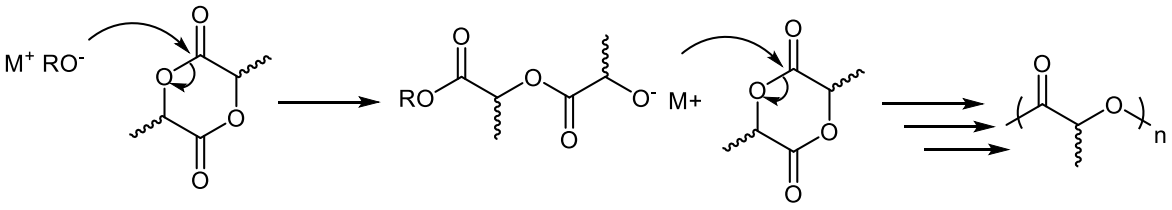

Scheme 1.5. Anionic ROP mechanism.

b) Coordination–insertion ROP: In this mechanism the Lewis acidic metal center binds to the carbonyl oxygen and activates the lactide monomer (Scheme 1.6).[16-18] Insertion of the metal alkoxide group causes the lactide ring to open, resulting in an extended metal alkoxide species. It has been shown that the coordination of the carbonyl oxygen of lactide monomer to a metal center can play a significant role in the stereocontrol of the system. Thus, the environment of the metal center, the ligands, as well as the growing polymer chain can make

a very significant difference in the rates of insertion of the different lactide enantiomers.

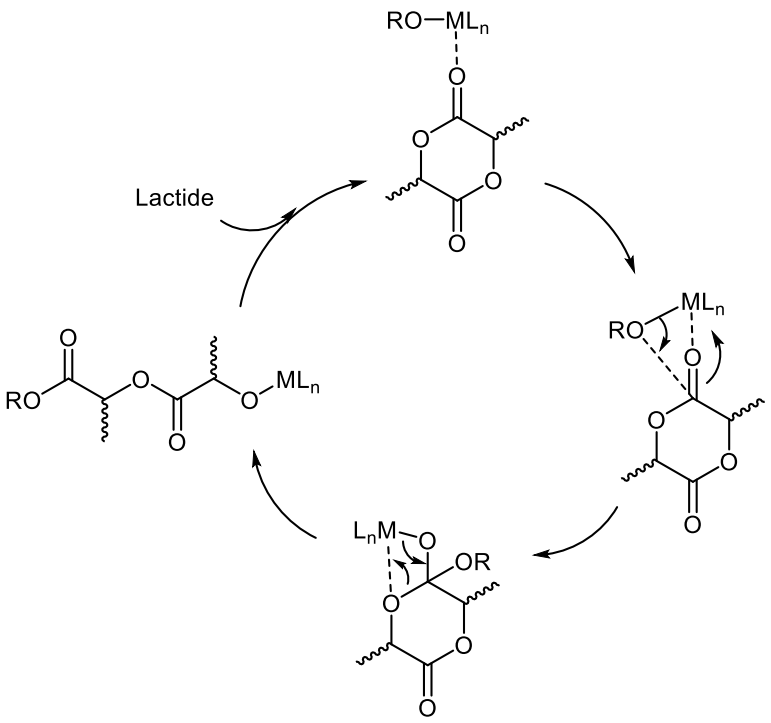

Scheme 1.6. Coordination-insertion ROP mechanism.

c) Activated monomer ROP mechanism: This mechanism was proposed for cationic initiating systems. In this mechanism, lactide monomer is activated by a protic acid or Lewis acid, then nucleophilic attack of exogenous alcohol at the carbonyl group leads to the opening of the lactide cycle (Scheme 1.7).[19, 20]

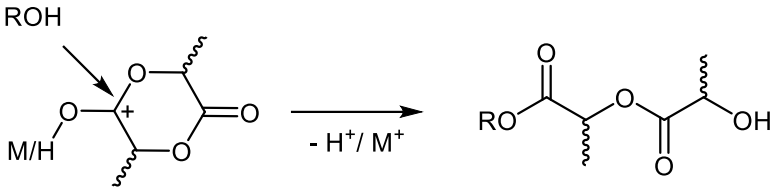

Scheme 1.7. Activated monomer ROP mechanism.

d) Organocatalytic ROP: Another class of catalysts for ROP lactide are organocatalysts. Two mechanisms have been proposed for organocatalysts: Monomer-activated or pseudo-anionic (similar to the anionic mechanism). One of the most famous organocatalysts are N-heterocyclic carbenes (NHCs) which operate through the monomer-activated mechanism. The reaction starts with nucleophilic attack of NHCs at the carbonyl carbon atom, then esterification by the initiating or propagating alcohol (Scheme 1.8).[21]

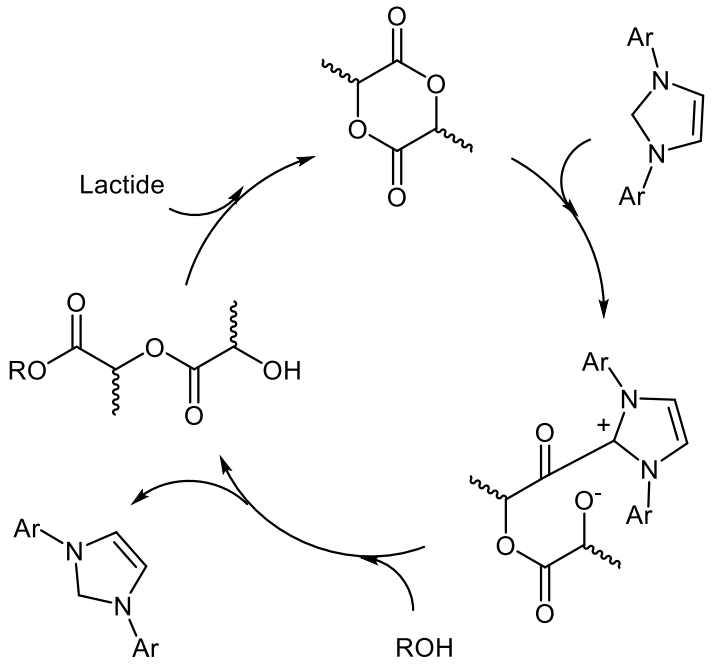

Scheme 1.8. N-heterocyclic carbene compounds as organic catalysts for ROP.

5. Stereocontrol mechanisms

In all cases, there are two main mechanisms for stereocontrol of lactide polymerization.[14]

a) Catalytic-site control mechanism: the chirality of the new lactide monomer to be inserted depends on the chirality of the Lewis-acidic metal center.

b) Chain-end control mechanism: In this mechanism, the chirality of the new lactide monomer to be inserted depends on the chirality of the last stereocenter of the growing PLA chain.

6. Metal- based catalysts

A large number of catalyst systems, have been used in the ROP of lactide such as traditional anionic, enzymatic and metal-mediated.[7, 8] Recently, metal-mediated catalysts have received considerable attention as stereocontrolled ROP catalyst systems. These systems mostly include an electropositive metal center, a ligand and an alkoxide or amide as an initiating group. So far, hundreds of these catalysts have been reported for ROP, which are often stereoselective, easily tunable and highly active. The mechanism of metal-mediated ring opening of lactide mostly proceeds via a coordination-insertion mechanism. Some representative examples of metal complexes will be discussed in the following sections.

6.1. Group 1 metal complexes

Environmentally friendly complexes based on alkali metals have been considered. Among this group, increasing attention has been dedicated to lithium, sodium and potassium, with ligands such as crown ethers, chelating phenoxide/N-donor, iminophenoxide or amidinate.

Recently, Wu and co-workers reported potassium amidinate complexes for ROP. At room temperature, they obtain high molecular weight polylactide (M_n = 117.7 kg/mol^{-1}) (Scheme 1.9). At -70 °C, the catalyst showed high isoselectivity P_m= 88.[22]

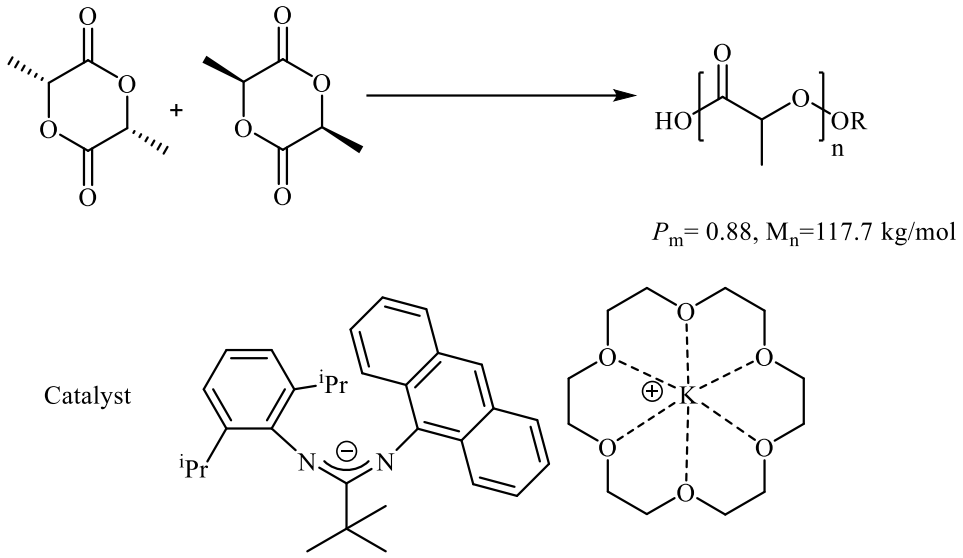

Scheme 1.9. Crown ether alkali metal complexes.

Wu's group also reported six salen−sodium complexes which can stereoselectively catalyze the ROP of lactide (Scheme 1.10). The best P_m value was 0.82, obtained at -40 °C. DFT studies proposed a ligand-assisted activated monomer mechanism rather a simple activated monomer mechanism. In this mechanism, the basic spectator phenoxide ligands participate by hydrogen bonding/ abstraction in the attack of the exogenous alcohol.[23]

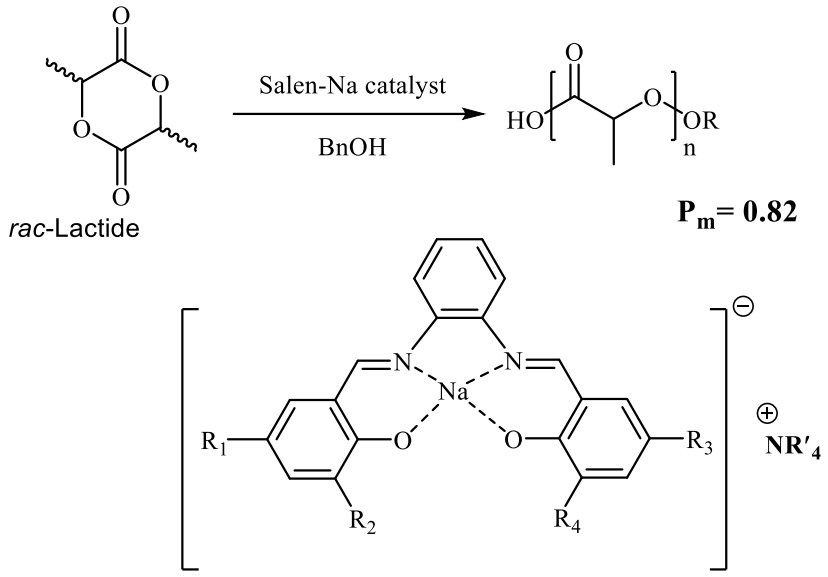

Scheme 1.10. Salen-sodium complexes.

6.2. Group 2 metal complexes

In addition to the group of alkali metal complexes, alkaline earth metal complexes have shown effective potential for ROP. Ligands include, for example phenoxides and alkoxides, imino/aminophenoxide, ketoiminates and nitrogen-based bidentate/tridentate/tetradentate ligands.

Ma and co-workers reported magnesium complexes, which are highly active and isoselective for ROP of *rac*-lactide at room temperature (Scheme 1.11). Using a racemic mixture of complexes, they achieved 90% conversion in 5 minutes with good selectivity (P_m = 0.80) (at high molar ratio of [*rac*-LA]$_0$:[Mg]$_0$:[^{i}PrOH]$_0$ = 5000:1:1). Based on the kinetic studies for the polymerization, the most reasonable mechanism for isoselectivity is a catalytic-site control mechanism, where the chirality of the catalyst site determines the stereoselectivity of the next insertion.[24]

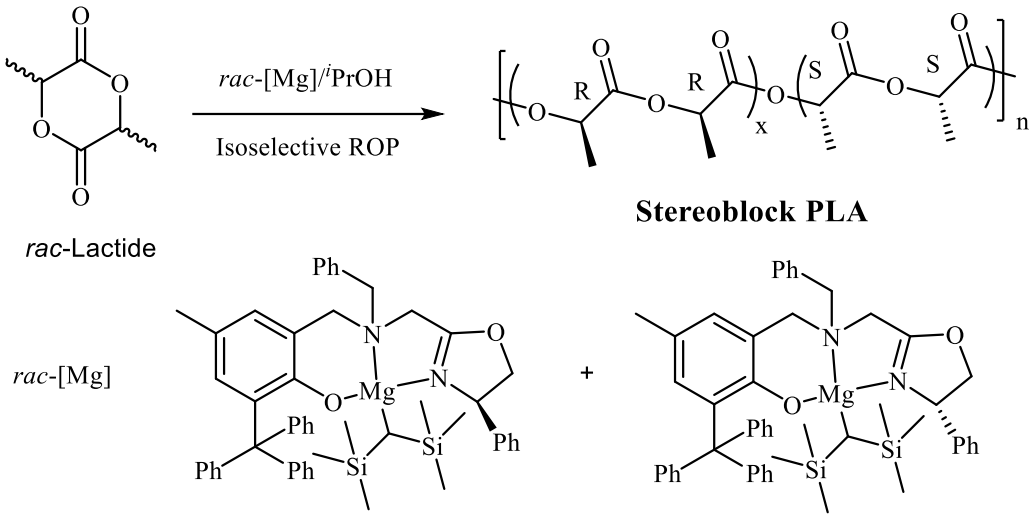

Scheme 1.11. Oxazolinyl-aminophenoxide magnesium complexes,

6.3. Group 13 metal complexes

In this group, the most extensively studied metal is aluminum. For example, aluminum complexes bearing aminomethylpyrrolidine-based salalen ligands (Scheme 1.12) have been reported by Kol's group.[25] The complexes showed isoselectivity for ROP, resulting isotactic multiblock microstructure. Highest conversion (90%) required one day at 80 °C. Stereoselectivity was reached P_m=0.82 with a molar ratio of [*rac*-LA]$_0$: [BnOH]$_0$: [Al]$_0$ = 100:1:1). The proposal mechanism was a combination of catalytic-site and chain-end control.

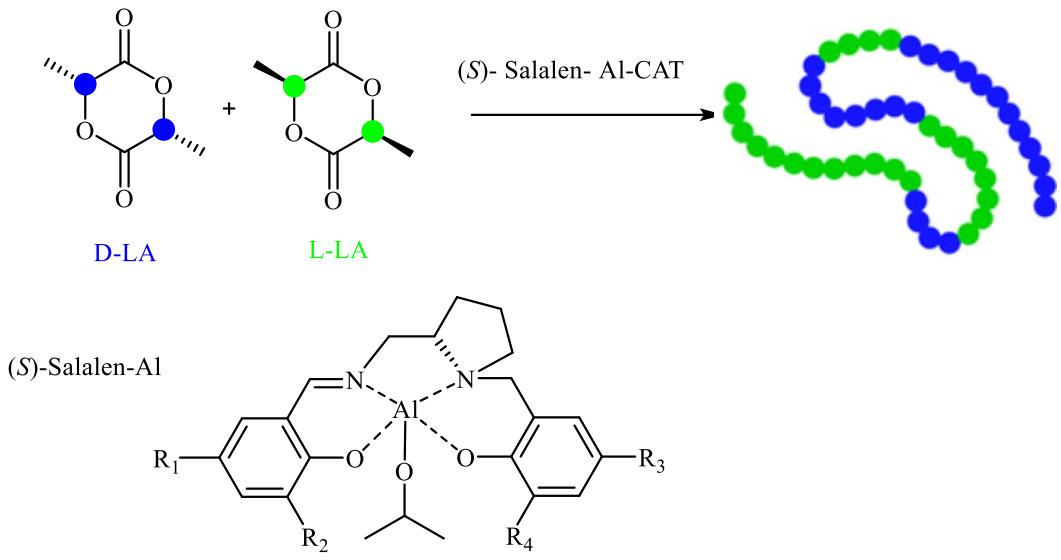

Scheme 1.12. Aluminum complexes supported by salen-derived ligands.

6.4. Transition Metals (Groups 4-11)

Transition metal-based catalysts are by far the most widely studied and also have yielded significant examples of stereocontrolled ROP. Metals such as titanium,[26] zirconium,[27] hafnium,[28] vanadium,[29] chromium,[30] manganese,[31] iron,[32] cobalt,[33] nickel,[34] copper,[35] zinc[36] and cadmium[37] have been reported for ring opening of lactide.

Efficient chiral Schiff-base zirconium complexes as catalysts in the ROP of *rac*-lactide were reported by Jones and co-workers (Scheme 1.13).[1] These complexes show good activity in toluene at both 80 °C and 20 °C. Polymerisation is well-controlled and heterotactic polymers were isolated (P_r = 0.68–0.71). Remarkably, the zirconium complexes were active, well-controlled and selective for ROP of *rac*-lactide even in the presence of water and/or unpurified monomer in the melt.

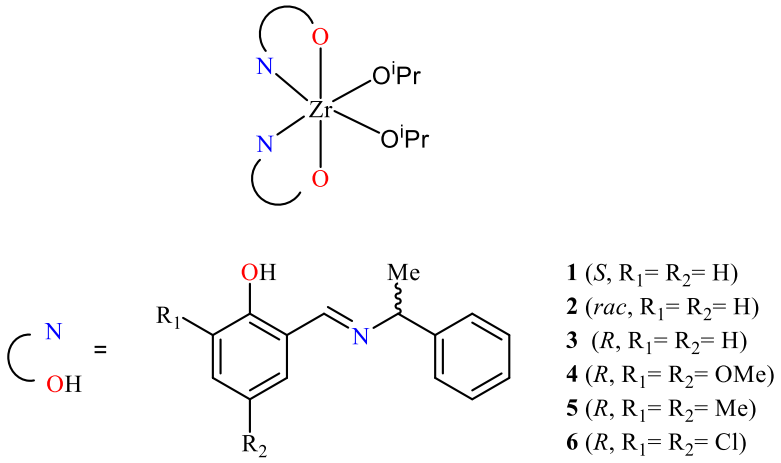

Scheme 1.13. Chiral Zr complexes.

Recently, Lee's group reported Cu(II)-iminomethylpyridine complexes for ROP of *rac*-lactide (Scheme 1.14).[35] The complexes showed moderate activities in CH_2Cl_2 with ratio of $[lactide]_0$: $[Cu]_0$ = 100:1 at room temperature as well as -25 °C in 2 hours. The obtained PLA was slightly heterotactic with polymerization following an activated monomer mechanism.

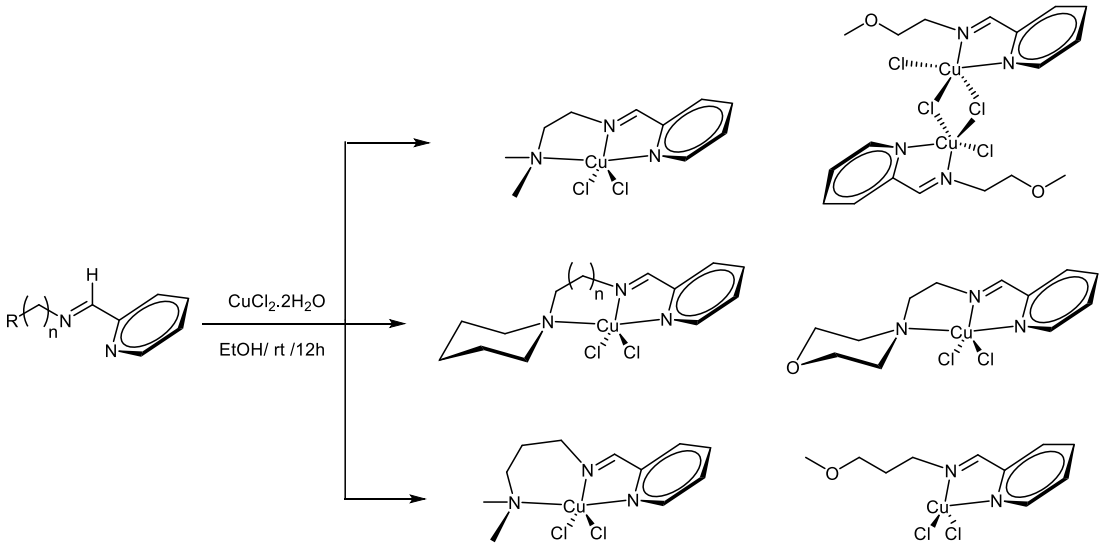

Scheme 1.14. Cu (II)-iminomethylpyridine complexes

Due to the use of PLA as a sustainable alternative to commodity plastics and their special application in medicine, their synthesis attracted considerable attention. In brief, significant advances have been made with group 1, 2, 13 Zn, and Zr complexes in the stereocontrolled ROP of lactide over the last decade. There are still challenges in improving catalyst stability and producing high molecular weight polymer with better stereocontrol. In spite of the continued appearance of designed ligands, there are thus still many opportunities to develop a catalyst for the synthesis off PLA with more desirable properties.

7. Aim of this work

There are many challenges in improving catalyst activity for lactide polymerization. One of the challenges is the control of the mechanism. Since chain-end control and catalytic-site control may happen simultaneously, it becomes very difficult to improve the catalyst. To give two examples: Williams and co-workers used the same ligand for lanthanum, lutetium and yttrium complexes and observed that by reducing the size of the metal the stereocontrol of polymerization first slightly changes and then suddenly inverts from isotactic to heterotactic PLA (Scheme 1.15).[38]

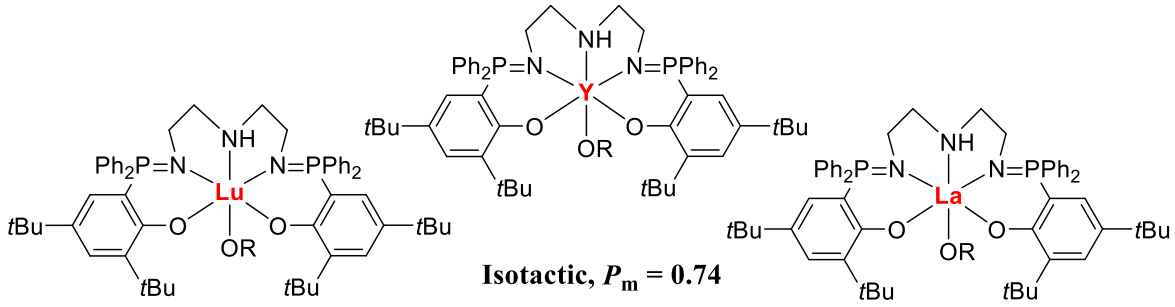

Isotactic, P_m = 0.82 **Isotactic, P_m = 0.74** **Heterotactic, P_m = 0.36**

Scheme 1.15. lanthanide, lutetium and yttrium complexes.

Also, Gibson observed that small changes to the ligand substituents might completely invert the stereocontrol of the polymerization.[39, 40] Kol found later that this inversion of stereocontrol is due to a change of the mechanism (Scheme 1.16).[37]

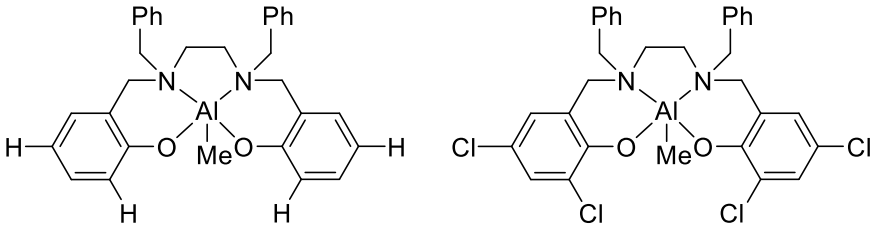

Isotactic, P_m = 0.79 **Heterotactic, P_m = 0.06**

Scheme 1.16. Aluminum complexes

My research project focused on the study of zinc and zirconium complexes carrying heteroatom-containing N and O ligands (Scheme 1.17). The purpose of this work is to investigate unusual stereocontrol mechanisms, which can avoid the competition between stereocontrol mechanisms and thus enable the catalytic-site to have a more predictable influence on polymerization.

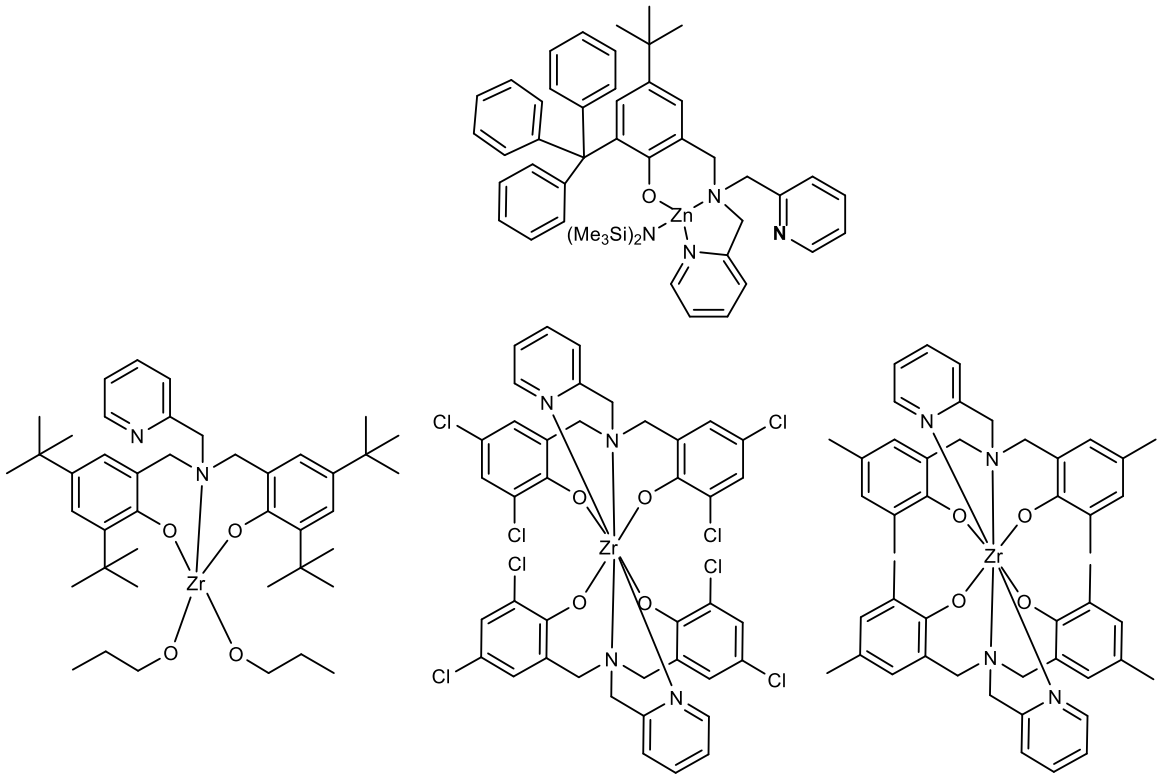

Scheme 1.17. Zinc and zirconium complex

In chapter 2, I studied a zinc complex for polymerization of *rac*-lactide using a catalytic-site mediated chain-end control mechanism. In this mechanism, the chirality of the flexible catalytic site is determined by the chain end, thus removing competition between the two stereocontrol mechanism.

In chapter 3, the polymerization of lactide using zirconium catalysts with tetradentate ligands was investigated. A ligand-assisted activated-monomer mechanism was targeted. Here, the idea was that a basic site on the ligand can participate in proton transfer and thus enable stereocontrol.

8. References chapter 1

1. Chmura, A. J.; Cousins, D. M.; Davidson, M. G.; Jones, M. D.; Lunn, M. D.; Mahon, M. F., Robust chiral zirconium alkoxide initiators for the room-temperature stereoselective ring-opening polymerisation of rac-lactide. *Dalton Transactions* **2008,** (11), 1437-1443.
2. Ragauskas, A. J.; Williams, C. K.; Davison, B. H.; Britovsek, G.; Cairney, J.; Eckert, C. A.; Frederick, W. J., Jr.; Hallett, J. P.; Leak, D. J.; Liotta, C. L.; Mielenz, J. R.; Murphy, R.; Templer, R.; Tschaplinski, T., The path forward for biofuels and biomaterials. *Science (New York, N.Y.)* **2006,** *311* (5760), 484-9.
3. Drumright, R. E.; Gruber, P. R.; Henton, D. E., Polylactic Acid Technology. **2000,** *12* (23), 1841-1846.
4. Dechy-Cabaret, O.; Martin-Vaca, B.; Bourissou, D., Controlled Ring-Opening Polymerization of Lactide and Glycolide. *Chemical Reviews* **2004,** *104* (12), 6147-6176.
5. Dove, A. P., Controlled ring-opening polymerisation of cyclic esters: polymer blocks in self-assembled nanostructures. *Chemical Communications* **2008,** (48), 6446-6470.
6. Garlotta, D., A Literature Review of Poly(Lactic Acid). *Journal of Polymers and the Environment* **2001,** *9* (2), 63-84.
7. Chisholm, M. H.; Iyer, S. S.; McCollum, D. G.; Pagel, M.; Werner-Zwanziger, U., Microstructure of Poly(lactide). Phase-Sensitive HETCOR Spectra of Poly(meso-lactide), Poly(rac-lactide), and Atactic Poly(lactide). *Macromolecules* **1999,** *32* (4), 963-973.
8. Ebdon, J. R., Introduction to polymers (second edition) R. J. Young and P. A. Lovell Chapman and Hall, London, 1991. pp. 443, price £16.95. ISBN 0-412-30640-9 (PB); ISBN 0–412–30630–1 (HB). **1992,** *27* (2), 207-208.
9. Fukushima, K.; Kimura, Y., Stereocomplexed polylactides (Neo-PLA) as high-performance bio-based polymers: their formation, properties, and application. **2006,** *55* (6), 626-642.
10. Zell, M. T.; Padden, B. E.; Paterick, A. J.; Thakur, K. A. M.; Kean, R. T.; Hillmyer, M. A.; Munson, E. J., Unambiguous Determination of the 13C and 1H NMR Stereosequence Assignments of Polylactide Using High-Resolution Solution NMR Spectroscopy. *Macromolecules* **2002,** *35* (20), 7700-7707.
11. Stanford, M. J.; Dove, A. P., Stereocontrolled ring-opening polymerisation of lactide. *Chemical Society Reviews* **2010,** *39* (2), 486-494.
12. Ko, B.-T.; Lin, C.-C., Synthesis, Characterization, and Catalysis of Mixed-Ligand Lithium Aggregates, Excellent Initiators for the Ring-Opening Polymerization of l-Lactide. *Journal of the American Chemical Society* **2001,** *123* (33), 7973-7977.
13. Ryner, M.; Stridsberg, K.; Albertsson, A.-C.; von Schenck, H.; Svensson, M., Mechanism of Ring-Opening Polymerization of 1,5-Dioxepan-2-one and l-Lactide with Stannous 2-Ethylhexanoate. A Theoretical Study. *Macromolecules* **2001,** *34* (12), 3877-3881.
14. Marshall, E. L.; Gibson, V. C.; Rzepa, H. S., A computational analysis of the ring-opening polymerization of rac-lactide initiated by single-site beta-diketiminate metal complexes: defining the mechanistic pathway and the origin of stereocontrol. *J Am Chem Soc* **2005,** *127* (16), 6048-51.
15. Kowalski, A.; Duda, A.; Penczek, S., Kinetics and Mechanism of Cyclic Esters Polymerization Initiated with Tin(II) Octoate. 3. Polymerization of l,l-Dilactide. *Macromolecules* **2000,** *33* (20), 7359-7370.
16. Basko, M., Activated monomer mechanism in the cationic polymerization of L,L-lactide %J Pure and Applied Chemistry. **2012,** *84* (10), 2081-2088.

17. Bourissou, D.; Martin-Vaca, B.; Dumitrescu, A.; Graullier, M.; Lacombe, F., Controlled Cationic Polymerization of Lactide. *Macromolecules* **2005,** *38* (24), 9993-9998.
18. Connor, E. F.; Nyce, G. W.; Myers, M.; Möck, A.; Hedrick, J. L., First example of N-heterocyclic carbenes as catalysts for living polymerization: organocatalytic ring-opening polymerization of cyclic esters. *J Am Chem Soc* **2002,** *124* (6), 914-5.
19. Chen, C.; Jiang, J.; Mao, X.; Cong, Y.; Cui, Y.; Pan, X.; Wu, J., Isoselective Polymerization of rac-Lactide Catalyzed by Ion-Paired Potassium Amidinate Complexes. *Inorg Chem* **2018,** *57* (6), 3158-3168.
20. Cui, Y.; Jiang, J.; Mao, X.; Wu, J., Mononuclear Salen–Sodium Ion Pairs as Catalysts for Isoselective Polymerization of rac-Lactide. *Inorganic Chemistry* **2019,** *58* (1), 218-227.
21. Rufino-Felipe, E.; Muñoz-Hernández, M.-Á.; Montiel-Palma, V., Lithium Complexes Derived of Benzylphosphines: Synthesis, Characterization and Evaluation in the ROP of rac-Lactide and ε-Caprolactone. **2018,** *23* (1), 82.
22. Hu, J.; Kan, C.; Wang, H.; Ma, H., Highly Active Chiral Oxazolinyl Aminophenolate Magnesium Initiators for Isoselective Ring-Opening Polymerization of rac-Lactide: Dinuclearity Induced Enantiomorphic Site Control. *Macromolecules* **2018,** *51* (14), 5304-5312.
23. Pilone, A.; Press, K.; Goldberg, I.; Kol, M.; Mazzeo, M.; Lamberti, M., Gradient Isotactic Multiblock Polylactides from Aluminum Complexes of Chiral Salalen Ligands. *Journal of the American Chemical Society* **2014,** *136* (8), 2940-2943.
24. Li, X.; Yang, B.; Zheng, H.; Wu, P.; Zeng, G., Synthesis and characterization of salen-Ti(IV) complex and application in the controllable polymerization of D, L-lactide. *PLOS ONE* **2018,** *13* (8), e0201054.
25. Dai, R.; Diaconescu, P. L., Investigation of a zirconium compound for redox switchable ring opening polymerization. *Dalton Transactions* **2019,** *48* (9), 2996-3002.
26. Mandal, D.; Chakraborty, D.; Ramkumar, V.; Chand, D. K., Group 4 alkoxide complexes containing [NNO]-type scaffold: synthesis, structural characterization and polymerization studies. *RSC Advances* **2016,** *6* (26), 21706-21718.
27. Ma, J.; Zhao, K.-Q.; Walton, M. J.; Wright, J. A.; Frese, J. W. A.; Elsegood, M. R. J.; Xing, Q.; Sun, W.-H.; Redshaw, C., Vanadyl complexes bearing bi-dentate phenoxyimine ligands: synthesis, structural studies and ethylene polymerization capability. *Dalton Transactions* **2014,** *43* (22), 8300-8310.
28. Vagin, S. I.; Reichardt, R.; Klaus, S.; Rieger, B., Conformationally Flexible Dimeric Salphen Complexes for Bifunctional Catalysis. *Journal of the American Chemical Society* **2010,** *132* (41), 14367-14369.
29. Yang, W.; Zhao, K.-Q.; Wang, B.-Q.; Redshaw, C.; Elsegood, M. R. J.; Zhao, J.-L.; Yamato, T., Manganese coordination chemistry of bis(imino)phenoxide derived [2 + 2] Schiff-base macrocyclic ligands. *Dalton Transactions* **2016,** *45* (1), 226-236.
30. Liang, Y.; Duan, R.-L.; Hu, C.-Y.; Li, L.-L.; Pang, X.; Zhang, W.-X.; Chen, X.-S., Salen-iron complexes: Synthesis, characterization and their reactivity with lactide. *Chinese Journal of Polymer Science* **2018,** *36* (2), 185-189.
31. Pradhan, H. C.; Mantri, S.; Routaray, A.; Maharana, T.; Sutar, A. K., Cobalt (II) complex catalyzed polymerization of lactide and coupling of CO2 and styrene oxide into cyclic styrene carbonate. *Journal of Chemical Sciences* **2020,** *132* (1), 25.
32. Routaray, A.; Mantri, S.; Nath, N.; Sutar, A. K.; Maharana, T., Nickel(II) complex catalyzed ring-opening polymerization of lactide. *Polyhedron* **2016,** *119*, 335-341.

33. Lee, J.; Yoon, M.; Lee, H.; Nayab, S., Stereoselective polymerization of methyl methacrylate and rac-lactide mediated by iminomethylpyridine based Cu(ii) complexes. *RSC Advances* **2020,** *10* (27), 16209-16220.
34. Zhu, D.; Li, Y.; Chen, J.; Song, X., L2Zn and LZnX complexes bearing half-salphen ligands and their catalysis of ring-opening polymerization of ε -caprolactone. *Journal of Organometallic Chemistry* **2020,** *920*, 121317.
35. Lee, J.; Lee, H.; Nayab, S.; Yoon, K. B., Synthesis, characterization and polymerisation studies of cadmium(II) complexes containing N,N′,X-tridentate X-substituted (X = N, O) 2-iminomethylpyridines. *Polyhedron* **2019,** *158*, 432-440.
36. Navarro, M.; Garcés, A.; Sánchez-Barba, L. F.; de la Cruz-Martínez, F.; Fernández-Baeza, J.; Lara-Sánchez, A., Efficient Bulky Organo-Zinc Scorpionates for the Stereoselective Production of Poly(rac-lactide)s. **2021,** *13* (14), 2356.

Chapter 2. Lactide polymerization using a sterically encumbered, flexible zinc complex

Fatemeh Dordahan, Frank Schaper*

Centre in Green Chemistry and Catalysis, Université de Montréal, Department of Chemistry, Montréal, Canada

This chapter was submitted for publication to : Canadian Journal of Chemistry, Manuscript ID: cjc-2021-0239

Fatemeh Dordahan : Design of experiments, all experimental work, writing of the manuscript.

Frank Schaper : Design of the project, supervision, suggestions of and corrections to the manuscript.

Abstract

4-(*tert*-Butyl)-2-trityl-6-(di-(2-picolyl)amine)phenol, LH, was prepared from paraformaldehyde, 4-(*tert*-butyl)-2-tritylphenol and di-(2-picolyl)amine. Reaction with $Zn(N(SiMe_3)_2)_2$ gave $LZnN(SiMe_3)_2$. The complex was shown by X-ray diffraction study, variable temperature NMR and DFT calculations to coordinate only one pyridine ligand, which allows for fast and facile complex isomerisation. $LZnN(SiMe_3)_2$ was active in *rac*-lactide polymerization upon activation with alcohol, but in contrast to previous complexes of this type did not show any evidence for isotactic monomer enchainment via a catalytic-site mediated chain-end control mechanism.

Keywords

zinc complexes, lactide polymerization, isotacticity, stereocontrol, reaction mechanism, catalysis, inorganic chemistry

Introduction

Polylactide (or polylactic acid, PLA) has one of the largest market shares in bio-based, biodegradable plastic materials, next to starch-based polymers and polyhydroxyalkanoates.[1] Due to growing concerns about the impact of plastics on the environment,[1, 2] the catalytic polymerization of lactide has attracted significant academic interest over the last two decades.[3-28] Of particular interest is isotactic PLA (or the stereocomplex of *all-R* and *all-S* PLA) and much effort has been invested into achieving isoselective polymerization of a racemic mixture of *RR*- and *SS*-lactide. Although several highly active and highly isoselective catalyst systems have been proposed,[29-42] stereocontrol still remains far below the levels which can be achieved in α-olefin polymerization and P_m values above 85% (P_m = probability of forming an isotactic dyad by insertion) can be considered "highly isoselective" for a catalyst with high activity.

A fundamental impediment to improved catalyst design is the stubborn resistance of lactide polymerization to accept rational catalyst development. Despite of what should be a straightforward mechanism of transesterification, finding selective catalysts is mostly empiric, with modifications often affording no further improvement or even loss of stereocontrol. Further complication arises from the fact that catalytic site control, i. e. selection of the lactide enantiomer based on the chirality of the catalytic site, is always accompanied and sometimes countered by chain end control, i. e. selection of the lactide enantiomer based on the chirality of the last inserted unit. Stereocontrol via a catalytic site with fixed chirality normally can only lead to isotactic PLA (although even here lactide polymerization is able to violate conventional wisdom[43, 44]). Chain-end control, on the other hand, can favour isotactic or heterotactic monomer enchainment, but most often produces heterotactic PLA.

The complications of rational catalyst design in lactide polymerization can be visualized by considering the example of diaminophenoxy zinc complexes. Williams, Hillmyer, Tolman and coworkers reported in 2003 complex **1** (Chart 2.1), which showed very high activity in *rac*-lactide polymerization (full conversion in solution at room temperature in less than 5 min), while retaining good polymer molecular weight control.[45] Although chiral and stereorigid, a racemic mixture of **1** produced only atactic PLA. Mehrkhodavandi and coworkers attempted to introduce stereocontrol via a catalytic-site control mechanism by replacing the ethylene diamine donor arm with (homo-)chiral cyclohexylenediamine, **2**, but the complex proved to be inactive in polymerization.[46] Activity could be restored by removal of the *N*-methyl substituent, but the obtained PLA remained atactic.[47] Ma and coworkers were more successful in installing catalytic-site control using several different (homo-)chiral *N*-donor arms, such as **3** (Chart 2.1).[48, 49] Although highly isoselective catalysts were obtained, chain-end control proved to be the dominant stereocontrol mechanism (here with preference for isotactic enchainment). Consequently, similar complexes with achiral *N*-donor arms, such as **4**, likewise produced isotactic PLA.[32, 50] Similar results were obtained by Kol and coworkers when they extended the *N*-donor arm by a further pyridine unit: both, homochiral **5** as well as racemic **6** with an achiral donor arm produced highly isotactic PLA via a chain-end control mechanism.[38, 51]

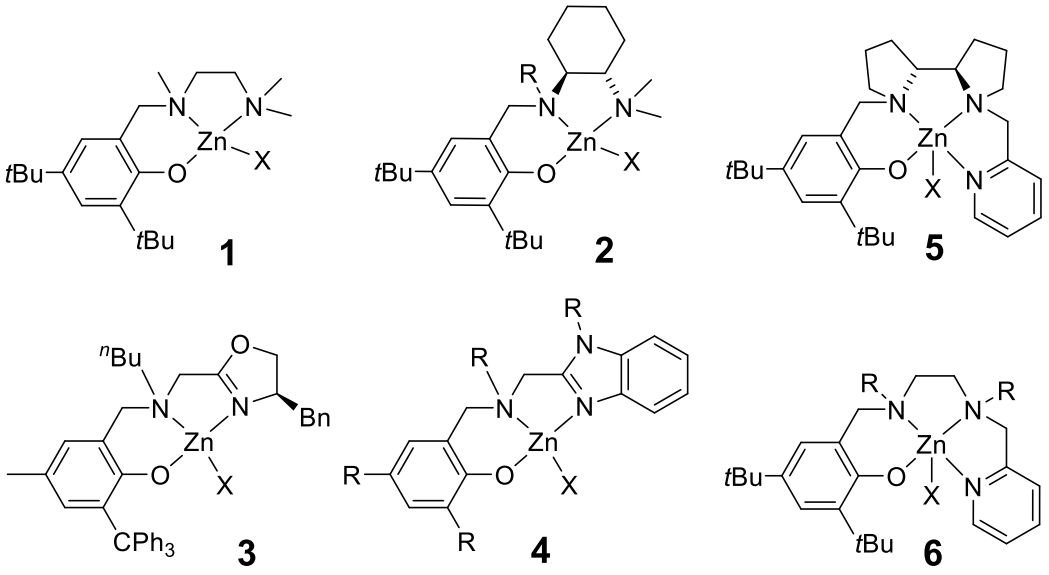

Chart 2.1.

While the chain-end control mechanism offers several advantages (longer isotactic blocks from the same amount of stereocontrol, stereocontrol is not affected by chain-shuttling and compatible with immortal polymerization), the chiral information and differentiation is always derived from the growing polymer chain. The ligand framework plays at best a passive role of amplifying selectivity by sterically crowding the transition states. This limitation can be circumvented by a *ligand-site mediated chain-end control mechanism*. The latter is based on initial observations by Ma, Okuda and Carpentier, that in several cases increased flexibility of the ligand framework is advantageous to stereocontrol.[52, 53] Follow-up work of Davidson and Jones showed that catalysts able to racemize between conformations actually performed better than stereorigid catalysts.[54-57] In this proposed mechanism, the flexible catalytic site adapts to the chirality of the last inserted monomer unit, but participates in/determines the selection of the monomer. We had previously found evidence that such a mechanism was also operating in isotactic lactide polymerization with copper iminopyrrolide complexes:[58-61] although stereoerror analysis clearly indicated a chain-end control mechanism, isotactic PLA was only obtained

with catalysts having a flexible, chiral ligand coordination, while catalysts with a C_s-symmetric coordination environment provided atactic PLA.[61]

We had decided to test whether such stereocontrol could be introduced into zinc complex **1** by providing a flexible coordination environment. Placing two identical *N*-donor arms on the central nitrogen in **7** and **8** (Chart 2.2) provided an easy pathway to catalyst racemization. Indeed, ^{1}H-NMR studies indicated redundant fast catalyst racemization at room temperature for four-coordinated **7**, as well as for five-coordinated **8**,[62] while the parent complex **1** was stereorigid.[45] Catalysts **7** and **8** (X = $N(SiMe_3)_2$) produced slightly isotactic PLA (P_m = 0.55 – 0.65), when activated with EtOH. While this served as proof-of-principle for the existence of the speculated stereocontrol mechanism, selectivities fell well short of useful levels. Here we present our investigation of trityl-substituted derivatives of **7** and **8**, which were intended to increase stereocontrol by providing additional steric crowding, but surprisingly and unfortunately showed the opposite effect.

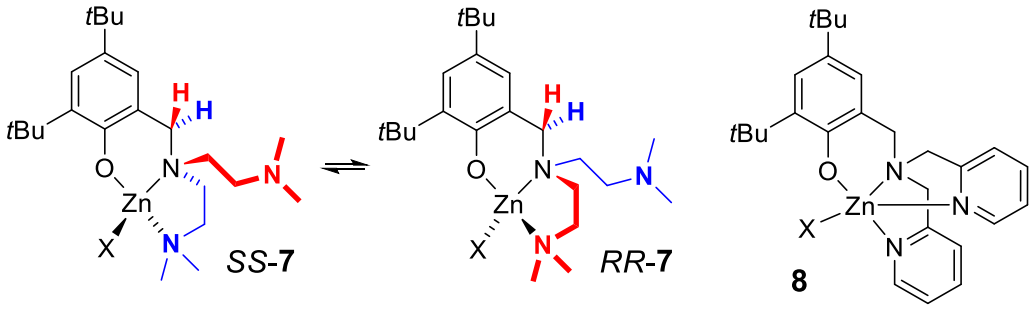

Chart 2.2.

Results and Discussion

Syntheses. Attempts to prepare ligand **L1**H carrying dimethylaminoethyl substituents, using procedures employed by Ma and coworkers,[63] were unfortunately unsuccessful (Scheme 2.1). Neither variation of solvent (EtOH, DMF, THF, MeCN, MeOH), nor heating in a Parr Monowave reactor to 150 °C yielded the expected product. On the other hand, pyridyl-substituted **L2**H was obtained in good yields by direct aminomethylation of 4-*t*Bu-2-trityl-phenol in refluxing ethanol. Subsequent reaction of **L2**H with $Zn(N(SiMe_3)_2)_2$ in toluene cleanly produced the respective amide complex **9** (Scheme 2.1).

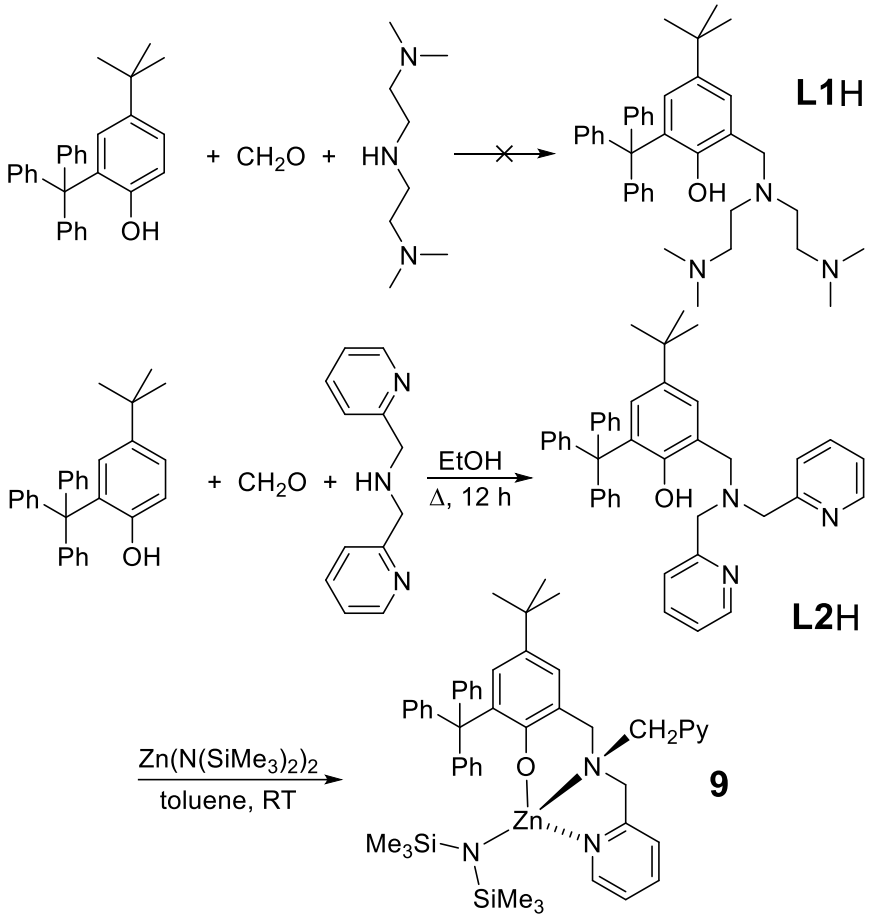

Scheme 2.1

Structural studies. The crystal structure of **9** gratifyingly showed a tetrahedral coordination of the zinc atom (Fig. 2.1), contrary to *t*Bu-substituted **8**, which displayed

coordination of both pyridine arms in its crystal structure.[62] As a consequence of the lower coordination number, Zn-N bond lengths are appr. 0.1 Å shorter in **9** then in **8**, but otherwise in the expected range for tetracoordinated zinc complexes (Zn-Py: 2.06(4) Å, *n*=7772; Zn-NR_3: 2.11(7) Å, *n*=2286; Zn-$N(SiMe_3)_2$: 1.92(2), *n*=120).[64] As observed in **8**, the phenolate ring adopts a π-stacking orientation with the coordinated pyridine. The increased steric crowding by the trityl substituent is reflected in a boat-like distortion of the phenolate ring from planarity, which is absent in **7** or **8**: planes through the respective *ipso, ortho, meta* and *para* atoms on both sides of the oxygen substituent show an angle of 10° to each other.

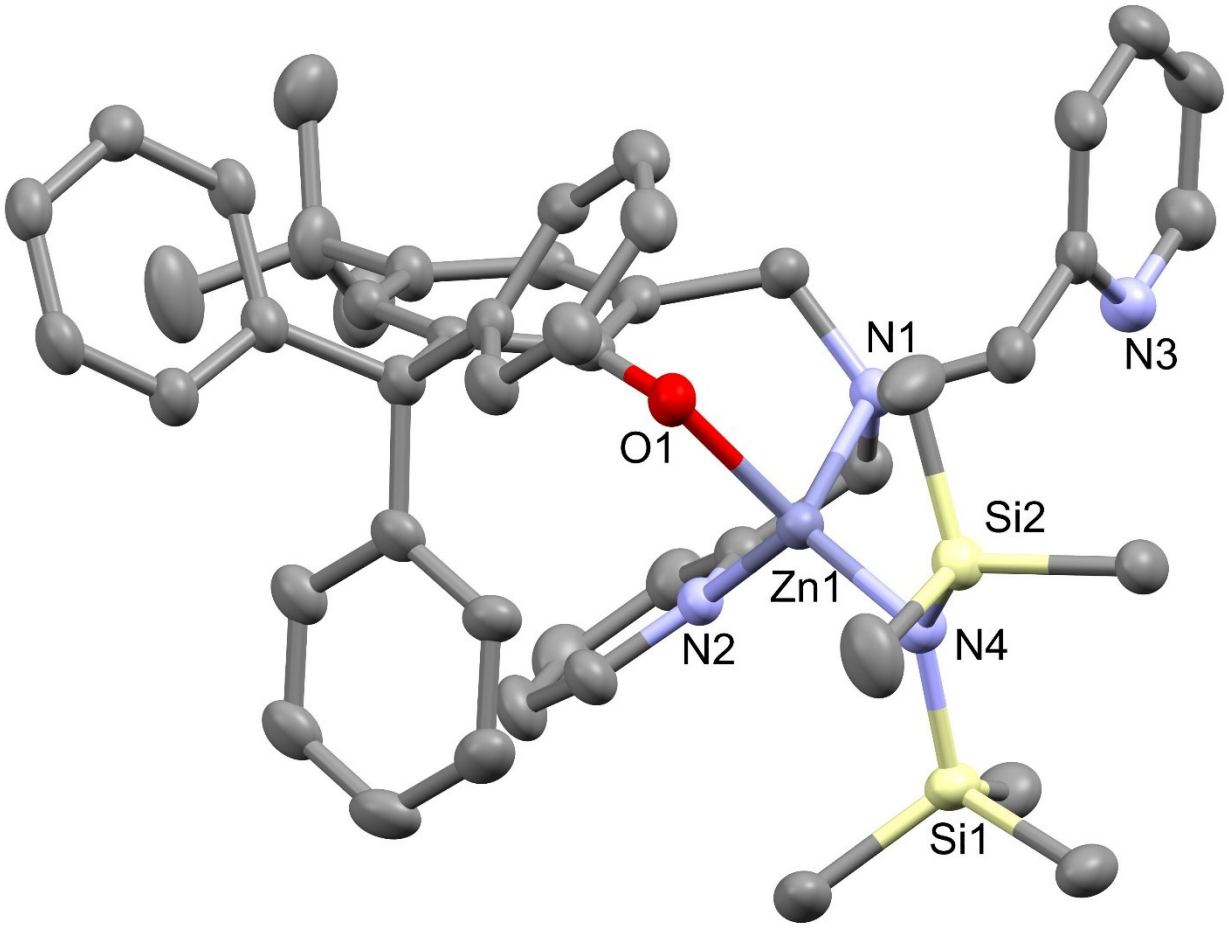

Figure 2.1 Crystal structure of 9. Hydrogen atoms and the minor part of the *tert*-butyl disorder omitted for clarity. Thermal ellipsoids are drawn at the 50% probability level. Zn1-O1: 1.929(4) Å, Zn1-N1: 2.160(5) Å, Zn1-N2: 2.091(4) Å, Zn1-N4: 1.910(5) Å.

The ^{1}H NMR spectrum of **9** at room temperature showed broadened peaks indicative of chemical exchange for the hydrogen atoms on the methylene groups and the pyridine ring. The observed changes are in agreement with apparent C_s symmetry at higher temperature and C_1 symmetry at low temperature. At 333 K, the methylene protons coalesce into three peaks, two doublets and a singlet (Fig. 2.1). The two CH_2Py moieties are thus rendered equivalent by chemical exchange, but the two protons of the CH_2Py methylene group remain diastereotopic. At low temperature, 6 doublets are observed, in agreement with chemically inequivalent CH_2Py moieties. Equivalent temperature-dependent changes occur in the aromatic region, which shows peaks for two inequivalent pyridine moieties at 223 K (Fig. S2.1). Notably, a signal assigned to the hydrogen atom at the *ortho*-position at the pyridine ring appears at 8.5 ppm, but there is no other such peak above 8.0 ppm, indicating a strongly different environment for the second pyridyl moiety. (Given the residual peaks from d^8-toluene and the broadened trityl peaks at low temperature, the second *ortho* pyridyl proton could not be located.) Trityl signals start to broaden at 223 K, indicating that trityl rotation remains fast until this temperature (Fig. S2.1). There is no significant broadening for the $SiMe_3$ signal even 223 K. From an Eyring plot of exchange rates, thermodynamic parameters of $\Delta H^{‡}$ = 41(1) kJ/mol, $\Delta S^{‡}$ = –44(4) J/(mol·K), and $\Delta G^{‡}_{298K}$ = 54(1) kJ/mol (Fig. S2.2) were determined. The facile Zn-amide rotation even at 223 K (in penta-coordinated **8**, Zn-amide rotation was slow below 278 K despite the smaller *t*Bu substituent), strongly different environments of the pyridine moieties and the negative activation entropy of –44(4) J/(mol·K) are all in agreement with **9** being tetra-

coordinated in solution and that it racemizes by coordination of the pending pyridine arm as indicated in Scheme 2.2.

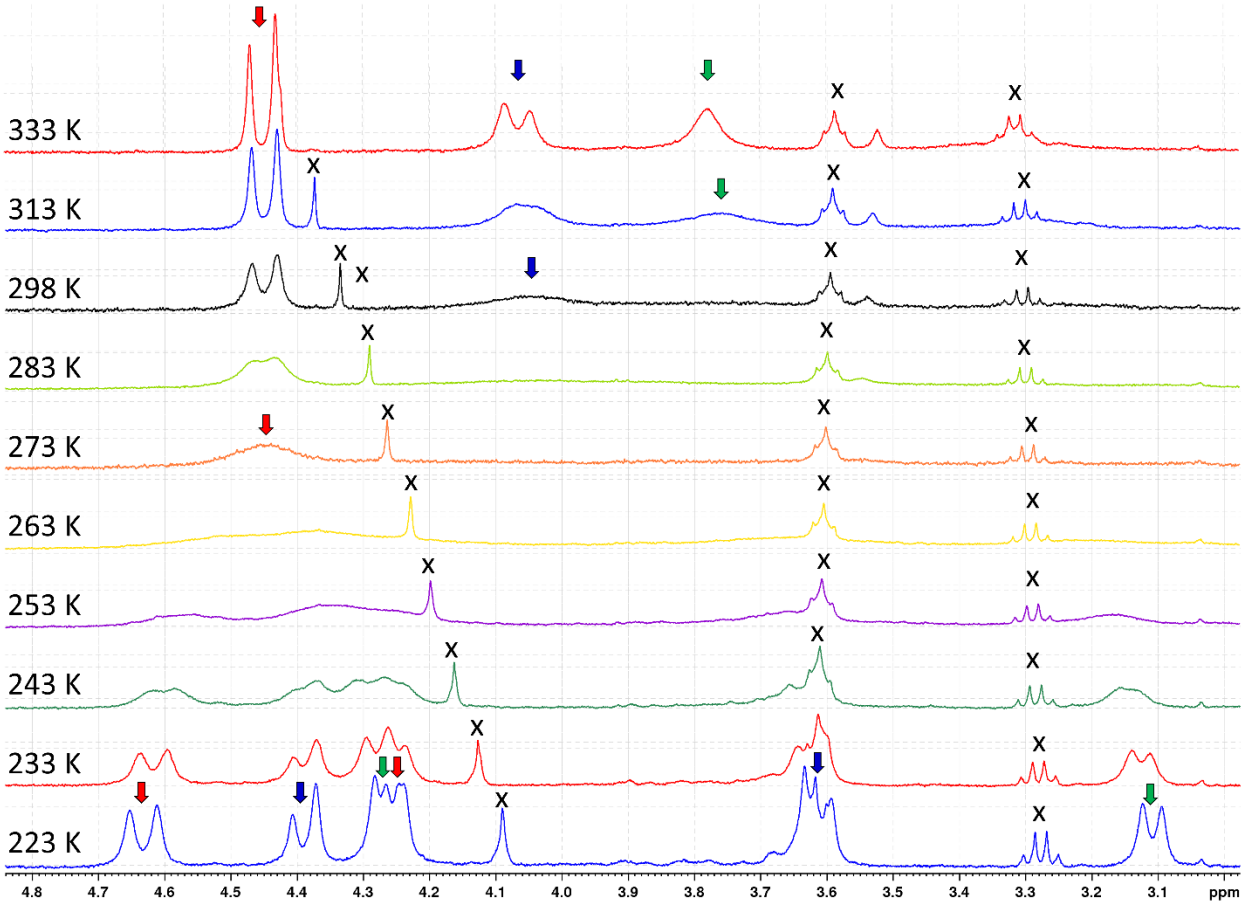

Figure 2.2 Methylene region of ^{1}H NMR spectra of **9** in d_8-toluene at 223 – 333 K.

To corroborate this assignment, we conducted DFT calculations on tetra- and penta-coordinated **8** and **9** (Fig. S2.3 and S2.4). DFT-calculated structures were in good agreement with the experimentally observed crystal structures (Fig. S2.5), but bond distances to Zn were up to 0.1 Å shorter in the calculated structures (Table S2.1). The steric influence of the trityl group was thus under- rather than overestimated by the calculations. Nevertheless, the calculations confirmed that the most stable isomer at 298 K is the penta-coordinated complex for **8**, while the tetra-coordinated isomer is more stable for **9** (Table

2.1). The small energy difference between **9-tetra** and **9-penta** is in good agreement with a fast racemization of **9**, most likely via the penta-coordinated intermediate.

Table 2.1. Results of DFT calculations

	Δ(E + ZPE) [kJ/mol]	**$\Delta G_{298\ K}$ [kJ/mol]**
8-tetra, one pyridine coordinated	23.8	8.4
8-penta, two pyridine coordinated [a]	0	0
9-tetra, one pyridine coordinated [a]	3.3	–4.2
9-penta, one pyridine coordinated	0	0

[a] coordination observed in the crystal structure

Lactide polymerization. Complex **9** was readily active in *rac*-lactide polymerization in C_6D_6 solution, albeit with lower activity than the highly active complex **1**,[45] most likely due to its increased steric crowding. Nevertheless, polymerizations typically reached completion in 15-90 minutes, depending on conditions (Table 2.2). P_m values determined from decoupled ^{1}H NMR showed slightly stronger variations than we usually observe in lactide polymerization, but clearly indicate that only atactic PLA was obtained. Exchange of the *ortho-t*Bu substituent against trityl thus surprisingly removed the slight stereocontrol which was observed in **7** and **8**.[62] Increased steric bulk is typically considered to favour existing stereocontrol mechanisms. For example, in Ma's complexes of type **4**, exchange of *ortho-t*Bu against trityl increased isoselectivity from P_m=0.64 to P_m=0.84.[48] While steric bulk can be detrimental in the postulated *ligand-site mediated chain-end control* mechanism if it impedes the required isomerization of the catalyst, variable temperature NMR of **9** provided an isomerization rate of appr. 2000 s^{-1}, still orders of magnitude faster than insertion rates, which were below 1 s^{-1} (insertion rate per Zn $\approx k_{obs}\cdot$[lactide]^0/[**9**]). The reasons for the loss of stereocontrol remains thus unclear at the moment.

Table 2.2 *rac*-Lactide polymerization with 9

#	c(9) [mM]	c(ROH) [mM]	Final conversion	k_{obs} [h]	P_m	M_n clcd. [kDa] [f]	M_n obs. [kDa] [f]	M_w/M_n [f]
1	1.0	-	95% – 98%	1.8±1.2	0.51 – 0.57	14.1	8.9	4.3
2	2.0	-	95% – 99%	3.0±1.3	0.45 – 0.57	14.3	8.7	1.4
3	3.0 [c]	-	95% – 99%	3.8±0.9 [d]	0.44 – 0.60	14.3	14.0	2.0
4	1.0 [e]	1.0	96%	1.6	0.48	13.8	9.0	1.5
5	2.0	2.0 / 4.0	98%	12.2±1.8	0.42 – 0.51	14.1 / 7.0	1.6 / 1.4	1.8 / 1.9
6	3.0	3.0 / 6.0	99%	20.4±5.6	0.46 – 0.50	14.3 / 7.1	2.8 / 1.1	1.9 / 1.8

[a] Average/range of three to five polymerizations. Conditions : [lactide]:[**9**] = 100, C_6D_6, ambient temperature, 15 – 90 min. ROH = EtOH or BnOH (see Table S2.2). [c] Three out of five polymerizations with [lactide]:[Zn] = 67 instead of 100. [d] One outlier rate constant ignored (see Table S2.2). [e] Single polymerization. [f] M_n determinations performed on isolated samples (see Table S2.2).

Although the bulky bis(trimethylsilyl)amide group is often considered a poor initiator for lactide polymerization, polymerizations with **9** proceeded smoothly to completion without addition of any co-initiator (Table 2.2). Polymerization kinetics at 1.0 mM catalyst concentration did not indicate the presence of an induction period and showed concentration profiles in agreement with the expected first-order dependence on lactide concentration (Fig. 2.3). Pseudo-first-order rate constants ranged from 1 h^{-1} – 3 h^{-1} (Table S2.2), and a comparable rate constant was obtained in the presence of 1 equiv of ethanol per catalyst, likewise in agreement with efficient initiation by bis(trimethylsilyl)amide. Polymerizations at 2.0 mM or 3.0 mM catalyst concentration were less well behaved, however, and we observed induction periods of variable lengths and notable deviations from first-order behaviour (Fig. S2.6-S2.9). Observed rate constants also barely increased with catalyst concentration (Table 2.2) and suggested a square-root dependence on catalyst concentration, rather than a linear dependence. Catalyst dimerization equilibria, even for the alkoxide complexes considered to be the active species, seem unlikely given the number of potential donor ligands on the zinc complex and the steric bulk of the ligand. We thus reinvestigated the influence of alcohol co-initiator at these catalyst concentrations.

At 2.0 and 3.0 mM catalyst concentration, addition of one equiv of ethanol or benzyl alcohol drastically increased catalytic activity (Table 2.2, Fig. S2.10 and S2.11). Addition of an additional equivalent of alcohol did not lead to further activity increase. Activities depend linearly on catalyst concentration, but show a zero-intercept at [**9**] = 0.8 mM (Fig. 2.4). We had previously observed a comparable concentration threshold of 0.5 mM for polymerizations with similarly sensitive copper catalysts under identical experimental conditions.[65]

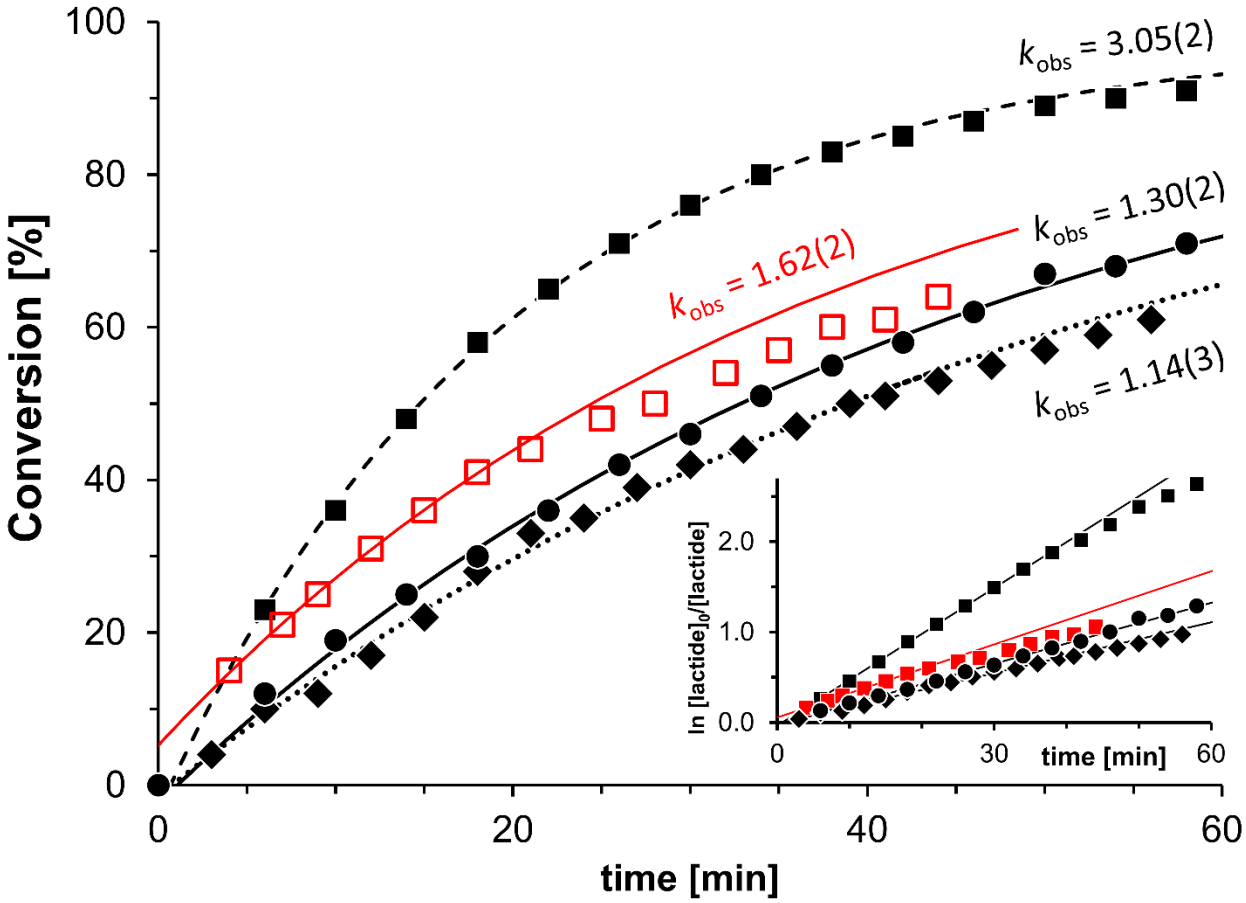

Figure 2.3 Concentration profiles for the polymerization of *rac*-lactide with 1.0 mM **9** in C_6D_6 at ambient temperature without (full symbols) and with addition of ethanol (hollow squares). The inset shows the linearized concentration-time profile.

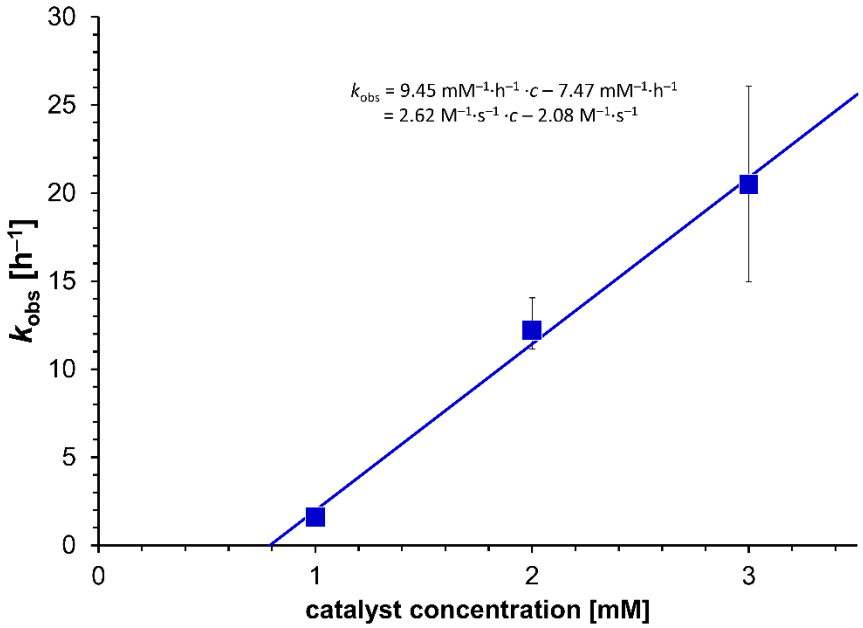

Figure 2.4 Dependence of average values of k_{obs} on catalyst concentration for *rac*-lactide polymerizations with **9** in the presence of ethanol or benzyl alcohol (C_6D_6, ambient temperature). The obtained second-order rate constant is 2.6 L/(mol·s).

While kinetic data thus seem to indicate poor initiation by bis(trimethylsilyl)amide, which is circumvented by *in-situ* formation of the alkoxide complex upon addition of alcohol, this was contradicted by GPC analyses of the polymers: Polymer molecular weights in the absence of alcohol are in good agreement with the expected values, although significantly broadened polydispersities indicate problems with molecular weight control, such as slow initiation. In the presence of alcohol (2.0 or 3.0 mM catalyst concentration), on the other hand, oligomers instead of polymers are obtained, without any correlation between the amount of added alcohol and the polymer molecular weight (Tables 2.2 and S2.2). The likeliest explanation is thus unfortunately that sterically hindered **9** is a capable, but slow initiator of lactide polynerization, but not stable in the presence of external

alcohol. The decomposed species is more active, but prone to chain-backbiting leading to oligomeric, instead of polymeric products.

The difference in the activity indicates that we do not obtain clean protonation of the amide with the alcohol. It can be assumed that by increasing the steric bulk from *tert*-butyl to triphenyl methane in the *ortho* position, we weakened the phenolate coordination to the zinc and the alcohol can now protonate this position. However, I do not believe that this enough to compete in the basicity with trimethylsilyl amide. I believe that the trimethylsilyl amide will still be protonated first. Then a second alcohol, either due to different reaction speeds or due to local overconcentration protonates the phenolate. I believe also that the amine pyridyl moiety still stays on the zinc. The results is a zinc dialkoxide complex, with two N-donor ligands, which is less bulky and thus more active in polymerization.

Conclusion

Zinc complex **9** is a competent initiator for lactide polymerization, albeit with poor molecular weight control. Increasing the steric bulk at the *ortho*-position of the aryloxide ligand destabilized, as hoped, the coordination of a second pyridine ligand, providing a complex with flexible coordination geometry. However, the increased steric bulk did not increase stereoselectivity compared to previous work, but unexpectedly led to atactic PLA. Contrary to the analogous complex with *ortho tert*-butyl substituents, the sterically more bulky complex investigated here does not seem to tolerate the presence of external alcohol in the reaction system. While *catalytic-site mediated chain-end control* is thus a valid alternative stereocontrol mechanism, it does not seem to exempt from the capricious nature of catalyst design in lactide polymerization, where “trial and error” often seems to trump any rational approach to catalyst design.

Experimental part

General considerations. All reactions were carried out using Schlenk or glove box techniques under nitrogen atmosphere. $Zn(N(SiMe_3)_2)_2$[66] and 4-*tert*-butyl-2-trityl-phenol[67] were prepared according to literature. Solvents were dried by passage through activated aluminum oxide (MBraun SPS), de-oxygenated by repeated extraction with nitrogen, and stored over molecular sieves. C_6D_6 was dried over molecular sieves. *rac*-Lactide (98%) was purchased from Sigma–Aldrich, purified by 3x recrystallisation from dry ethyl acetate and kept at –30 °C. All other chemicals were purchased from common commercial suppliers and used without further purification. ^1H and ^{13}C NMR spectra were acquired on a Bruker Advance 400 spectrometer. Chemical shifts were referenced to the residual signals of the deuterated solvents ($CDCl_3$: ^1H: δ 7.26 ppm, ^{13}C: δ 77.16; C_6D_6: 1H: δ 7.16 ppm, ^{13}C: δ 128.06 ppm).

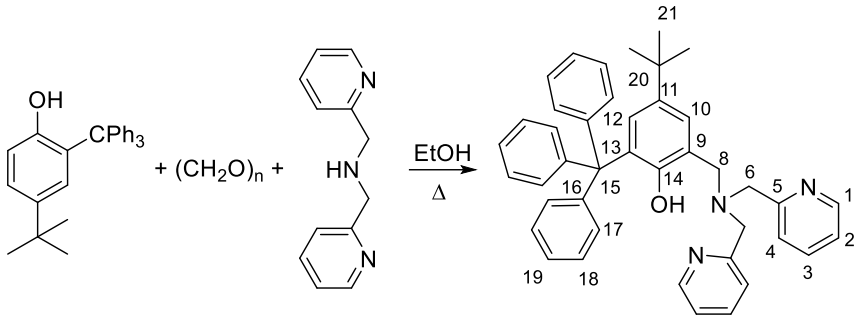

4-(*tert*-butyl)-2-trityl-6-(di-(2-picolyl)amine)phenol, L2. Paraformaldehyde (0.300 g, 10.0 mmol) and 4-(*tert*-butyl)-2-tritylphenol (1.96 g, 5.0 mmol) were added to a solution of di-(2-picolyl)amine (0.90 ml, 5.0 mmol) in ethanol (15 mL) and heated to reflux for 12 h with magnetic stirring. The mixture was cooled to ambient temperature. The solution was concentrated to 20% of its volume. After filtration and washing with EtOH, **L2** was obtained as a white powder (2.01 g, 67%).

^1H NMR (400 MHz, C_6D_6): δ 1.25 (s, 9H, C*Me*$_3$), 3.57 (s, 2H, ArC(8)*H*$_2$), 3.69 (s, 4H, PyC*H*$_2$), 6.56 (t, 2H, Py C(2)*H*), 6.82 (d, *J* = 8 Hz, 2H, Py C(4)*H*), 6.98 (dt, *J* = 8 Hz & 2 Hz, 3H, *para* Ph), 7.01-7.05 (m, 3H, C(10)*H* + Py C(3)*H*), 7.10 (vt, *J* = 8 Hz, 6H, *ortho*

Ph), 7.53 (d, *J* = 2 Hz, 1H, C(12)*H*), 7.59 (d, *J* = 8 Hz, 6H, *meta* Ph), 8.32 (d, *J* = 5 Hz, 2H, Py C(1)*H*), 10.99 (s, 1H, OH). ^{1}H NMR (400 MHz, $CDCl_3$): δ 1.15 (s, 9H, C*Me*$_3$), 3.70 (s, 4H, PyC*H*$_2$), 3.79 (s, 2H, ArC(8)*H*$_2$), 6.98 (m, 3H) 7.12-7.26 (m, 17H), 7.53 (td, *J* = 8 Hz, 2H, Py C(3)*H*), 8.44 (d, 2H, Py C(1)*H*), 10.54 (s, 1H, OH). ^{13}C{^{1}H} NMR (100 MHz, $CDCl_3$): δ 31.9 (C*Me*$_3$), 34.44 (*C*Me$_3$), 58.81 (*C*Ph$_3$), 59.20 (Py*C*H$_2$), 63.98 (Ar*C(8)*H$_2$), 121.84 (Ar), 122.51 (Py C2), 124.22 (Py C4), 125.65 (CPh$_3$ C19), 125.72 (Ar), 127.27 (CPh$_3$ C17) 128.46 (Ar), 131.66 (CPh$_3$ C18), 133.61 (Ar), 137.09 (Py C3), 140.46 (Ar), 146.70 (CPh$_3$ C16), 149.17 (Py C1), 154.01 (*C*(14)OH), 158.04 (Py C5). EI-HRMS (m/z): $[M+H]^+$ ($C_{42}H_{41}N_3O$) calcd 604.3322; found 604.3316.

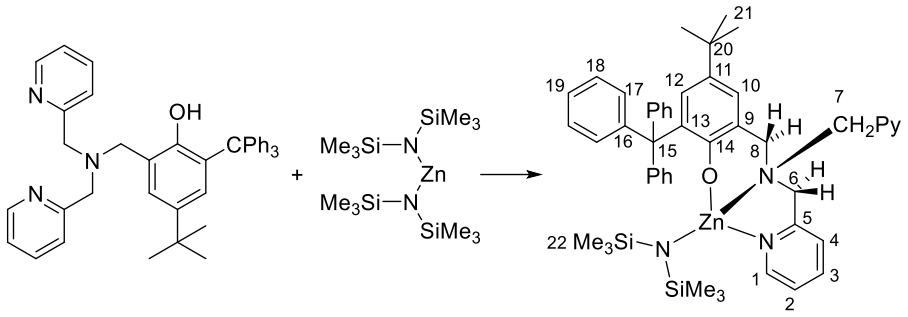

(L2)ZnN(SiMe$_3$)$_2$, 9. Zn(N(SiMe$_3$)$_2$)$_2$ (444 mg, 1.2 mmol) was suspended in toluene (3 ml). 4-(*tert*-butyl)-2-trityl-6-(di-(2-picolyl)amine)phenol (933 mg, 1.2 mmol) in toluene (2 ml) was added dropwise, resulting in a light yellow solution. The reaction was stirred 24 hours at RT. Evaporation of the solvent yielded a yellow-orange solid (947 mg, 98%).

^{1}H NMR (400 MHz, C_6D_6): δ 0.31 (s, 18H, SiC*Me*$_3$), 1.03 (s, 9H, C*Me*$_3$), 3.76 (bs, 1H, ArC(8)*H*$_2$) 4.03 (bs, 2H, PyC*H*$_2$), 4.43 (d, 2H, PyC*H*$_2$), 6.34 (bs, 3H, Py), 6.46 (d, 1H, *J* = 3 Hz, C(10)H), 6.72 (bs, 1H, Py), 6.98 (t, *J* = 8 Hz, 3H, *para* Ph), 7.21 (t, *J* = 8 Hz, 6H, *meta* Ph), 7.31 (d, 1H, C(12)*H*), 7.70 (d, *J* = 7 Hz, 6H, *ortho* Ph). ^{13}C{^{1}H} NMR (100 MHz, C_6D_6): δ 5.88 (Si*Me*$_3$), 31.64 (C*Me*$_3$), 33.32 (*C*Me$_3$), 61.38 (*C6* + *C7*), 63.69 (*C8*), 121.05 (Ar), 122.76 (Py C2), 124.54 (CPh$_3$ C19), 125.13 (Ar), 126.87 (CPh$_3$ C17), 128.84 (Ar), 131.35 (CPh$_3$ C18), 132.36 (Ar), 133.63 (Ar), 136.64 (bs, Py C3), 147.48 (CPh$_3$ C16),148.49 (bs, Py C1), 154.90 (Py C5), 164.97 (C14). (Py C4 not located)

Lactide polymerization. In a glove box, the desired amount of *rac*-lactide was placed into a J.-Young tube and dissolved in C_6D_6. If required, a stock solution of an additive (EtOH, etc.) was added, followed by a stock solution of the catalyst (≈20 mM in C_6D_6). The reaction was followed by ^{1}H NMR. The reaction was quenched by addition of ≈5 equiv of a $CDCl_3$ solution of acetic acid (5 mM). The volatiles were immediately evaporated and solid polymer samples were stored at –80 °C for further analysis. Conversion was determined from ^{1}H NMR by comparison to remaining lactide. P_m values were determined from homodecoupled ^{1}H NMR spectra and calculated from $P_m = 1 - 2 \cdot I_1/(I_1+I_2)$, with I_1 = 5.15 – 5.21 ppm (*rmr, mmr/rmm*), I_2 = 5.21 – 5.25 ppm (*mmr/rmm, mmm, mrm*). Molecular

weight analyses were performed on *crude reaction products* using an Agilent 1260 Infinity GPC/SEC gel permeation chromatograph equipped with a refractive index and a viscosity detector at 30 °C. THF was used as the eluent at a flow rate of 0.4 mL·min-1. Molecular weights were obtained from universal calibration using polystyrene standards.

DFT calculations were performed with Gaussian16[68] using the M06 functional.[69] In geometry optimization and frequency calculation (ZPE and thermal correction to 298 K), a 6-31+G(d,p) basis set was used for all light atoms and a LANL2DZ effective-core potential basis set for zinc and silicon. All optimized geometries showed real frequencies only. Single-point energies on the optimized geometries were obtained with the Def2TZVPP basis set.

X-ray diffraction. Diffraction data were collected on a Bruker APEXII with a Cu microsource/Quazar MX using the APEX2 software package.[70] Data reduction was performed with SAINT,[71] absorption corrections with SADABS.[72] Structures were solved by dual-space refinement (SHELXT).[73] All non-hydrogen atoms were refined anisotropic using full-matrix least-squares on F^2 and hydrogen atoms refined with fixed isotropic U using a riding model (SHELXL97).[74] Further experimental details can be found in Table 2.3 and in the supporting information (CIF). Data indicates the possible presence of a (slight) non-merohedral twin (or a contaminating crystallite), but no twin domain was found.

Table 2.3. Details of the X-ray diffraction study

	9
Formula	$C_{48}H_{58}N_4OSi_2Zn$
M_w (g/mol); $d_{calcd.}$ (g/cm^3)	828.53; 1.232
T (K); F(000)	100; 1760
Crystal System	monoclinic
Space Group	*C*2

Unit Cell:	a (Å)	20.5019(5)
	b (Å)	10.0347(3)
	c (Å)	23.4815(5)
	β (°)	112.4320(10)
V (Å^3); Z		4465.3(2); 4
μ (mm^{-1}); Abs. Corr.		1.575; multi-scan
θ range (°); completeness		2.0 – 72.6; 0.985
collected reflections; R_σ		27311; 0.056
unique reflections; R_{int}		7292; 0.057
R1(F) ($I > 2\sigma(I)$)		0.059
wR(F^2) (all data)		0.157
GoF(F^2); Flack-x		1.082; 0.04(4)
Residual electron density		1.92; -0.43

Supplementary data

Supplementary data are available with the article through the journal Web site at xxxxx. ^{1}H and ^{13}C NMR spectra of **L2**H and 9, and additional tables and figures, as mentioned in the text, are included, as well as calculated structures (PDB) and details of the crystal structure determination (CIF). CCDC 2096839 contains the supplementary crystallographic data for this paper. The data can be obtained free of charge from The Cambridge Crystallographic Data Centre via www.ccdc.cam.ac.uk/structures.

Conflicts of interest

There are no conflicts to declare.

Acknowledgements

Funding was supplied by the NSERC discovery program (RGPIN-2016-04953) and the Centre for Green Chemistry and Catalysis (FQRNT). DFT calculations were enabled by support provided by Calcul Québec (www.calculquebec.ca) and Compute Canada (www.computecanada.ca). F. D. received partial funding by MITACS (Summer research stipend). We thank Dr. Daniel Chartrand for support with X-ray crystallography and Dr. René Gagnon (Université de Sherbrooke) for support with GPC measurements.

References chapter 2

1. Filiciotto, L.; Rothenberg, G., Biodegradable Plastics: Standards, Policies, and Impacts. *ChemSusChem* **2021,** *14* (1), 56-72.
2. Abdelmoez, W.; Dahab, I.; Ragab, E. M.; Abdelsalam, O. A.; Mustafa, A., Bio- and oxo-degradable plastics: Insights on facts and challenges. *Polym. Adv. Technol.* **2021,** *32* (5), 1981-1996.
3. Lyubov, D. M.; Tolpygin, A. O.; Trifonov, A. A., Rare-earth metal complexes as catalysts for ring-opening polymerization of cyclic esters. *Coord. Chem. Rev.* **2019,** *392*, 83-145.
4. Li, X.; Chen, C.; Wu, J., Lewis Pair Catalysts in the Polymerization of Lactide and Related Cyclic Esters. *Molecules* **2018,** *23* (1).
5. Kuroishi, P. K.; Dove, A. P., On like a light. *Nature Catalysis* **2018,** *1* (7), 486-487.
6. Redshaw, C., Use of Metal Catalysts Bearing Schiff Base Macrocycles for the Ring Opening Polymerization (ROP) of Cyclic Esters. *Catalysts* **2017,** *7* (5).
7. Osten, K. M.; Mehrkhodavandi, P., Indium Catalysts for Ring Opening Polymerization: Exploring the Importance of Catalyst Aggregation. *Acc. Chem. Res.* **2017,** *50* (11), 2861-2869.
8. Fuoco, T.; Pappalardo, D., Aluminum Alkyl Complexes Bearing Salicylaldiminato Ligands: Versatile Initiators in the Ring-Opening Polymerization of Cyclic Esters. *Catalysts* **2017,** *7* (2).
9. Paul, S.; Zhu, Y.; Romain, C.; Brooks, R.; Saini, P. K.; Williams, C. K., Ring-Opening Copolymerization (Rocop): Synthesis and Properties of Polyesters and Polycarbonates. *Chem. Commun. (Cambridge, U. K.)* **2015,** *51* (30), 6459-6479.
10. MacDonald, J. P.; Shaver, M. P., Aluminum Salen and Salan Polymerization Catalysts: From Monomer Scope to Macrostructure Control. In *Green Polymer Chemistry: Biobased Materials and Biocatalysis*, American Chemical Society: 2015; Vol. 1192, pp 147-167.
11. Guillaume, S. M.; Kirillov, E.; Sarazin, Y.; Carpentier, J.-F., Beyond Stereoselectivity, Switchable Catalysis: Some of the Last Frontier Challenges in Ring-Opening Polymerization of Cyclic Esters. *Chem.-Eur. J.* **2015,** *21* (22), 7988-8003.
12. Sauer, A.; Kapelski, A.; Fliedel, C.; Dagorne, S.; Kol, M.; Okuda, J., Structurally Well-Defined Group 4 Metal Complexes as Initiators for the Ring-Opening Polymerization of Lactide Monomers. *Dalton Trans.* **2013,** *42* (25), 9007-9023.
13. Dagorne, S.; Normand, M.; Kirillov, E.; Carpentier, J.-F., Gallium and Indium Complexes for Ring-Opening Polymerization of Cyclic Ethers, Esters and Carbonates. *Coord. Chem. Rev.* **2013,** *257* (11–12), 1869-1886.
14. Dagorne, S.; Fliedel, C., Organoaluminum Species in Homogeneous Polymerization Catalysis. In *Modern Organoaluminum Reagents: Preparation, Structure, Reactivity and Use*, Woodward, S.; Dagorne, S., Eds. Springer Berlin Heidelberg: Berlin, Heidelberg, 2013; pp 125-171.
15. Carpentier, J.-F.; Liu, B.; Sarazin, Y., Charge-Neutral and Cationic Complexes of Large Alkaline Earths for Ring-Opening Polymerization and Fine Chemicals Catalysis. In *Advances in Organometallic Chemistry and Catalysis*, John Wiley & Sons, Inc.: 2013; pp 359-378.
16. dos Santos Vieira, I.; Herres-Pawlis, S., Lactide Polymerisation with Complexes of Neutral N-Donors – New Strategies for Robust Catalysts. *Eur. J. Inorg. Chem.* **2012,** *2012* (5), 765-774.
17. Wheaton, C. A.; Hayes, P. G., Designing Cationic Zinc and Magnesium Catalysts for Coordination–Insertion Polymerization of Lactide. *Comments Inorg. Chem.* **2011,** *32* (3), 127-162.
18. Dutta, S.; Hung, W.-C.; Huang, B.-H.; Lin, C.-C., Recent Developments in Metal-Catalyzed Ring-Opening Polymerization of Lactides and Glycolides: Preparation of Polylactides,

Polyglycolide, and Poly(Lactide-Co-Glycolide). In *Synthetic Biodegradable Polymers*, Rieger, B.; Künkel, A.; Coates, G. W.; Reichardt, R.; Dinjus, E.; Zevaco, T. A., Eds. Springer-Verlag: Berlin, 2011; pp 219-284.
19. Dijkstra, P. J.; Du, H.; Feijen, J., Single Site Catalysts for Stereoselective Ring-Opening Polymerization of Lactides. *Polym. Chem.* **2011,** *2* (3), 520-527.
20. Thomas, C. M., Stereocontrolled Ring-Opening Polymerization of Cyclic Esters: Synthesis of New Polyester Microstructures. *Chem. Soc. Rev.* **2010,** *39* (1), 165.
21. Stanford, M. J.; Dove, A. P., Stereocontrolled Ring-Opening Polymerization of Lactide. *Chem. Soc. Rev.* **2010,** *39*, 486-494.
22. Jones, M. D., Heterogeneous Initiators for Sustainable Polymerization Processes. In *Heterogenized Homogeneous Catalysts for Fine Chemicals Production*, Barbaro, P.; Liguori, F., Eds. Springer Netherlands: 2010; Vol. 33, pp 385-412.
23. Wheaton, C. A.; Hayes, P. G.; Ireland, B. J., Complexes of Mg, Ca and Zn as Homogeneous Catalysts for Lactide Polymerization. *Dalton Trans.* **2009**, 4832 - 4846.
24. Williams, C. K.; Hillmyer, M. A., Polymers from Renewable Resources: A Perspective for a Special Issue of Polymer Reviews. *Polym. Rev.* **2008,** *48* (1), 1-10.
25. Platel, R. H.; Hodgson, L. M.; Williams, C. K., Biocompatible Initiators for Lactide Polymerization. *Polym. Rev.* **2008,** *48* (1), 11 - 63.
26. Amgoune, A.; Thomas, C. M.; Carpentier, J.-F., Controlled Ring-Opening Polymerization of Lactide by Group 3 Metal Complexes. *Pure Appl. Chem.* **2007,** *79* (11), 2013-2030.
27. Dechy-Cabaret, O.; Martin-Vaca, B.; Bourissou, D., Controlled Ring-Opening Polymerization of Lactide and Glycolide. *Chem. Rev.* **2004,** *104* (12), 6147-6176.
28. O'Keefe, B. J.; Hillmyer, M. A.; Tolman, W. B., Polymerization of Lactide and Related Cyclic Esters by Discrete Metal Complexes. *J. Chem. Soc., Dalton Trans.* **2001,** (15), 2215-2224.
29. Yuntawattana, N.; McGuire, T. M.; Durr, C. B.; Buchard, A.; Williams, C. K., Indium phosphasalen catalysts showing high isoselectivity and activity in racemic lactide and lactone ring opening polymerizations. *Catalysis Science & Technology* **2020,** *10* (21), 7226-7239.
30. Rosen, T.; Rajpurohit, J.; Lipstman, S.; Venditto, V.; Kol, M., Isoselective Polymerization of rac-Lactide by Highly Active Sequential {ONNN} Magnesium Complexes. *Chem. Eur. J.* **2020,** *26* (71), 17183-17189.
31. Fernández-Millán, M.; Ortega, P.; Cuenca, T.; Cano, J.; Mosquera, M. E. G., Alkali-Metal Compounds with Bio-Based Ligands as Catalysts for Isoselective Lactide Polymerization: Influence of the Catalyst Aggregation on the Polymerization Control. *Organometallics* **2020,** *39* (12), 2278-2286.
32. Gong, Y.; Ma, H., High performance benzoimidazolyl-based aminophenolate zinc complexes for isoselective polymerization of rac-lactide. *Chem. Commun. (Cambridge, U. K.)* **2019,** *55* (68), 10112-10115.
33. Hu, J.; Kan, C.; Wang, H.; Ma, H., Highly Active Chiral Oxazolinyl Aminophenolate Magnesium Initiators for Isoselective Ring-Opening Polymerization of rac-Lactide: Dinuclearity Induced Enantiomorphic Site Control. *Macromolecules* **2018,** *51* (14), 5304-5312.
34. Xu, T.-Q.; Yang, G.-W.; Liu, C.; Lu, X.-B., Highly Robust Yttrium Bis(Phenolate) Ether Catalysts for Excellent Isoselective Ring-Opening Polymerization of Racemic Lactide. *Macromolecules* **2017,** *50* (2), 515-522.
35. Myers, D.; White, A. J. P.; Forsyth, C. M.; Bown, M.; Williams, C. K., Phosphasalen Indium Complexes Showing High Rates and Isoselectivities in Rac-Lactide Polymerizations. *Angew. Chem., Int. Ed.* **2017,** *56* (19), 5277-5282.

36. Bhattacharjee, J.; Harinath, A.; Nayek, H. P.; Sarkar, A.; Panda, T. K., Highly Active and Iso-Selective Catalysts for the Ring-Opening Polymerization of Cyclic Esters Using Group 2 Metal Initiators. *Chem.-Eur. J.* **2017,** *23* (39), 9319-9331.
37. Sun, Y.; Xiong, J.; Dai, Z.; Pan, X.; Tang, N.; Wu, J., Stereoselective Alkali-Metal Catalysts for Highly Isotactic Poly(Rac-Lactide) Synthesis. *Inorg. Chem.* **2016,** *55* (1), 136-143.
38. Rosen, T.; Popowski, Y.; Goldberg, I.; Kol, M., Zinc Complexes of Sequential Tetradentate Monoanionic Ligands in the Isoselective Polymerization of Rac-Lactide. *Chem.-Eur. J.* **2016,** *22* (33), 11533-11536.
39. Aluthge, D. C.; Ahn, J. M.; Mehrkhodavandi, P., Overcoming aggregation in indium salen catalysts for isoselective lactide polymerization. *Chem. Sci.* **2015,** *6* (9), 5284-5292.
40. Wang, H.; Yang, Y.; Ma, H., Stereoselectivity Switch between Zinc and Magnesium Initiators in the Polymerization of Rac-Lactide: Different Coordination Chemistry, Different Stereocontrol Mechanisms. *Macromolecules* **2014,** *47* (22), 7750-7764.
41. Mou, Z.; Liu, B.; Wang, M.; Xie, H.; Li, P.; Li, L.; Li, S.; Cui, D., Isoselective Ring-Opening Polymerization of Rac-Lactide Initiated by Achiral Heteroscorpionate Zwitterionic Zinc Complexes. *Chem. Commun. (Cambridge, U. K.)* **2014,** *50* (77), 11411-11414.
42. Bakewell, C.; White, A. J. P.; Long, N. J.; Williams, C. K., Metal-Size Influence in Iso-Selective Lactide Polymerization. *Angewandte Chemie International Edition* **2014,** *53* (35), 9226-9230.
43. Hador, R.; Botta, A.; Venditto, V.; Lipstman, S.; Goldberg, I.; Kol, M., The Dual-Stereocontrol Mechanism: Heteroselective Polymerization of rac-Lactide and Syndioselective Polymerization of meso-Lactide by Chiral Aluminum Salan Catalysts. *Angew. Chem., Int. Ed.* **2019,** *58* (41), 14679-14685.
44. Press, K.; Goldberg, I.; Kol, M., Mechanistic Insight into the Stereochemical Control of Lactide Polymerization by Salan–Aluminum Catalysts. *Angewandte Chemie International Edition* **2015,** *54* (49), 14858-14861.
45. Williams, C. K.; Breyfogle, L. E.; Choi, S. K.; Nam, W.; Young, V. G.; Hillmyer, M. A.; Tolman, W. B., A Highly Active Zinc Catalyst for the Controlled Polymerization of Lactide. *J. Am. Chem. Soc.* **2003,** *125* (37), 11350-11359.
46. Labourdette, G.; Lee, D. J.; Patrick, B. O.; Ezhova, M. B.; Mehrkhodavandi, P., Unusually Stable Chiral Ethyl Zinc Complexes: Reactivity and Polymerization of Lactide. *Organometallics* **2009,** *28* (5), 1309-1319.
47. Ebrahimi, T.; Mamleeva, E.; Yu, I.; Hatzikiriakos, S. G.; Mehrkhodavandi, P., The Role of Nitrogen Donors in Zinc Catalysts for Lactide Ring-Opening Polymerization. *Inorg. Chem.* **2016,** *55* (18), 9445-9453.
48. Wang, H.; Ma, H., Highly Diastereoselective Synthesis of Chiral Aminophenolate Zinc Complexes and Isoselective Polymerization of Rac-Lactide. *Chem. Commun. (Cambridge, U. K.)* **2013,** *49* (77), 8686-8688.
49. Kan, C.; Hu, J.; Huang, Y.; Wang, H.; Ma, H., Highly Isoselective and Active Zinc Catalysts for Rac-Lactide Polymerization: Effect of Pendant Groups of Aminophenolate Ligands. *Macromolecules* **2017,** *50* (20), 7911-7919.
50. Hu, J.; Kan, C.; Ma, H., Exploring Steric Effects of Zinc Complexes Bearing Achiral Benzoxazolyl Aminophenolate Ligands in Isoselective Polymerization of rac-Lactide. *Inorg. Chem.* **2018,** *57* (17), 11240-11251.

51. Stasiw, D. E.; Luke, A. M.; Rosen, T.; League, A. B.; Mandal, M.; Neisen, B. D.; Cramer, C. J.; Kol, M.; Tolman, W. B., Mechanism of the Polymerization of Rac-Lactide by Fast Zinc Alkoxide Catalysts. *Inorg. Chem.* **2017,** *56* (22), 14366-14372.
52. Ma, H.; Spaniol, T. P.; Okuda, J., Highly Heteroselective Ring-Opening Polymerization of Rac-Lactide Initiated by Bis(Phenolato)Scandium Complexes. *Angew. Chem., Int. Ed.* **2006,** *45* (46), 7818-7821.
53. Amgoune, A.; Thomas, C. M.; Roisnel, T.; Carpentier, J.-F., Ring-Opening Polymerization of Lactide with Group 3 Metal Complexes Supported by Dianionic Alkoxy-Amino-Bisphenolate Ligands: Combining High Activity, Productivity, and Selectivity. *Chem.-Eur. J.* **2006,** *12* (1), 169-179.
54. Chmura, A. J.; Chuck, C. J.; Davidson, M. G.; Jones, M. D.; Lunn, M. D.; Bull, S. D.; Mahon, M. F., A Germanium Alkoxide Supported by a C3-Symmetric Ligand for the Stereoselective Synthesis of Highly Heterotactic Polylactide under Solvent-Free Conditions. *Angew. Chem., Int. Ed.* **2007,** *46* (13), 2280-2283.
55. Chmura, A. J.; Davidson, M. G.; Frankis, C. J.; Jones, M. D.; Lunn, M. D., Highly Active and Stereoselective Zirconium and Hafnium Alkoxide Initiators for Solvent-Free Ring-Opening Polymerization of Rac-Lactide. *Chem. Commun. (Cambridge, U. K.)* **2008,** (11), 1293-1295.
56. Jones, M. D.; Hancock, S. L.; McKeown, P.; Schafer, P. M.; Buchard, A.; Thomas, L. H.; Mahon, M. F.; Lowe, J. P., Zirconium Complexes of Bipyrrolidine Derived Salan Ligands for the Isoselective Polymerisation of Rac-Lactide. *Chem. Commun. (Cambridge, U. K.)* **2014,** *50* (100), 15967-15970.
57. Jones, M. D.; Brady, L.; McKeown, P.; Buchard, A.; Schafer, P. M.; Thomas, L. H.; Mahon, M. F.; Woodman, T. J.; Lowe, J. P., Metal Influence on the Iso- and Hetero-Selectivity of Complexes of Bipyrrolidine Derived Salan Ligands for the Polymerisation of Rac-Lactide. *Chem. Sci.* **2015,** *6* (8), 5034-5039.
58. Fortun, S.; Daneshmand, P.; Schaper, F., Isotactic Rac-Lactide Polymerization with Copper Complexes: The Influence of Complex Nuclearity. *Angew. Chem., Int. Ed.* **2015,** *54* (46), 13669-13672.
59. Daneshmand, P.; Fortun, S.; Schaper, F., Diiminopyrrolide Copper Complexes: Synthesis, Structures and *Rac*-Lactide-Polymerization Activity. *Organometallics* **2017,** *36*, 3860–3877.
60. Daneshmand, P.; van der Est, A.; Schaper, F., Mechanism and Stereocontrol in Isotactic *rac*-Lactide Polymerization with Copper(II) Complexes. *ACS Catal.* **2017,** *7*, 6289-6301.
61. Daneshmand, P.; Jiménez-Santiago, J. L.; Aragon--Alberti, M.; Schaper, F., Catalytic-Site-Mediated Chain-End Control in the Polymerization of Rac-Lactide with Copper Iminopyrrolide Complexes. *Organometallics* **2018,** *37*, 1751–1759.
62. Daneshmand, P.; Michalsky, I.; Aguiar, P. M.; Schaper, F., Configurationally flexible zinc complexes as catalysts for rac-lactide polymerisation. *Dalton Trans.* **2018,** *47*, 16279 - 16291.
63. Wang, H.; Yang, Y.; Ma, H., Exploring Steric Effects in Diastereoselective Synthesis of Chiral Aminophenolate Zinc Complexes and Stereoselective Ring-Opening Polymerization of Rac-Lactide. *Inorg. Chem.* **2016,** *55* (15), 7356-7372.
64. Groom, C. R.; Bruno, I. J.; Lightfoot, M. P.; Ward, S. C., The Cambridge Structural Database. *Acta Crystallogr., Sect. B: Struct. Sci.* **2016,** *72* (2), 171-179.
65. Whitehorne, T. J. J.; Schaper, F., *Nacnac*^{Bn}CuO*i*Pr: A Strained Geometry Resulting in Very High Lactide Polymerization Activity. *Chem. Commun. (Cambridge, U. K.)* **2012,** *48*, 10334-10336.
66. Lee, D. Y.; Hartwig, J. F., *Org. Lett.* **2005,** *7*, 1169−1172.

67. Kochnev, A. I.; Oleynik, I. I.; Oleynik, I. V.; Ivanchev, S. S.; Tolstikov, G. A., Synthesis of salicylaldehydes bearing bulky substituents in the positions 3 and 5. *Russian Chemical Bulletin* **2007,** *56* (6), 1125-1129.
68. Frisch, M. J.; Trucks, G. W.; Schlegel, H. B.; Scuseria, G. E.; Robb, M. A.; Cheeseman, J. R.; Scalmani, G.; Barone, V.; Petersson, G. A.; Nakatsuji, H.; Li, X.; Caricato, M.; Marenich, A. V.; Bloino, J.; Janesko, B. G.; Gomperts, R.; Mennucci, B.; Hratchian, H. P.; Ortiz, J. V.; Izmaylov, A. F.; Sonnenberg, J. L.; Williams; Ding, F.; Lipparini, F.; Egidi, F.; Goings, J.; Peng, B.; Petrone, A.; Henderson, T.; Ranasinghe, D.; Zakrzewski, V. G.; Gao, J.; Rega, N.; Zheng, G.; Liang, W.; Hada, M.; Ehara, M.; Toyota, K.; Fukuda, R.; Hasegawa, J.; Ishida, M.; Nakajima, T.; Honda, Y.; Kitao, O.; Nakai, H.; Vreven, T.; Throssell, K.; Montgomery Jr., J. A.; Peralta, J. E.; Ogliaro, F.; Bearpark, M. J.; Heyd, J. J.; Brothers, E. N.; Kudin, K. N.; Staroverov, V. N.; Keith, T. A.; Kobayashi, R.; Normand, J.; Raghavachari, K.; Rendell, A. P.; Burant, J. C.; Iyengar, S. S.; Tomasi, J.; Cossi, M.; Millam, J. M.; Klene, M.; Adamo, C.; Cammi, R.; Ochterski, J. W.; Martin, R. L.; Morokuma, K.; Farkas, O.; Foresman, J. B.; Fox, D. J. *Gaussian 16 Rev. C.01*, Wallingford, CT, 2016.
69. Zhao, Y.; Truhlar, D. G., The M06 suite of density functionals for main group thermochemistry, thermochemical kinetics, noncovalent interactions, excited states, and transition elements: two new functionals and systematic testing of four M06-class functionals and 12 other functionals. *Theor. Chem. Acc.* **2008,** *120* (1), 215-241.
70. *Apex2*, Release 2.1-0; Bruker AXS Inc.: Madison, USA, 2006.
71. *Saint*, Release 7.34A; Bruker AXS Inc.: Madison, USA, 2006.
72. Sheldrick, G. M. *Sadabs*, Bruker AXS Inc.: Madison, USA, 1996 & 2004.
73. Sheldrick, G., Shelxt - Integrated Space-Group and Crystal-Structure Determination. *Acta Crystallogr., Sect. A: Found. Adv.* **2015,** *71* (1), 3-8.
74. Sheldrick, G. M., A Short History of Shelx. *Acta Crystallogr.* **2008,** *A64*, 112-122.

Supporting Information

Lactide polymerization using a sterically encumbered, flexible zinc complexe

Fatemeh Dordahan, Frank Schaper*

Centre in Green Chemistry and Catalysis, Université de Montréal, Department of Chemistry, Montréal, Canada

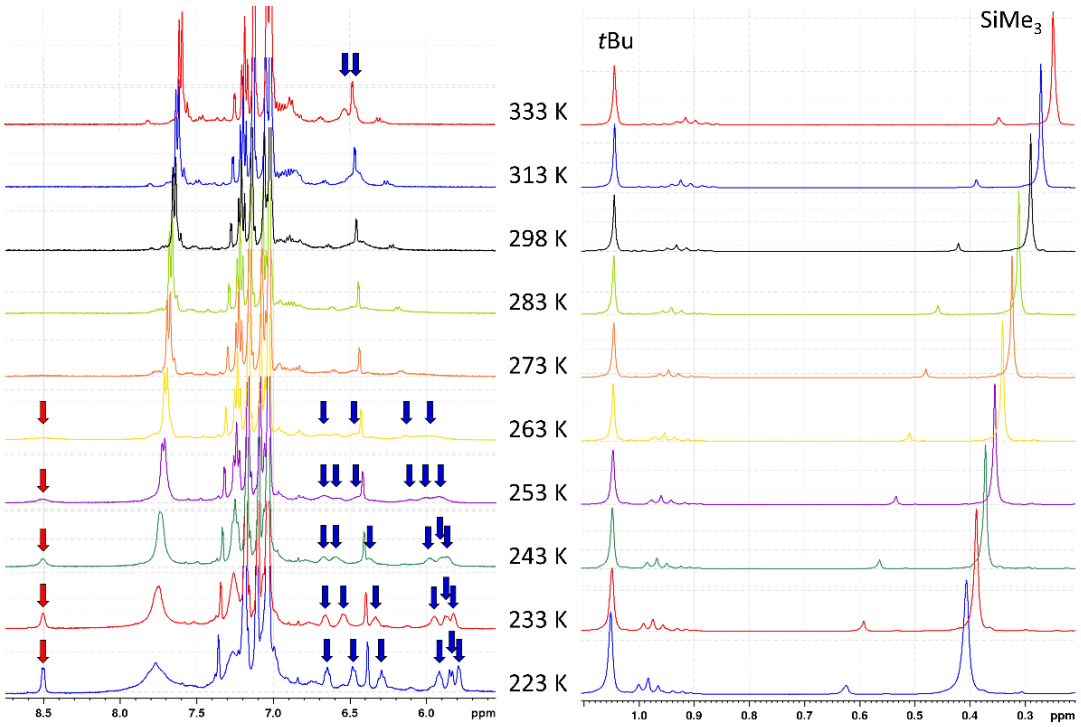

Figure S2.1. Aromatic and aliphatic regions of ^{1}H NMR spectra of **9** in d_8-toluene at 223 – 333 K. Arrows indicate peaks assigned to the pyridine ring.

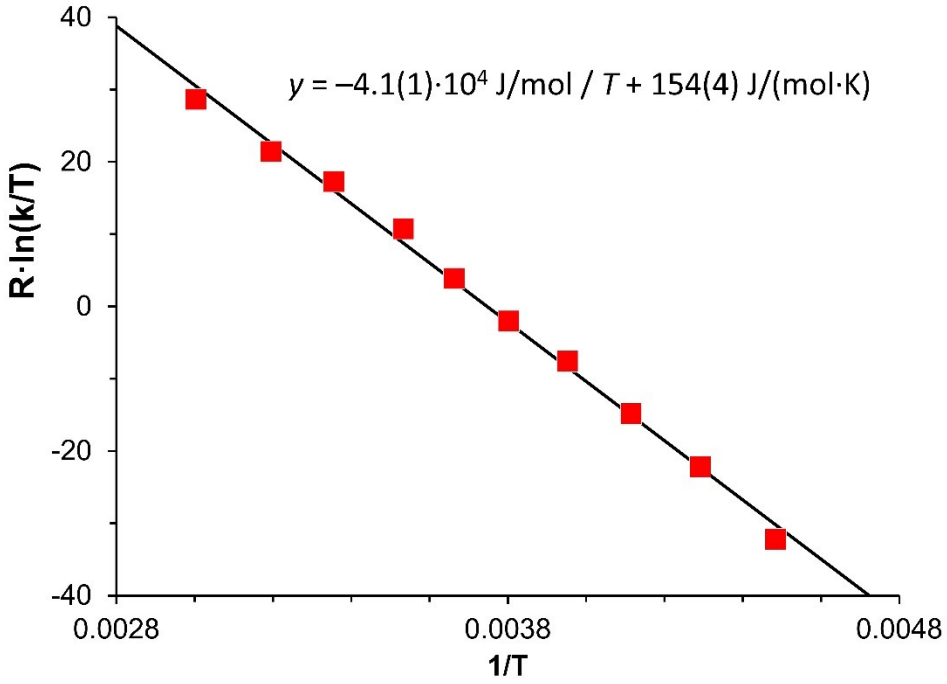

Figure S2.2. Eyring plot of exchanged constants determined from the methylene region of ^{1}H NMR spectra of **9** in d_8-toluene at 223 – 333 K.

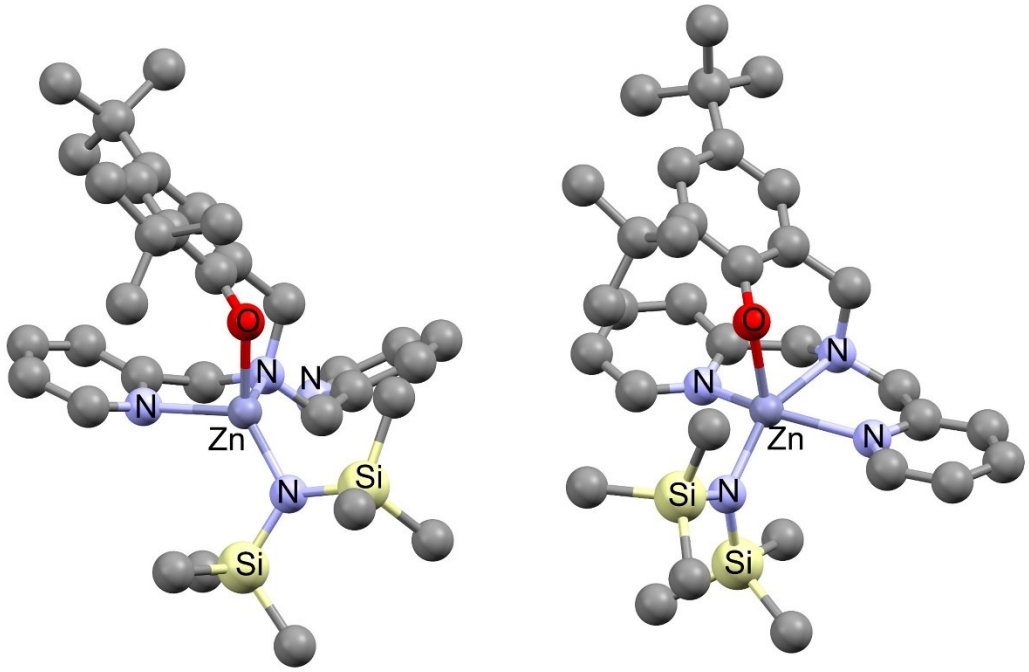

Figure S2.3. DFT-optimized structures of **8** and **9** with both pyridine arms coordinated to Zn, **8-penta** and **9-penta**.

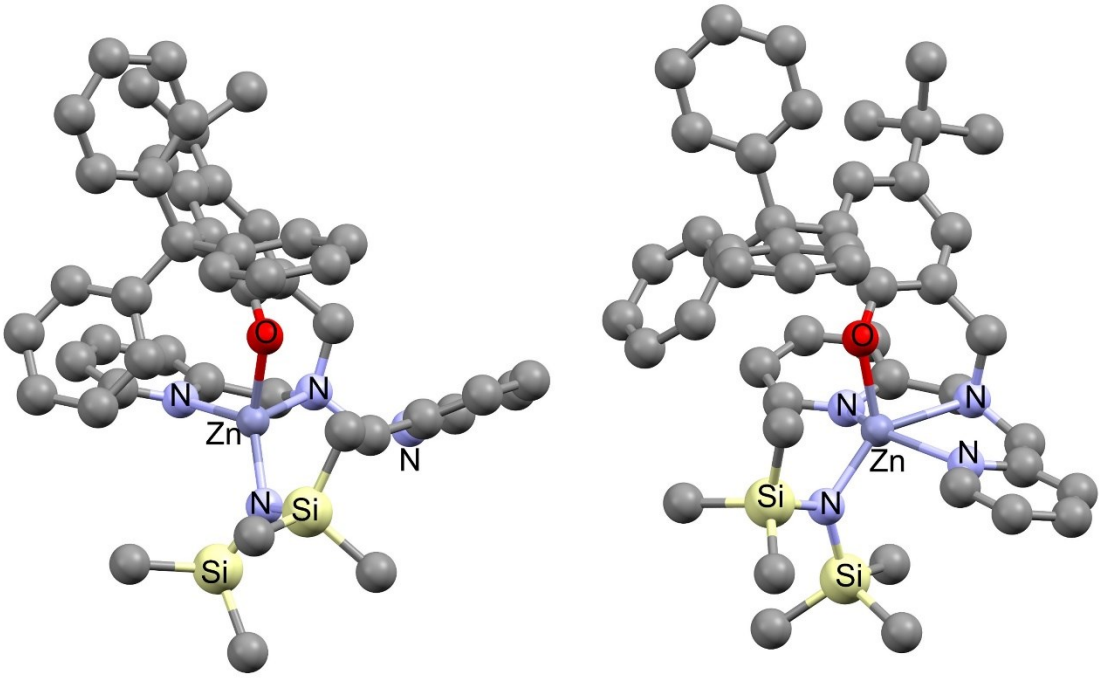

Figure S2.4. DFT-optimized structures of **8** and **9** with only one pyridine arms coordinated to Zn, **8-tetra** and **9-tetra**.

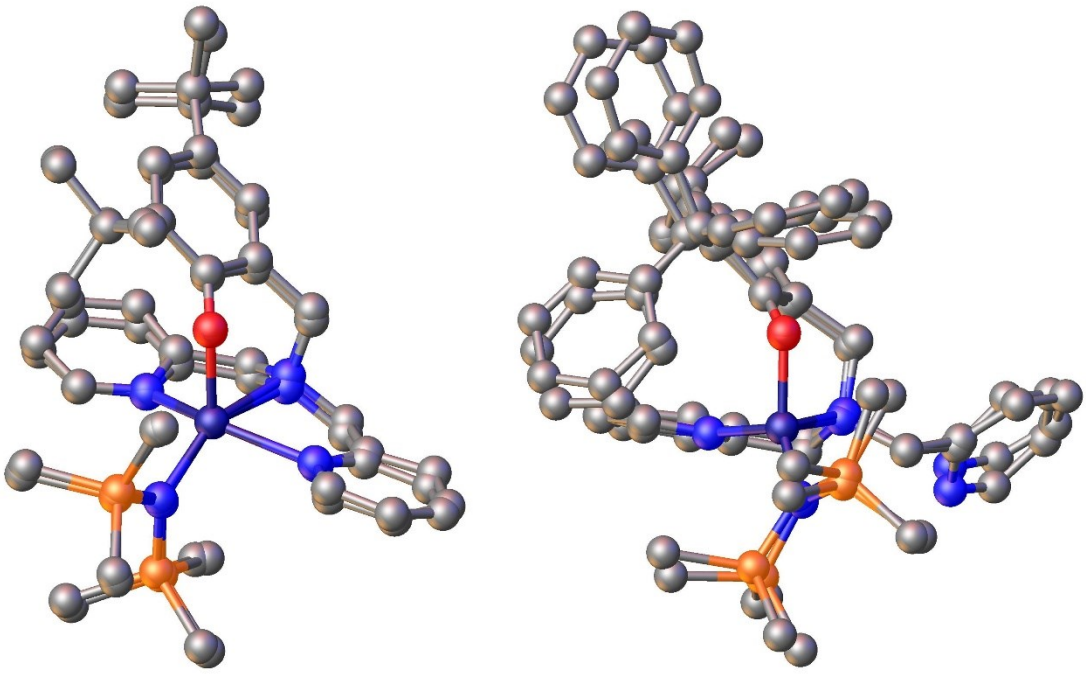

Figure S2.5. Overlay of experimental (X-ray) and calculated (DFT) structures. Left : **8** and **8-penta**, right: **9** and **9-tetra**.

Table S2.1. Calculated and experimental bond distances and calculated energies for complexes **8** and **9** with one or two pyridine arms coordinated. [a]

	8-tetra	**8**-penta	Experimenta l **8** (penta) [b]	**9**-tetra	Experimenta l **9** (tetra) [b]	**9**-penta
Zn-O [Å]	1.968	2.007	1.972(1)	1.967	1.929(4)	2.007
Zn-N_{amine} [Å]	2.226	2.410	2.307(2)	2.255	2.160(5)	2.374
Zn-$N_{pyridine,\ 1}$ [Å]	2.189	2.229	2.211(1)	2.176	2.091(4)	2.227
Zn-$N_{pyridine,\ 2}$ [Å]		2.239	2.225(2)			2.291
Zn-N_{amide} [Å]	1.928	1.979	1.977(2)	1.928	1.910(5)	1.970

E (small basis) [c]	-1655.33455	-1655.35238	-2230.11405	-2230.12092
ZPE (small basis) [c]	0.784754	0.786273	0.943028	0.943138
Thermal correction to Gibbs energy [c]	0.702100	0.709474	0.850128	0.853099
E (large basis) [c]	-3941.02237	-3941.03294	-4515.97723	-4515.97859
E+ZPE [c]	-3940.23761	-3940.24667	-4515.0342	-4515.03545
$G_{298\ K}$ [c]	-3940.32027	-3940.32347	-4515.1271	-4515.12549

[a] tetra : tetra-coordinated zinc, one pyridine coordinated; penta : penta-coordinated zinc, two pyridine coordinated. [b] experimentalX-ray structures in taken from this work and from Daneshmand, P.; Michalsky, I.; Aguiar, P. M.; Schaper, F., *Dalton Trans.* **2018,** *47*, 16279 - 16291. [c] All energies given in Hartree. [d] Small basis : 6-31+G(d,p) for light atoms and LANL2DZ for Si and Zn. Large basis : Def2TZVPP on all atoms. Small basis used for geometry optimization and frequencies calculations (= thermal corrections), large basis used in single point calculation on the optimized geometry.

Table S2.2. Details of *rac*-lactide polymerization with **9**.

#	*c*(**9**) [mM]	ROH	Final conversion	k_{obs} [h]	P_m	M_n (theo.) [kDa] [b]	M_n (obs) [kDa]	M_w/M_n
1	1	-	98%	1.12(2)	0.57	14.1	8.9	4.3
2	1	-	98%	3.05(2)	0.51			
3	1	-	95%	1.35(2)	0.56			
4	2	-	99%	1.75(6)	0.54			
5	2	-	99%	3.34(6)	0.47	14.3	8.7	1.4
6	2	-	97%	2.88(6)	0.47			
7	2	-	95%	3.47(10)	0.57			
8	2	-	97%	3.83(4)	0.45			
9	3	-	99%	10.1(4)	0.44			
10	3	-	99%	3.85(13)	0.44	14.3	14.0	2.0
11	3 [a]	-	97%	3.76(6)	0.60			
12	3 [a]	-	95%	3.8(3)	0.55			
13	3 [a]	-	97%	3.81(5)	0.57			
14	1	1 mM EtOH	96%	1.62(2)	0.48	13.8	9.0	1.5
15	2	2 mM BnOH	98%	14.0(2)	0.46	14.1	0.5	2.2
16	2	4 mM BnOH	98%	11.8(4)	0.51	7.0	1.4	1.8
17	2	2 mM EtOH	98%	11.7(11)	0.42	14.1	1.6	1.9
18	2	2 mM EtOH	98%	11.1(9)	0.50			
19	3	3 mM BnOH	99%	14.9(6)	0.46	14.3	2.8	1.9
20	3	6 mM BnOH	99%	26(n. d.)	0.50	7.1	1.1	1.8

Conditions : [lactide]:[**9**] = 100, C_6D_6, ambient temperature, 60 – 90 min. (see supp. inform.)

[a] [lactide]:[Zn] = 67 instead of 100. [b] Assuming no further participation of amide

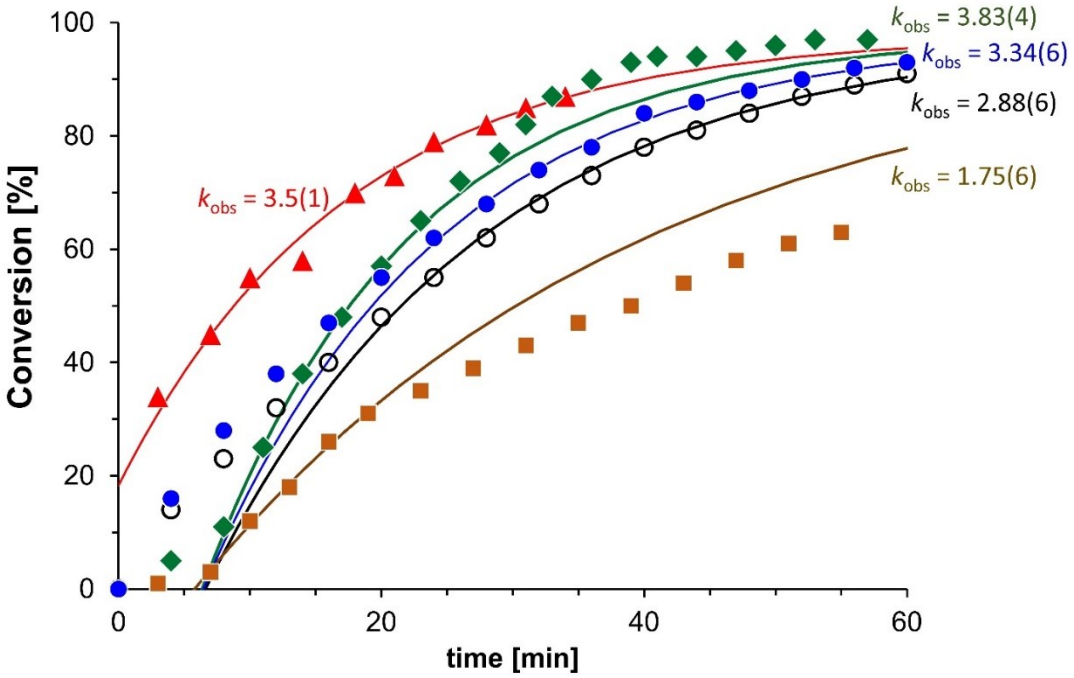

Figure S2.6. Concentration profiles for the polymerization of *rac*-lactide with 2.0 mM **9** without addition of alcohol (2.0 mM **9**, 200 mM lactide, ambient temperature, C_6D_6).

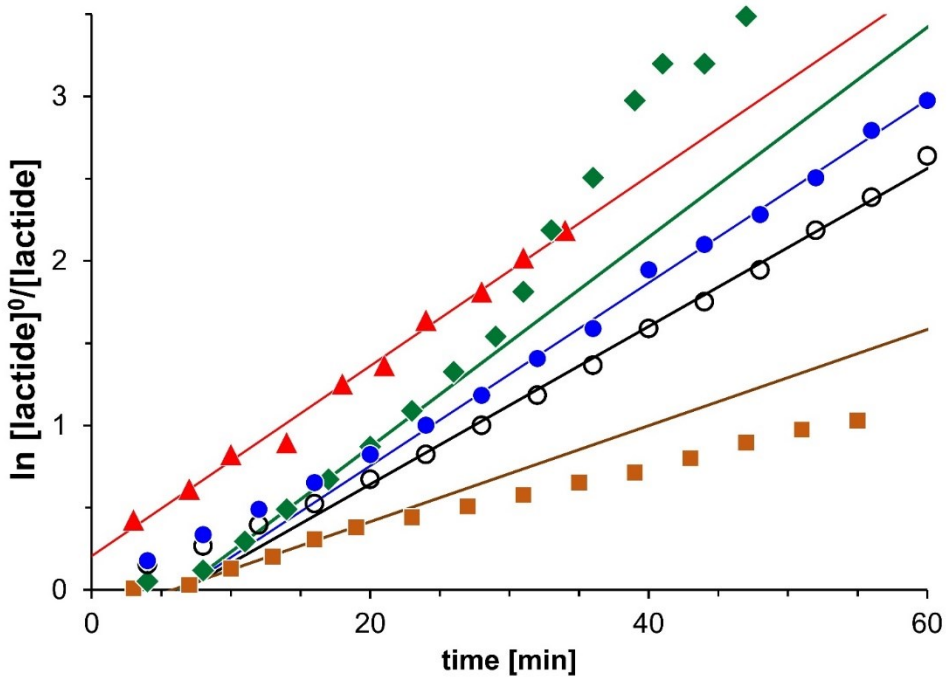

Figure S2.7. Linearized concentration profiles for the polymerization of *rac*-lactide with 2.0 mM **9** without addition of alcohol (2.0 mM **9**, 200 mM lactide, ambient temperature, C_6D_6).

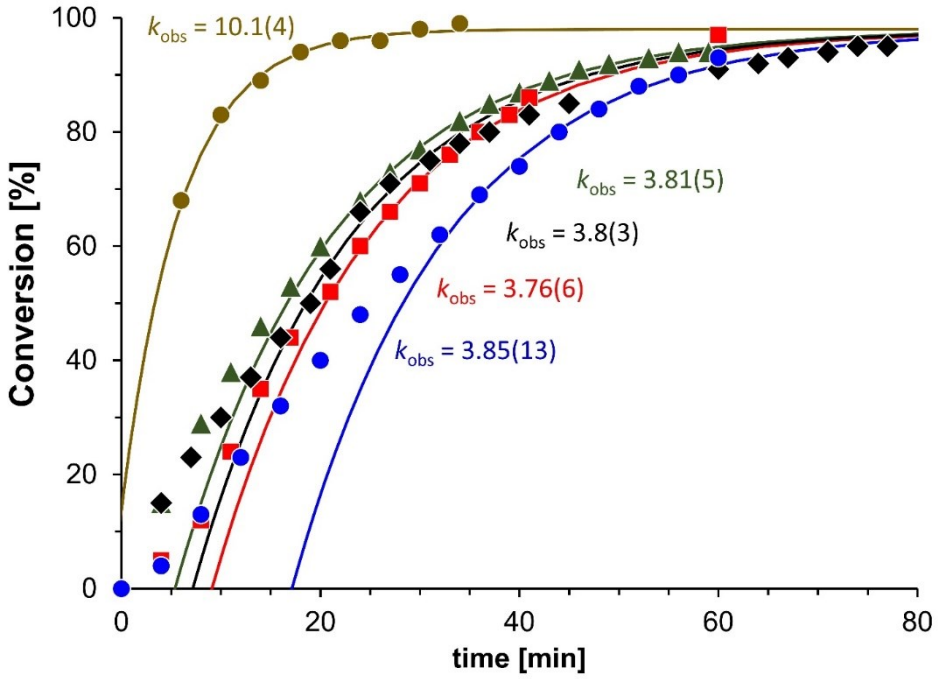

Figure S2.8. Concentration profiles for the polymerization of *rac*-lactide with 3.0 mM **9** without addition of alcohol (3.0 mM **9**, 200 or 300 mM lactide, ambient temperature, C_6D_6).

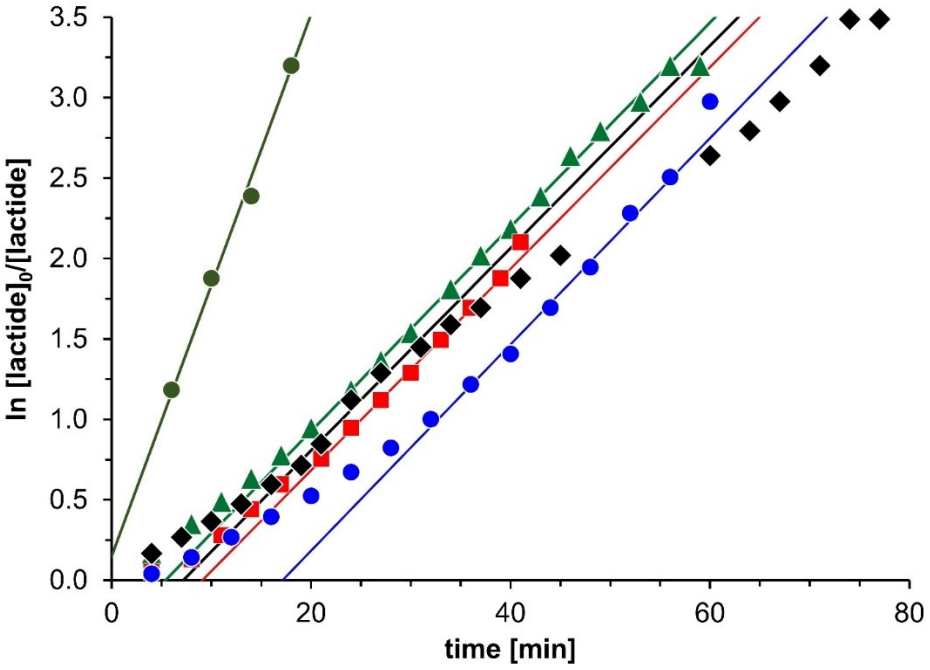

Figure S2.9. Linearized concentration profiles for the polymerization of *rac*-lactide with 3.0 mM **9** without addition of alcohol (3.0 mM **9**, 200 or 300 mM lactide, ambient temperature, C_6D_6).

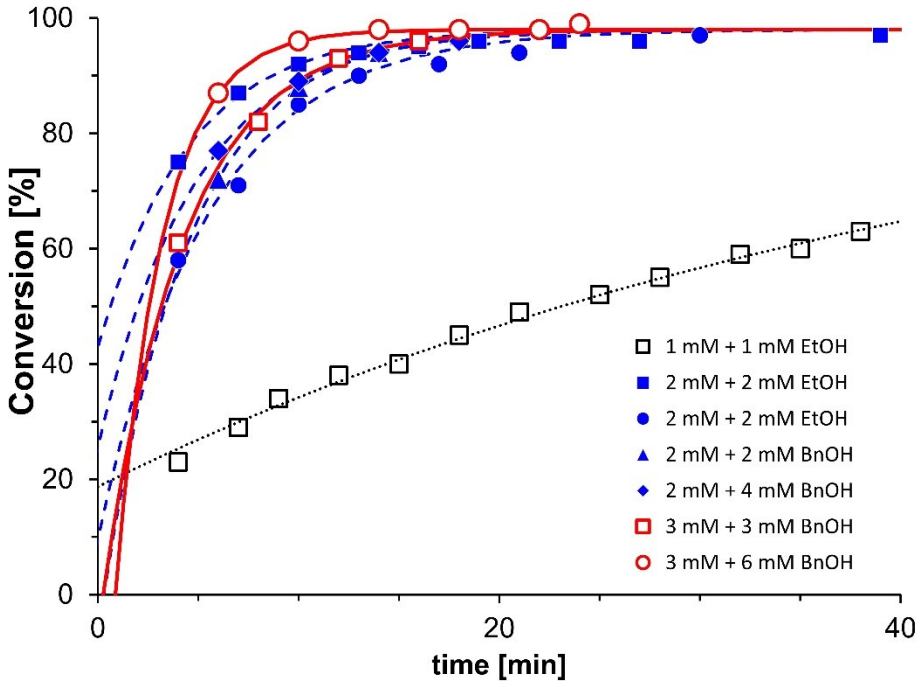

Figure S2.10. Concentration profiles for the polymerization of *rac*-lactide with **9** in the presence of 1 or 2 equiv of ethanol or benzyl alcohol as co-initiator (1.0 - 3.0 mM **9**, [lactide]:[catalyst] = 100:1, ambient temperature, C_6D_6).

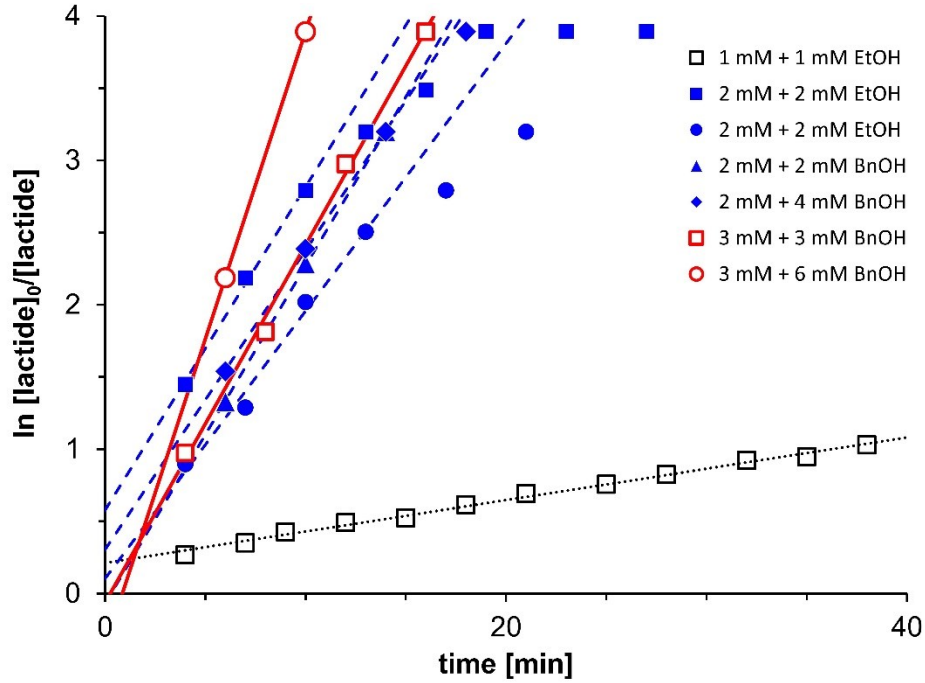

Figure S2.11. Linearized concentration-time profiles for the polymerization of *rac*-lactide with **9** in the presence of 1 or 2 equiv of ethanol or benzyl alcohol as co-initiator (1.0 - 3.0 mM **9**, [lactide]:[catalyst] = 100:1, ambient temperature, C_6D_6).

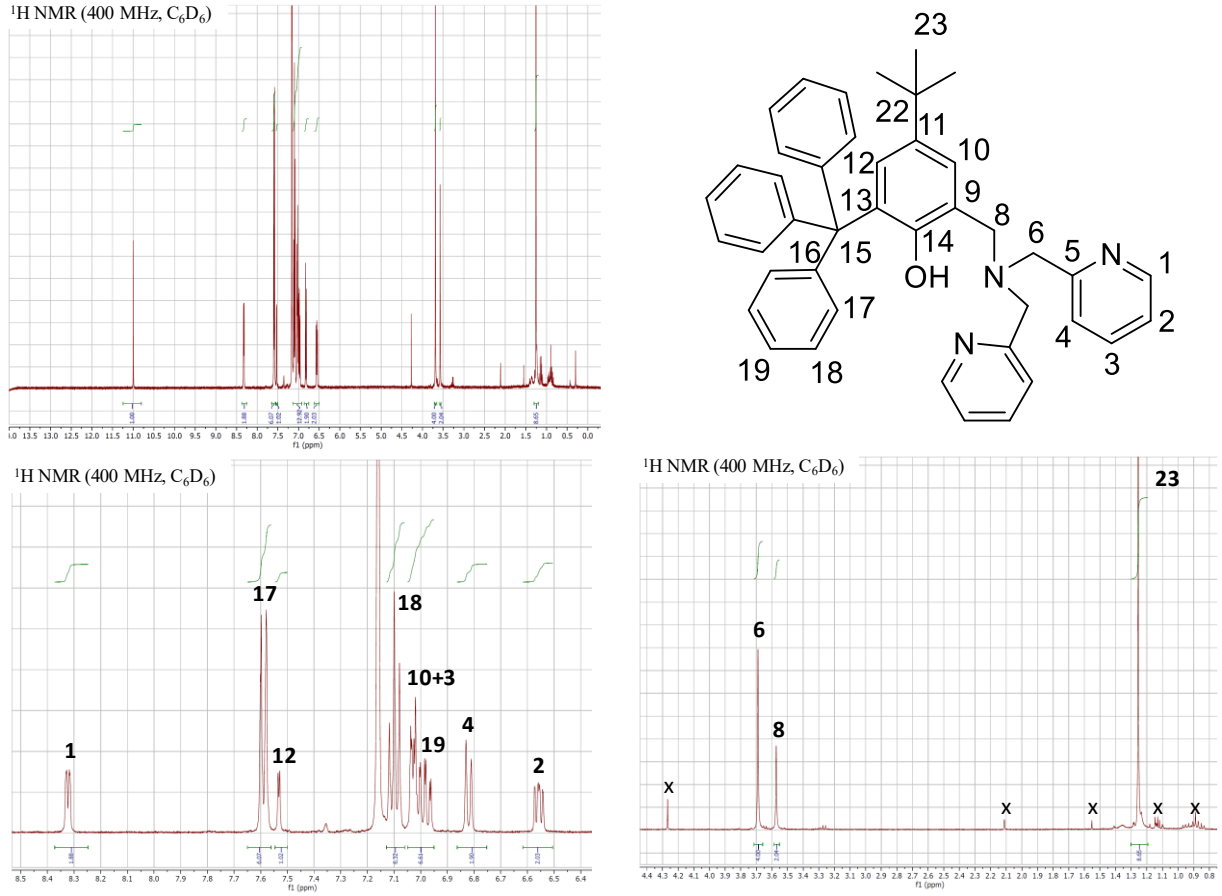

Figure S2.12. ^{1}H NMR spectrum of **L2**H in C_6D_6 at 400 MHz.

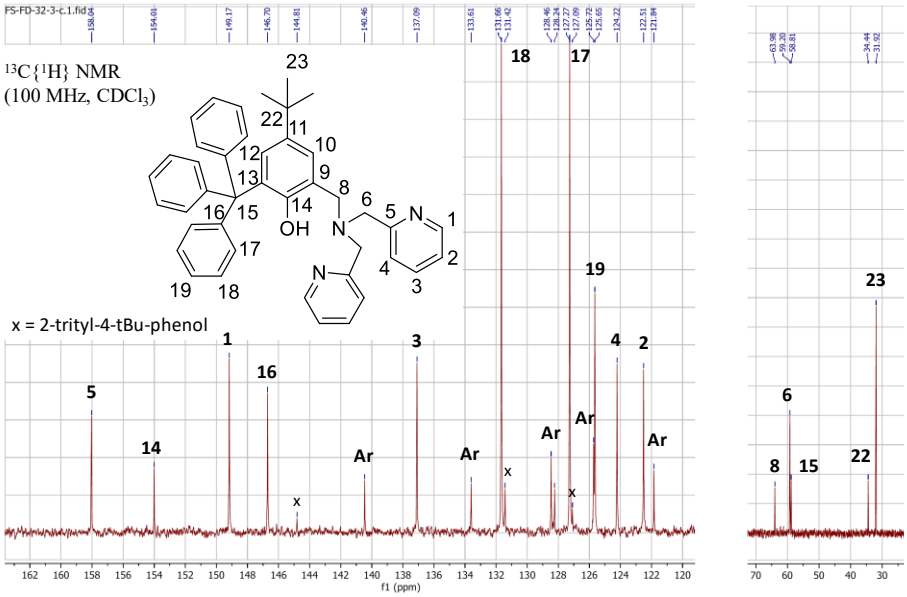

Figure S2.13. $^{13}C\{^{1}H\}$ NMR spectrum of **L2**H in $CDCl_3$ at 125 MHz.

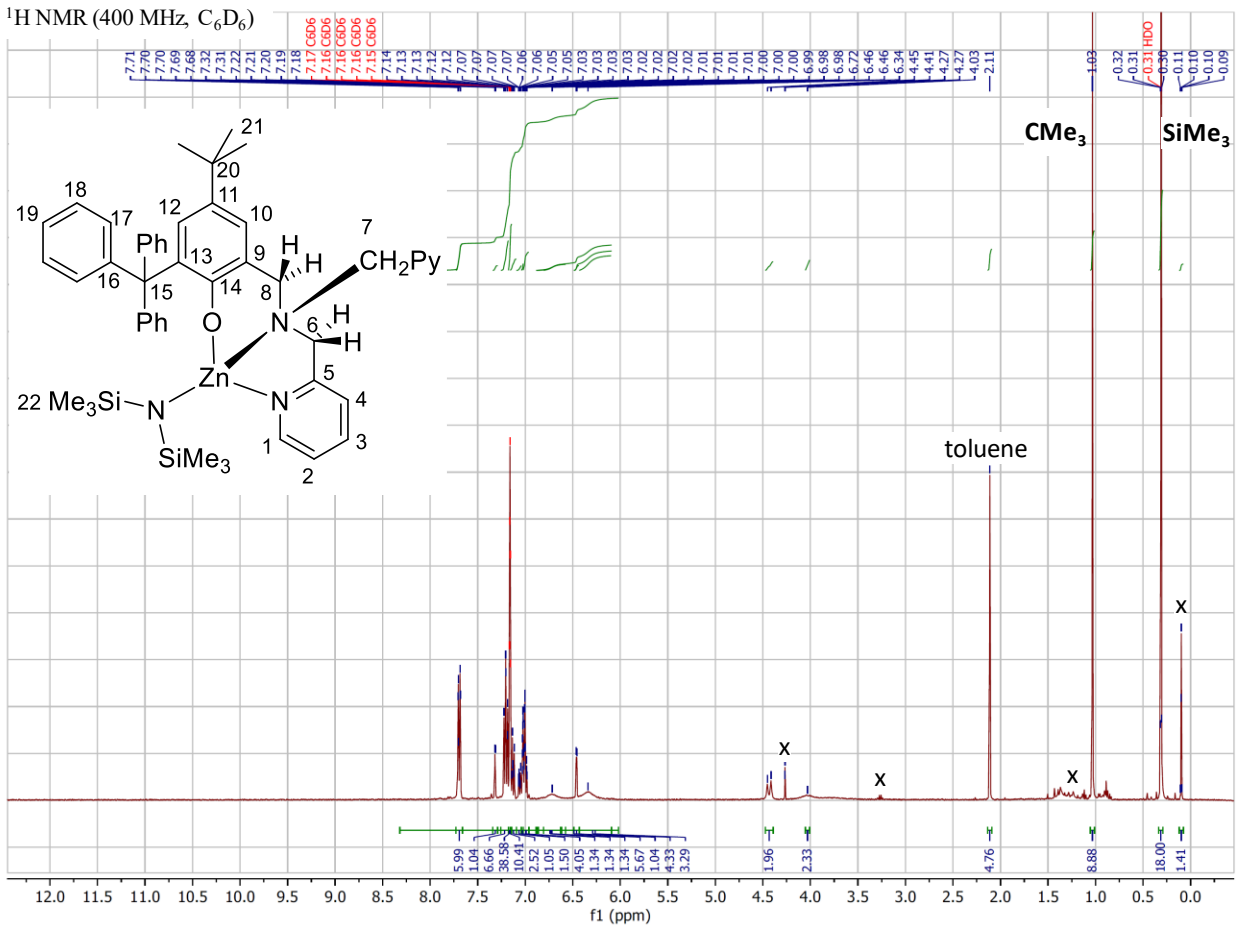

Figure S2.14. ^{1}H NMR spectrum of **9** in C_6D_6 at 400 MHz.

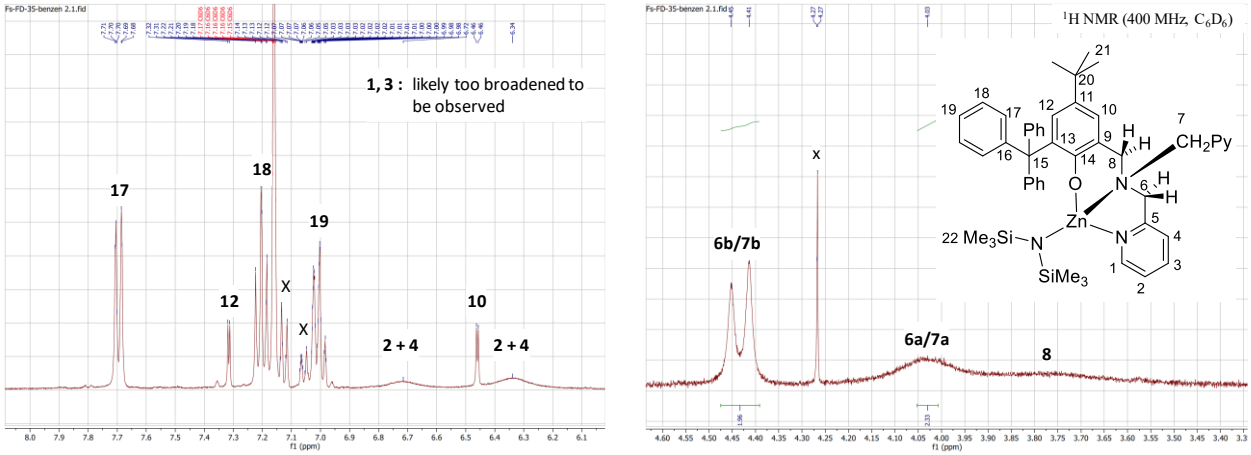

Figure S2.15. ^{1}H NMR spectrum of **9** in C_6D_6 at 400 MHz with peak assignments.

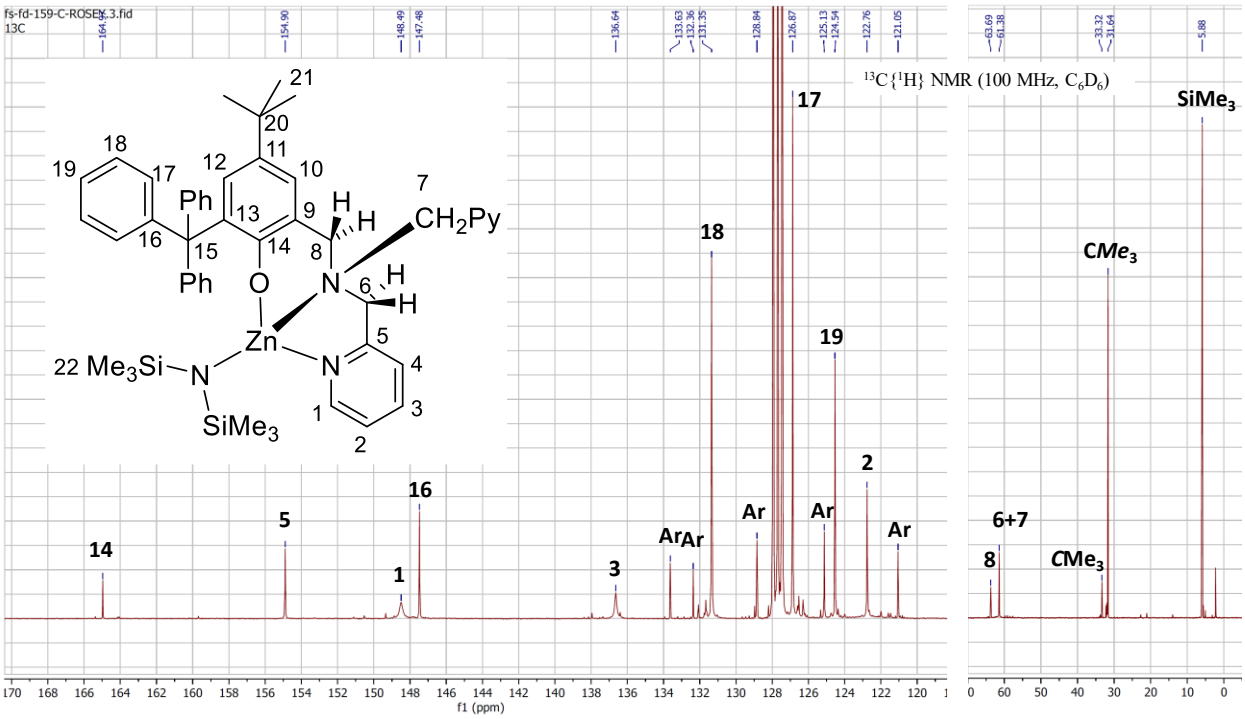

Figure S2.16. $^{13}C\{^{1}H\}$ NMR spectrum of **9** in C_6D_6 at 125 MHz.

Chapter 3. Lactide polymerization with 8-coordinated zirconium complexes

To be submitted after receiving the GPC and MS data.

Introduction

Growing concerns about the impact of plastics on the environment motivated the interest in bio-based, biodegradable plastic materials,[1, 2] of which polylactide (or polylactic acid, PLA) has one of the largest market shares, next to starch-based polymers and polyhydroxyalkanoates.[2] Of commercial interest is isotactic PLA (*all-R* or *all-S* PLA) and, potentially, the stereocomplex or block-copolymer *all-R*/*all-S* PLA.

To date, academic research in this area has been focussed on the challenge presented by the catalytic sterreoselective polymerization, i. e. obtaining isotactic PLA from a racemic mixture of *RR*- and *SS*-lactide. For the vast majority of metal-based catalysts,[3-28] including those studied by our group,[29-36] stereocontrol has been attempted by the use of metal alkoxide catalysts that catalyse lactide via a coordination-insertion mechanism. Lactide coordination to the metal center is followed by insertion into a metal alkoxide bond, forming a new, chain-extended, metal-bound polymeryl alkoxide. The rigid four-membered transition state of the insertion step enables control of transition state energies by the ligand environment in catalytic-site control mechanisms. It also offers likewise a tight catalytic pocket, that can maximize transition state energy differences, in chain-end control mechanisms.

The drawback of coordination-insertion based mechanisms is the lack of stability of the required metal-alkoxide catalysts. Water and lactic acid, which are present in notable amounts in commercially used lactide monomer, act as deactivating reagents by protonation of the alkoxide. Studies using metal alkoxide catalysts thus typically require purified monomer and the majority of the studied catalysts would not survive typical industrial conditions, i. e. presence of water and lactic acid in molten monomer at 180 °C.

Less sensitive catalysts can be employed in polymerizations systems designed to proceed via an activated-monomer mechanism. In the latter, monomer coordination to a Lewis-acidic catalyst is followed by external attack of a polymeryl alcohol at the carbonyl

site. Since neither the catalyst nor the polymeryl alcohol reacts (irreversibly) with water or lactic acid, the presence of such impurities typically does not affect catalyst activity though it might have an effect on the resulting polymer's molecular weight. The main disadvantage of the activated-monomer approach is that stereocontrole is much more difficult to achieve in the latter mechanism because the transition state is further away from the metal center and has a much higher degree of flexibility. Despite some exceptions, particularly in the overlapping regions of an activated monomer mechanism and organo-ring opening polymerization,[37] polymers obtained from an activated monomer mechanism are often atactic.[38]

Davidson and García-Vivo proposed that the unreactive alkoxide group in (polyamine) sodium aryloxide complexes participates in lactide polymerization by hydrogen bonding to the polymeryl alcohol.[39] Carpentier and Sarazin proposed a similar mechanism for lactide polymerizations with alkoxy or aryloxy group II or rare-earth complexes, where the anionic ligand was tethered to an aza-15-crown-5 ligand, which they named "*ligand-assisted activated monomer mechanism*".[40] In this mechanism, the anionic spectator ligand does not remain innocent, but activates the polymeryl alcohol by hydrogen bonding (or outright deprotonation) and thus facilitates the addition of the nucleophile to the activated monomer. The simultaneous interaction of the incoming alcohol with the monomer and a basic site on the ligand is thought to restrict removes the conformational flexibility of the transition state in the activated-monomer mechanism. In a series of studies, Wu succeeded in employing this tightened transition state to achieve unprecedented isotacticities in aryloxide/crown ether complexes of first row metals.[41-50] While this development or result was impressive, the catalytic system had two inherent limitations: the highest isotacticities reported required polymerization temperatures below 0 °C and the described alkoxide complexes were unlikely to withstand industrial polymerization conditions, i. e. the presence of water and lactic acid.

In 2017, Hu et al. reported zirconium bis(diaminodiphenolate) complexes **A** (Scheme 3.1), that can polymerized lactide with an isotactic preference (P_m = 0.67 – 0.81) via an activated-monomer mechanism in toluene at 130 °C.[51] The authors ascribed the source of stereocontrol to the chirality at the coordinated amine, featuring two different *N*-substituents. While Hu did not report the crystal structures for complexes **A**, it is nevertheless known that such bis(diaminodiphenolate) zirconium complexes are either octahedral with two pendant amines or octa-coordinated ; in the latter case, the complex would require dissociation of one amine arm prior to monomer coordination. Given the presence of a non-coordinated amine in any lactide-coordinated intermediate, we wondered that these complexes might in fact, follow a *ligand-assisted activated monomer mechanism* (and thus chain-end control). If this were indeed the case, the chirality at the nitrogen center would not be essential for stereospecificity, although it could of course still have an impact. The only previously reported lactide polymerization with a symmetric bis(diaminodiphenolate) zirconium complex yielded heterotactic PLA, but the employed complex was six-coordinated with pending morpholine arms.[52]

To test this hypothesis, we prepared 8-coordinated bis(diaminodiphenolate) complexes with symmetrical *N*-substituents and investigated their solution and solid-state structures, as well as their performance in lactide polymerization.

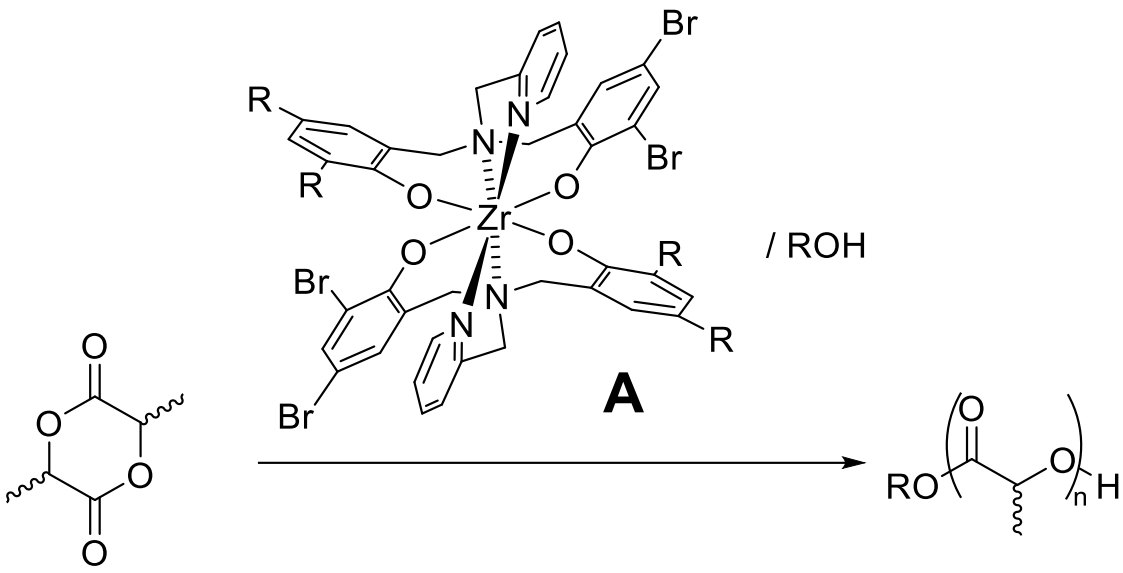

Scheme 3.1

Results and Discussion

Synthesis and structures. Ligands **L1**H_2 – **L3**H_2 were prepared as described in the literature (Scheme 3.2).[53-55] Complex **1** has been prepared previously from $ZrCl_4$ and **L1**Na_2 or from **L1**H_2 and $Zr(CH_2SiMe_3)_4$,[56] but in this work, was prepared from **L1**H_2 and commercially available $Zr(O\textit{n}Pr)_4$ (Scheme 3.2). The reported crystal structure of **1** showed an eight-coordinated zirconium complex with *cis*-positioned, inequivalent phenolate moieties in each **L1** ligand. Both ligands are related by approximate C_2 symmetry. The reported ^{1}H NMR spectrum of **1** was in agreement with C2 symmetry, i. e. showing signals for two equivalent ligands with inequivalent phenolate moieties.[56] In contrast to this, the NMR of the crude reaction mixture obtained from the reaction of **L1**H_2 with $Zr(O\textit{n}Pr)_4$ in ether showed two sets of signals in an approximate 1:1 ratio (Fig. 1a, S1 and S2): the reported complex **1** and a second isomer, **1b**, which likewise showed signals for equivalent

L1 ligands (i. e., only four signals for 8 hydrogen atoms on pyridine and six doublets for 12 methylene hydrogen atoms) with inequivalent phenolate moieties (i. e., four signals for the aromatic hydrogen atoms of the phenolates, $PyCH_2$ appearing as two doublets). Dissolution of the crude product in toluene and cooling to –80 °C, produced a precipitate in appr. 50% yield, which contained **1** and **1b** in an appr. 7:1 ratio (Fig. 1b). The supernatant solution, however, contained *only* **1** (Fig. 3.1b). Complex **1b** is thus likely to be the kinetic product of the reaction and transforms into **1** reported by Mountford upon standing. The reported crystal structure of **1**[56] shows weak hydrogen bonding of the *ortho*-pyridine proton in **1** to a phenolate oxygen, which is likely responsible for the strong low-field displacement of its signal in the ^1H NMR (9.9 ppm). The likewise displaced *ortho*-pyridine proton at 9.2 ppm of **1b** thus indicates coordination of the pyridine and that **1b** is also an eight-coordinated complex. Its apparently C_2-symmetric NMR spectra in combination with the inequivalent phenolate moieties, as well as the clean transformation into **1**, suggests that **1b** is the eight-coordinated complex with *trans*-phenolate ligands, while the latter are *cis* in **1**. The inequivalence of the *trans*-phenolate ligands is caused by the π-stacking interaction of one of the phenolate moieties with pyridine, which was observed in the crystal structure of **1**.[56] We have previously observed that such π-stacking leads to inequivalent pyridine moieties in five-coordinated zinc complexes with a related dipyridine amino phenolate ligand.[29]

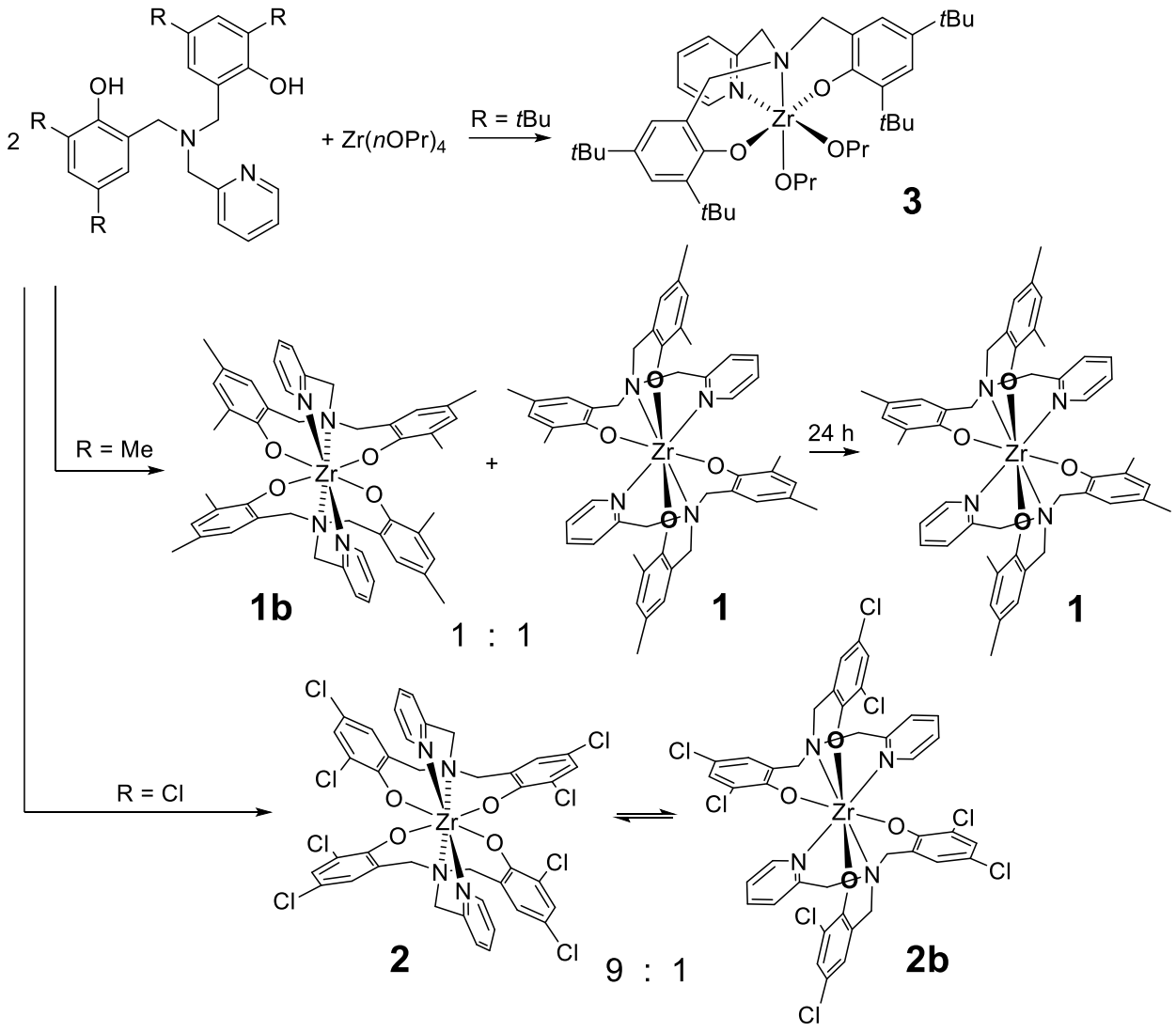

Scheme 3.2

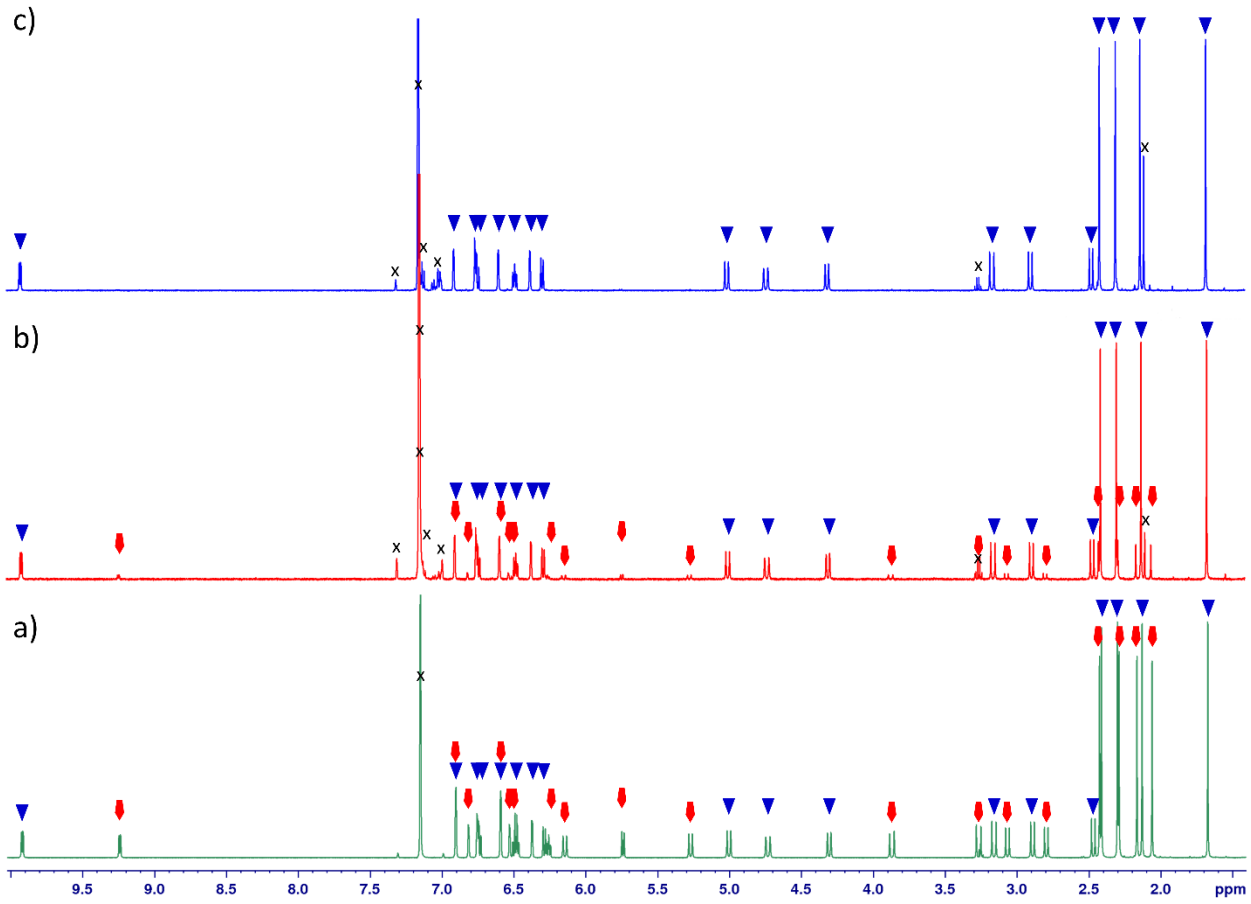

Figure 3.1. ^{1}H NMR spectra of **1** in C_6D_6. a) crude reaction mixture; b) precipitate from toluene solution at –80 °C; c) supernatant solution from precipitation at –80 °C. Triangles denote compound **1**, arrows compound **1b**. Crosses indicate impurities (traces of ether or toluene) and C_6D_5H.

To verify the tentative assignment of **1b**, we calculated the geometries of C_2-symmetric *cis*,*cis*-**1** and *trans*,*trans*-**1b** (Fig. 3.2) by DFT. The calculated structure *cis*,*cis*-**1** agreed well with the previously obtained crystal structure (Fig. S3.3, Table S3.1),[56] although it showed slightly longer Zr-N/O distances (0.01-0.05 Å). We also included C_1-symmetric *cis*,*trans*-**1c**, even though the NMR showed a symmetric complex. In agreement with the assignment of **1b** as the transient *trans*,*trans*-isomer, **1b** was found to be slightly less stable (ΔG^0 = 8 kJ/mol) than the experimentally observed *cis*,*cis*-isomer (Tables 3.1, S3.1, S3.2).

The unobserved C_1-symmetric *cis,trans*-isomer was of much lower stability (ΔG^0 = 59 kJ/mol). The isomerization between *cis*,*cis*-**1** and *trans*,*trans*-**1b** can be most easily envisioned as the exchange of coordination sites between the two non-π-stacked phenolate ligands in both structures (Fig. S3.4). To further corroborate the assignment of **1b**, we calculated ^{1}H NMR spectra for both complexes. While calculated chemical shifts differ in some detail from the experimental values, the calculations reproduce the most notable features and differences in the experimental ^{1}H NMR spectra: (i) A single methyl group in **1** is displaced high-field to 1.68 ppm (calculated: 1.50 ppm), while the remaining methyl groups in **1** and all methyl groups in **1b** are found above 2.0 ppm (Fig. S3.5). The calculation identified the high-field methyl group as the *ortho*-methyl group of the non-π-stacked phenolate in **1**, which is positioned above the pyridine ring of the other **L1** ligand. This interaction is absent in **1b** (Fig. S3.6). (ii) A methylene proton in **1b** is displaced downfield to 6.15 ppm (calculated 5.54 ppm, Fig. S3.7). The latter is caused by stronger hydrogen bonding of this proton to the phenolate oxygen atom (**1b**: 2.3 Å vs. **1**: 2.5 Å). (iii) The general order of aromatic peaks, e. g. the high field displacement of the pyridine hydrogen atoms in **1b** in comparison to **1**, is well reproduced in the calculated spectra (Fig. S3.8 and S3.9). Overall, the comparison of the calculated and experimental NMR spectra support the assignment of **1b** as the *trans,trans*-isomer.

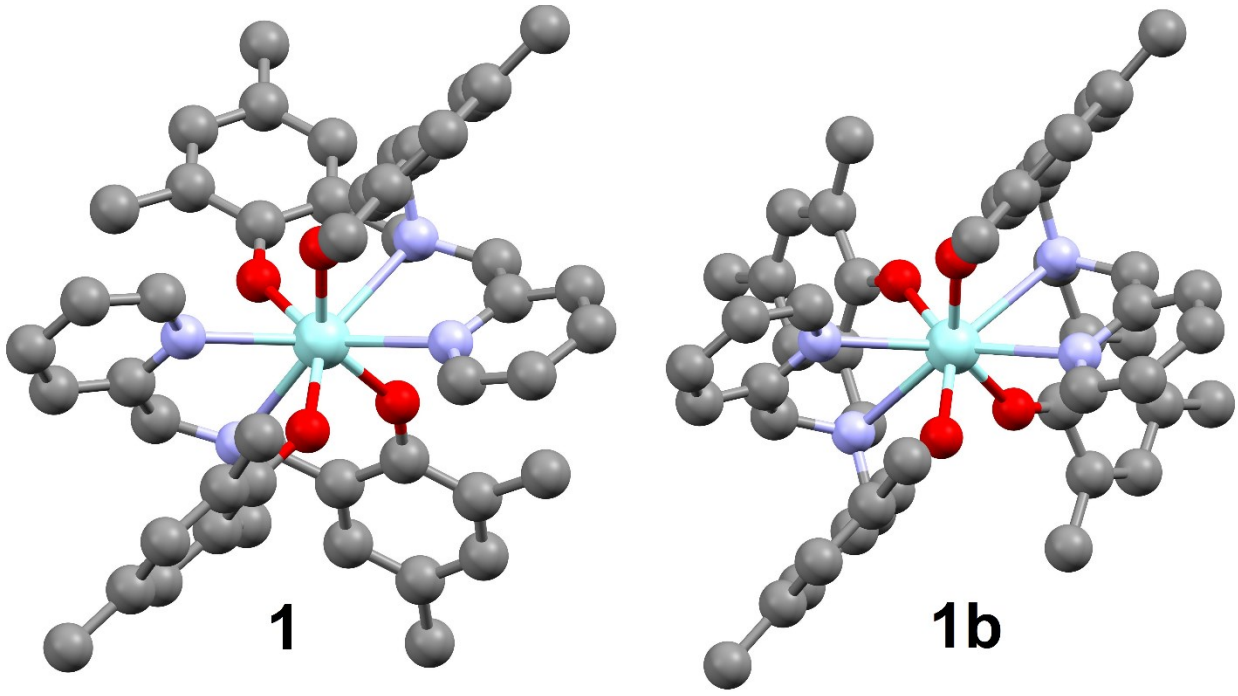

Figure 3.2. DFT-optimized structures of (*cis*-L1)$_2$Zr, **1** (left) and **(***trans*-L1)$_2$Zr, **1b** (right).

Table 3.1. Relative energies of DFT-calculated structures of 1 and 2.

	Total energy + ZPE [kJ/mol]	ΔG^0 (298 K) [kJ/mol]
(*cis*-L1)$_2$Zr, **1**	0	0
(*trans*-L1)$_2$Zr, **1b**	11.0	7.8
(*cis*-L1)(*trans*-L1)Zr, **1c**	66.1	59.0
(*cis*-L3)$_2$Zr, **2b**	0	0
(*trans*-L3)$_2$Zr, **2**	17.5	16.1

M06 functional, basis sets for geometry optimization and thermal corrections (frequency calculations): LANL2DZ (Zr and Cl), 6-31+G(d,p) (all others), basis set for single-point energy calculations: Def2TZVPP (all atoms).

Reaction of the chlorinated ligand **L2**H$_2$ with Zr(O*n*Pr)$_4$ in ether afforded (**L2**)$_2$Zr, **2** (Scheme 3.2). Complex **2** displayed the same symmetry in its ^{1}H NMR spectrum as **1**, i. e.

six doublets for the methylene groups, indicating two symmetry-related ligands **L2** with inequivalent phenolate moieties. A second, minor species with the same symmetry was observed in the ^{1}H NMR of the crude reaction mixture in a ratio of 85:15 (Fig. S3.10 and S3.11). In contrast to **1**, neither different purification procedures nor aging of the complex in benzene or toluene changed this ratio. ^{1}H NMR spectra in $CDCl_3$ showed the minor species in appr. the same ratio. When NMR spectra were recorded in DMSO solution, however, a ratio of 70:30 was observed with no indication of precipitation or complex decomposition (Fig. S3.10 and S3.11). The two species thus seem to be in a solvent-dependent equilibrium and we assign them again to the *cis,cis*- and the *trans,trans*-isomers of (**L2**)$_2$Zr.

Calculations of the respective *cis,cis*- and *trans,trans*-isomers of **2** by DFT-methods did not reproduce a reduced energy difference between the two isomers. On the contrary, the *cis,cis*-isomer was even more strongly favoured for (**L2**)$_2$Zr (16 kJ/mol compared to a 7 kJ/mol difference for **1**/**1b;** Tables 3.1, S3.1). Inclusion of a solvent environment did not change this observation (Table S3.2). Contrary to this, comparison of calculated and experimental NMR spectra, as well as interpretation of the ROESY spectrum indicated that the major species **2** is *trans,trans*-(**L2**)$_2$Zr rather than the *cis,cis*-isomer as observed for **1** (Scheme 3.2). The three major features supporting this assignment are the high-field displacement of the hydrogen atom at the 3-position of the pyridine ring in the major species, which the calculations reproduced for the *trans,trans*-, but not for the *cis,cis*-isomer (Fig. S3.12). Likewise, the calculation reproduced for the *trans,trans*-isomer the fact that three high-field methylene hydrogen atoms were found at a very similar displacement (Fig. 3.3). The calculation also identified (in agreement with the ROESY spectrum) the most-deshielded methylene proton as belonging to the stacked phenolate ligand (*trans,trans*-isomer & major species) or belonging to a pyridine methylene group (*cis,cis*-isomer & minor species).

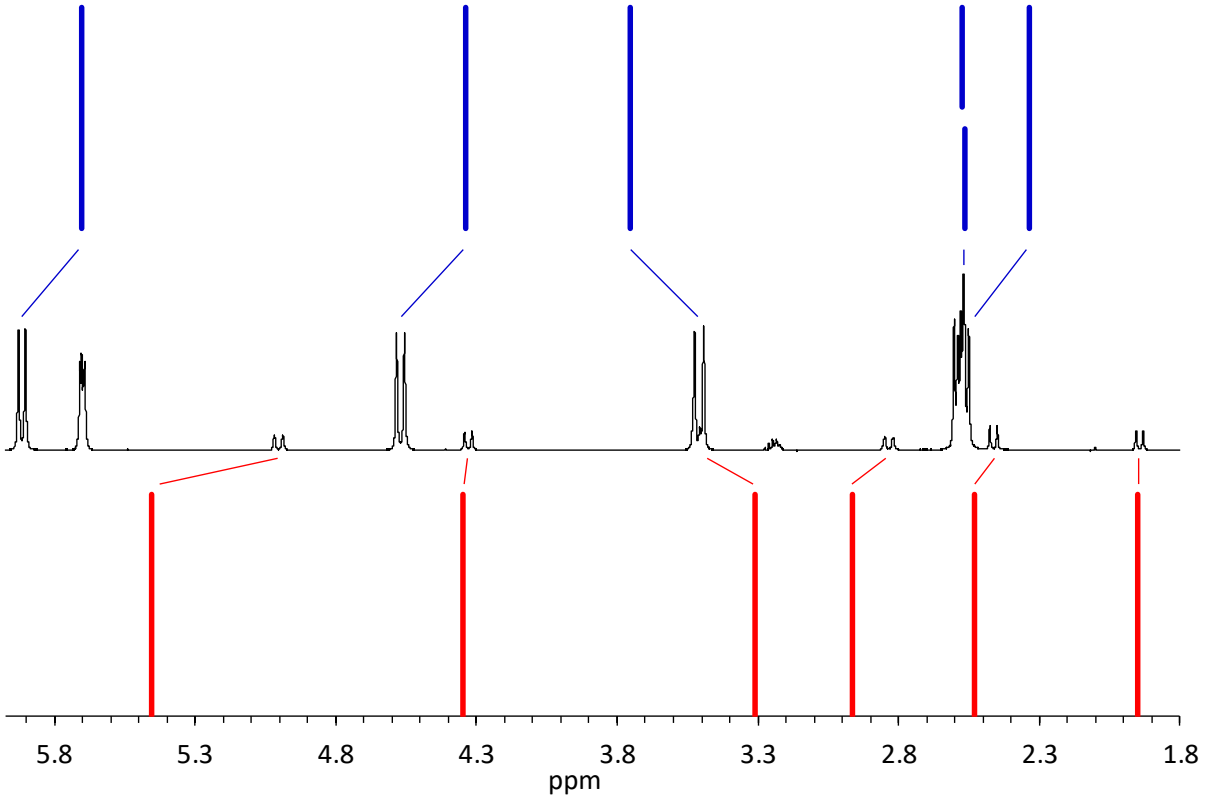

Figure 3.3. Comparison of calculated ^{1}H NMR spectra of *trans,trans*-**2** (blue, top) and *cis,cis*-**2b** (red, bottom) with the experimental spectrum of the equilibrium mixture obtained in C_6D_6.

The ROESY spectrum of **2** further confirmed the assignment of the major species **2** as *trans,trans*-(**L2**)$_2$Zr: The change of coordination sites of the non-π-stacked phenolate leads to an inversion of the Zr-N-C-C_{Ar} dihedral angle for this ligand moiety. Thus in *cis,cis*-(**L2**)$_2$Zr the methylene group of the non-π-stacked phenolate is eclipsed to CH_2Py and in *trans,trans*-(**L2**)$_2$Zr it is eclipsed to CH_2(phenolate) (Fig. S3.13 and S3.14). The ROESY spectrum shows the corresponding crosspeaks of *trans,trans*-(**L2**)$_2$Zr for the major species, **2**, and those of *cis,cis*-(**L2**)$_2$Zr for the minor species, **2b** (Fig. S3.13 and S3.14). No exchange peaks were observed in the ROESY spectrum, thus any exchange between **2** and **2b** is slow on the NMR time scale.

The crystal structure of **2** finally indicated that *trans,trans*-(**L2**)$_2$Zr was also the preferred isomer in the solid state (Fig. 3.4). In agreement with NMR spectroscopy, the complex displayed a non-crystallographic C_2-symmetry and thus two equivalent ligands. Apart from the *trans*-orientation of the phenolate ligands, the structure of **2** is highly similar to the methyl-substituted derivative **1**. Zr shows a C_2-symmetric, tetragonal anti-prismatic coordination environment. Bond lengths of **L2** to Zr show very slightly shorter (0.01-0.03 Å) Zr-O distances and slightly longer Zr-N distances (0.03-0.07 Å) than in **1**. Comparison with the DFT-calculated structures indicate that this is caused by the difference of *cis,cis*- vs. *trans,trans*-coordination rather than by the substitution of methyl by chloride (Table S3.1).

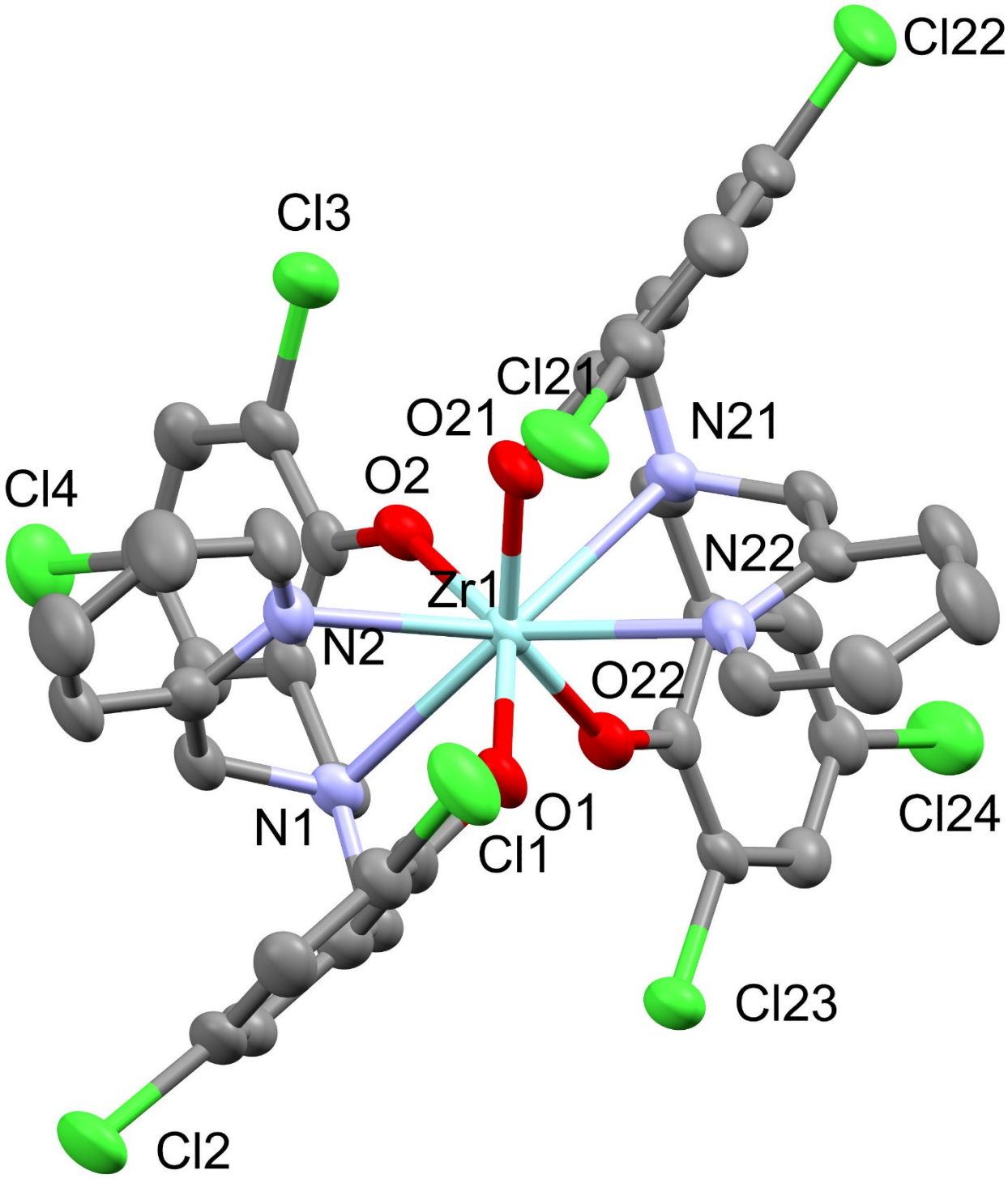

Figure 3.4. Crystal structure of *trans,trans*-(**L2**)$_2$Zr, **2**. Thermal ellipsoids are shown at the 50% probability level. Hydrogen atoms, co-crystallized toluene solvent and second independent molecule in the asymmetric unit omitted for clarity.

Reaction of two equivalents of the more bulky *tert*-butyl substituted ligand **L3**H_2 with Zr(O*n*Pr)$_4$ resulted in an incomplete reaction, forming (**L3**)Zr(O*n*Pr)$_2$, **3**, together with unreacted **L3**H_2 (Scheme 3.2). Prolonged reaction times, higher reaction temperatures, or solvent-less synthesis led to (partial) decomposition of **3**, but without any indication of formation of (**L3**)$_2$Zr. Mountford has reported similar problems in preparing (**L3**)$_2$Zr from Zr(CH_2SiMe_3)$_4$ and **L3**H_2.[56] Reactions of $ZrCl_4$ with **L3**H_2 in the presence of NEt_3 were likewise unsuccessful. Complex **3** was then resynthesized from reaction with one equivalent of **L3**H_2. The crystal structure of **3** at 100 K was of mediocre quality due to a phase transition into space group *P*c. A higher quality structure was obtained at 200 K, where it crystallized in space group $P2_1/c$. Coordination around Zr is octahedral with approximate (non-crystallographic) C_s symmetry, presuming fast O-*n*Pr rotation in solution (Fig. 3.5). The phenolate ligands are mutually *trans*-coordinated, while the *n*-propoxide ligands are *cis*. This agrees with the apparent symmetry of the ^{1}H NMR spectrum, which shows only one set of signals for the phenolate ligands, while two sets of signals are obtained for the propoxide ligands *trans* to amine and *trans* to pyridine. Coordination geometry and bond lengths are unsurprisingly very similar to previously reported (**L3**)Zr(O*i*Pr)$_2$ and (**L4**)Zr(O*i*Pr)$_2$ (**L4** : CH_2Py replaced by $C_2H_4NMe_2$).[57, 58]

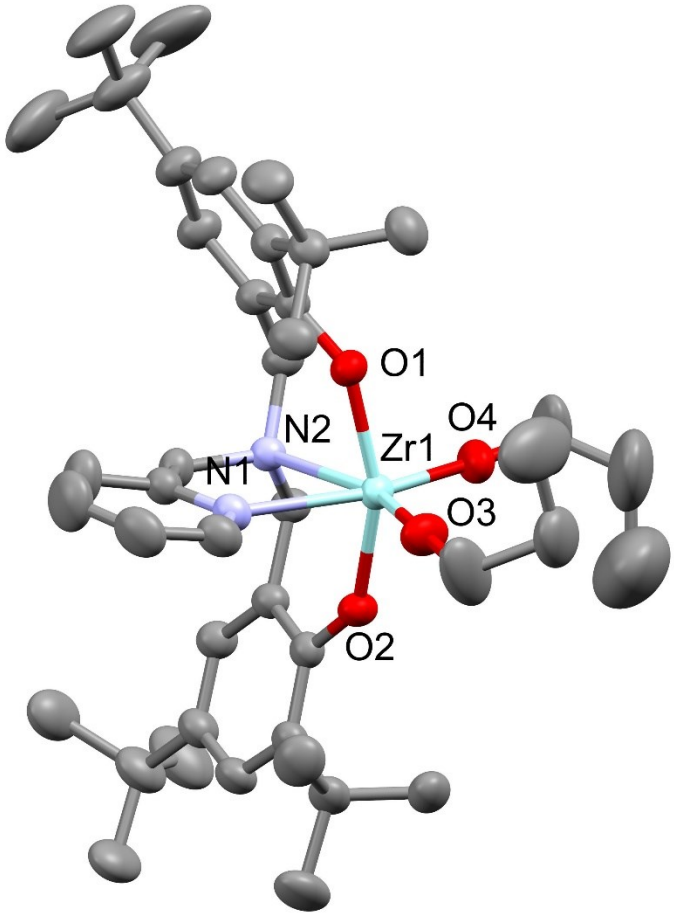

Figure 3.5. X-ray structure of **3**. Thermal ellipsoids are shown at the 50% probability level. Hydrogen atoms and the minor fraction of disordered *para*-*t*Bu and the two *n*Pr groups omitted for clarity. Selected bond lengths: Zr-O1: 2.034(1), Zr1-O2: 2.029(1), Zr1-O3: 1.938(2), Zr1-O4: 1.945(2), Zr1-N1: 2.426(2), Zr1-N2: 2.440(2).

While **3** did not react with free **L3**H_2, addition of the less bulky chloride-substituted ligand **L2**H_2 at room temperature led to the disappearance of the *n*-propoxide signals and the appearance of a new set of peaks, in agreement with the formation of a mixed ligand complex (**L2**)(**L3**)Zr. However, despite variations of reaction conditions (order of addition, relative stoichiometries, solvent), the complex was consistently accompanied by at least 15% of (**L2**)$_2$Zr, **2**. The data thus agrees with formation of a mixed ligand complex, but

since all purification attempts were unsuccessful putative (**L2**)(**L3**)Zr could not be isolated in pure form.

Lactide polymerization. Although it was not the target of this study, performance of alkoxide complex **3** was briefly investigated. The complex is active for polymerization at 130 °C without addition of a co-initiator and produced polymer with a slight heterotactic preference (Table 3.2, #6). Previously, polymerization with (**L3**)Zr(O*i*Pr)$_2$ was reported to be atactic.[57]

Of more interest was the performance of eight-coordinated L_2Zr complexes **1** and **2** in the presence of benzyl alcohol as co-initiator. While no activity was observed for *rac*-lactide polymerization in toluene at 70 °C or 100 °C, both complexes were moderately active at 140 °C in molten monomer/C_6D_6 mixtures (Table 3.2 and S3.3). Unfortunately, all of the produced polymers were atactic. We were thus unable to reproduce the isoselectivity reported by Hu et al. for comparable complexes with different phenolate substituents on nitrogen.[51] Despite our initial doubts Hu's claim of the importance of chirality at the nitrogen atom thus seems to be substantiated.

Table 3.2. *rac*-Lactide polymerization with complexes 1-3

#	catalyst	*c*(cat.) [mM] [a]	BnOH:Zr	Time [h]	conversion	P_m
1	**1**	12	1	2	97%	0.47
2	**2**	12	1	4	44%	0.46
				24	82%	0.44
3	**2**	38	0	1	0%	-
				2	17%	-
				20	86%	0.40
4	**2**	38	1	1	17%	-
				2	20%	-
				20	85%	0.46
5	**2**	38	5	1	48%	0.47

				2	72%	0.48
				20	93%	0.50
6	**3**	2	0	1	24%	-
				2	43%	0.41
				4	61%	0.37
				24	61%	0.31

Conditions: T = 140 °C, [lactide]:[catalyst] = 100:1, BnOH added as C_6D_6 stock solution, additional C_6D_6 added, if required, to adjust to targeted catalyst concentration. P_m values determined from decoupled ^{1}H NMR spectra (see experimental part). Values were also determined for low conversions, but not provided since chain-end effects have a notable influence on the chemical shift for shorter chain lengths. For additional experiments, see Table S3.

Contrary to expectations, methyl substituted **1** was significantly more active than chloride-substituted **2** (Table 3.2, #1 and #2), although the latter would be expected to furnish the more Lewis-acidic metal center. The polymerization mechanism was thus briefly investigated in the presence of different equivalents of benzyl alcohol. Some activity was still observed without co-initiator, but long induction times indicate activation by impurities. Between 1 and 5 equiv BnOH, activities correlated with the concentration of external alcohol (Table 3.2, #4 and #5). At lower catalyst concentration, activity is observer only with 5 equiv of benzyl alcohol (Table S3.3). An activated-monomer mechanism thus remains the most likely mechanistic scenario. Since formation of a putative L_2Zr(lactide) intermediate would require prior dissociation of a pyridine ligand, the decreased activity of **2** can be assigned to hindered pyridine dissociation from the more Lewis-acidic Zr center.

Conclusions

Eight-coordinated zirconium complexes are surprisingly active for polymerization of lactide in the melt, given the coordinative oversaturation of the zirconium center.

Polymerization data agrees with polymerization following an activated-monomer mechanism, which most likely implies the presence of an uncoordinated, basic pyridine moiety in the lactide-coordinated intermediate, which is available for assisting in deprotonating the incoming alcohol. However, no stereocontrol was observed in these reactions and the implication of the basic site remains for the moment speculative.

Experimental section. All reactions were carried out using Schlenk or glove box techniques under nitrogen atmosphere. 2-pyridylamino-*N,N*-bis(2-methylene-4,6-methylphenol), **L1**H_2,[53] 2-pyridylamino-*N,N*-bis(2-methylene-4,6-*tert*-butylphenol), **L3**H_2,[54] and 2-pyridylamino-*N,N*-bis(6-methylene-2,4-chlorophenol), **L2**H_2,[55] were prepared according to literature (but using water as solvent for **L2**H_2). Solvents were dried by passage through activated aluminum oxide (MBraun SPS), de-oxygenated by repeated extraction with nitrogen, and stored over molecular sieves. C_6D_6 was dried over molecular sieves. *rac*-Lactide (98%) was purchased from Sigma–Aldrich, purified by 3x recrystallisation from dry ethyl acetate and kept at –30 °C. All other chemicals were purchased from common commercial suppliers and used without further purification. ^{1}H and ^{13}C NMR spectra were acquired on a Bruker Advance 400 spectrometer. Chemical shifts were referenced to the residual signals of the deuterated solvents ($CDCl_3$: ^{1}H: δ 7.26 ppm, ^{13}C: δ 77.16; C_6D_6: 1H: δ 7.16 ppm, ^{13}C: δ 128.06 ppm).

(**L1**)$_2$Zr, **1**.[56] Zr(IV) *n*-propoxide (140 mg, 0.30 mmol, 70 wt.% in 1-propanol) was suspended in diethyl ether (3 ml). **L1**H_2 (225 mg, 0.60 mmol) in diethyl ether (4 ml) was added dropwise, resulting in a colorless solution. The reaction as stirred for 2 hours at ambient temperature. The solvent was evaporated. The crude reaction mixture contained **1** and **1b** in appr. equal amounts. The crude product dissolved in toluene and kept at –80 °C for 24 h. The supernatant solution was separated with a syringe from the precipitate. Evaporation of the solvent afforded **1** as a white powder (100 mg, 42%). The precipitate was mixture of **1** and **1b** in an appr. 7:1 ratio.

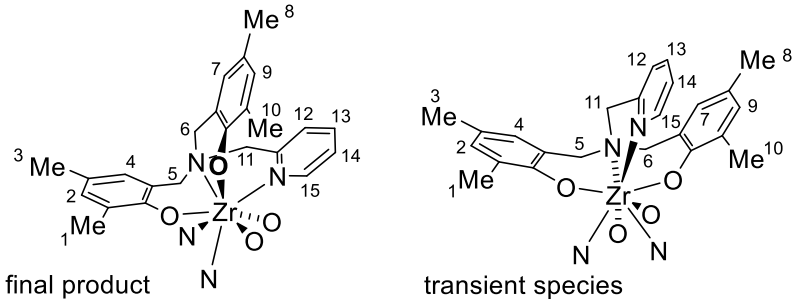

^{1}H NMR (500 MHz, C_6D_6): δ 1.68 (s, 3H, *ortho* Me H1), 2.13 (s, 3H, *para* Me H8), 2.30 (s, 3H, *para* Me H3), 2.42 (s, 3H, *ortho* Me H10), 2.47 (d, $^{3}J_{HH}$ = 13 Hz, 1H, CH_2 H6), 2.89 (d, $^{3}J_{HH}$ = 13 Hz, 1H, CH_2 H5), 3.16 (d, $^{3}J_{HH}$ = 14 Hz, 1H, PyCH_2), 4.31 (d, $^{3}J_{HH}$ = 12 Hz, 1H, CH_2 H6), 4.73 (d, $^{3}J_{HH}$ = 14 Hz, 1H, CH_2 H5), 5.01 (d, $^{3}J_{HH}$ = 13 Hz, 1H, PyCH_2), 6.29 (d, $^{3}J_{HH}$ = 8 Hz, 1H, *meta* Py H12), 6.38 (d, $^{3}J_{HH}$ = 2 Hz 1H, Ar H9), 6.48 (t, $^{3}J_{HH}$ = 6 Hz, 1 H, *meta* Py H14), 6.60 (d, $^{3}J_{HH}$ = 2 Hz, 1H, Ar H7), 6.75 (d, $^{3}J_{HH}$ = 2 Hz, 1H, Ar H4), 6.75-6.77 (m, 1H, *para* Py H13), 6.91 (d, $^{3}J_{HH}$ = 2 Hz, 1H, Ar H2), 9.92 (dd, $^{3}J_{HH}$ = 6 Hz, $^{4}J_{HH}$ = 2 Hz, 1H, *ortho* Py). ^{13}C{^{1}H} NMR (125 MHz, C_6D_6): δ 16.23 (*ortho* Me C10), 18.41 (*ortho* Me C10), 20.25 (*para* Me C8), 20.48 (*para* Me C8), 60.10 (Ar*C*H2), 63.93 (Ar*C*H2), 65.35 (Py*C*H2), 119.80, 120.96, 123.81, 123.83, 124.12, 124.51, 124.64, 124.72, 125.33, 128.97, 130.84 (meta Ar), 131.38 (meta Ar), 136.24 (*para* Py), 148.17 (*ortho* Py C15), 156.88 (*ortho* Py), 158.36 (*ipso* Ar), 160.96 (*ipso* Ar).

Transient species: δ 2.06 (s, 3H, *ortho* Me H10), 2.17 (s, 3H, *para* Me H3), 2.29 (s, 3H, *ortho* Me H1), 2.43 (s, 3H, *ortho* Me H8), 2.80 (d, $^{3}J_{HH}$ = 12 Hz, 1H, CH_2 H6), 3.07 (d, $^{3}J_{HH}$ = 12 Hz, 1H, CH_2 H5), 3.27 (d, $^{3}J_{HH}$ = 15 Hz, 1H, PyCH_2), 3.87 (d, $^{3}J_{HH}$ = 15 Hz, 1H, PyCH_2), 5.27 (d, $^{3}J_{HH}$ = 12 Hz, 1H, CH_2 H5), 5.74 (d, $^{3}J_{HH}$ = 8 Hz, 1H, *meta* Py H12), 6.15 (d, $^{3}J_{HH}$ = 12 Hz, 1H, CH_2 H6), 6.26 (t, $^{3}J_{HH}$ = 6 Hz, 1 H, *meta* Py H14), 6.50 (t, $^{3}J_{HH}$ = 6 Hz, 1H, *para* Py), 6.53 (d, $^{3}J_{HH}$ = 2 Hz, 1H, Ar H9), 6.60 (d, $^{3}J_{HH}$ = 2 Hz, 1H, Ar H4), 6.82 (d, $^{3}J_{HH}$ = 2 Hz, 1H, Ar H7), 6.91 (d, $^{3}J_{HH}$ = 2 Hz, 1H, Ar H7), 9.25 (dd, $^{3}J_{HH}$ = 6 Hz, $^{4}J_{HH}$ = 2 Hz, 1H, *ortho* Py).

(**L3**)Zr(O*n*Pr)$_2$, **3**. Zr(IV) *n*-propoxide (140 mg, 0.30 mmol, 70 wt.% in 1-propanol) was suspended in diethyl ether (3 ml). **L3**H$_2$ (167 mg, 0.31 mmol) in diethyl ether (4 ml) was added dropwise, resulting in a colorless solution. The reaction was stirred 2 hours at ambient temperature. The solution was concentrated to 10% of its volume by slow evaporation. Remaining solvent was removed via syringe and **3** was obtained as a crystalline powder (215 mg, 95%).

^{1}H NMR (500 MHz, C_6D_6): δ 1.12 (t, $^3J_{HH}$ = 7 Hz, 3H, CH_2*Me*), 1.31 (t, $^3J_{HH}$ = 7 Hz, 3H, CH_2*Me*), 1.38 (s, 18H, C*Me*$_3$), 1.56 (s, 18H, C*Me*$_3$), 1.81(m, 2H, C*H*$_2$Me), 2.03(m, 2H, C*H*$_2$Me), 2.97 (d, $^3J_{HH}$ = 14 Hz, 2H, ArC*H*$_2$), 3.27 (s, 2H, PyC*H*$_2$), 4.31 (t, $^3J_{HH}$ = 6 Hz, 2H, OC*H*$_2$), 4.58 (t, $^3J_{HH}$ = 6 Hz, 2H, OC*H*$_2$), 4.71(d, $^3J_{HH}$ = 14 Hz, 2H, ArC*H*$_2$), 5.63 (d, $^3J_{HH}$ = 8 Hz, 1H, *meta* Py), 6.23 (vt, $^3J_{HH}$ = 6 Hz, 1H, *meta* Py), 6.39 (td, $^3J_{HH}$ = 8 Hz, $^4J_{HH}$ = 2 Hz, 1H, *para* Py), 6.94 (d, $^3J_{HH}$ = 3 Hz, 2H, Ar H3) 7.33 (d, $^3J_{HH}$ = 3 Hz, 2H, Ar H5), 8.61 (d, $^3J_{HH}$ = 5 Hz, 1H, *ortho* Py). ^{13}C{^{1}H} NMR (125 MHz, C_6D_6): δ 10.73 (CH_2*Me*), 10.83 (CH_2*Me*), 27.95 (*CH*$_2$Me), 28.32 (*CH*$_2$Me), 29.78 (C*Me*$_3$), 31.84 (C*Me*$_3$), 33.91 (*C*Me$_3$), 34.99 (*C*Me$_3$), 59.68 (C*H*$_2$Ar), 63.62 (C*H*$_2$Py), 71.89 (OCH_2), 71.97 (OCH_2), 120.01 (Ar), 121.01 (Ar), 123.63 (Ar), 123.68 (Ar), 124.73 (Ar), 136.41 (Ar), 137.39 (Ar), 138.09 (Ar), 149.17 (Ar), 157.52 (Ar), 159.70 (Ar).

(**L2**)$_2$Zr, **1**. Zr(IV) *n*-propoxide (140 mg, 0.30 mmol, 70 wt.% in 1-propanol) was suspended in diethyl ether (3 ml). **L2**H$_2$ (274 mg, 0.60 mmol) in diethyl ether (4 ml) was added dropwise, resulting in a colorless solution. The reaction as stirred 2 hours at ambient temperature. Evaporation of the solvent yielded a white powder, the NMR spectra of which showed **2** and **2b** in a thermal equilibrium (295 mg, 98%).

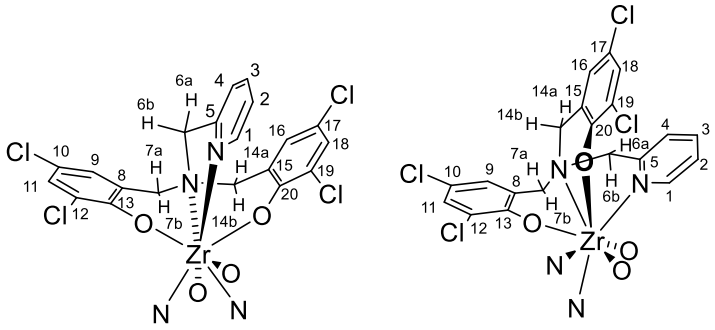

^{1}H NMR (500 MHz, C_6D_6): δ 2.54 – 2.62 (m, 3H, CH_2 6a, 7a & 14a), 3.51 (d, $^{3}J_{HH}$ = 14 Hz, 1H, CH_2 6b), 4.57 (d, $^{3}J_{HH}$ = 14 Hz, 1H, CH_2 7b), 5.71 (m, 1H, Py 4), 5.92 (d, $^{3}J_{HH}$ = 11 Hz, 1H, CH_2 14b), 6.51-6.55 (m, 3 H, Ar 9, Py 2 & 3), 6.74 (d, $^{3}J_{HH}$ = 2 Hz, 1H, Ar 16), 7.02 (d, $^{4}J_{HH}$ = 2 Hz, 1H, Ar 18), 7.18 (d, $^{4}J_{HH}$ = 2 Hz, 1H, Ar 11), 10.06-10.09 (m, 1H, Py 1). ^{13}C{^{1}H} NMR (125 MHz, C_6D_6): δ 59.19 (C6), 61.99 (C7), 62.32 (C14), 119.51 (C4), 121.19, 121.39, 121.79 (C2), 122.42, 123.24, 127.07, 128.00, 128.23 (C16), 128.60 (C9), 129.15 (C11), 129.38 (C18), 136.97 (C3), 150.86 (C1), 155.74 (C13), 156.23 (C13), 157.50 (C5).

Minor species: ^{1}H NMR (500 MHz, C_6D_6): δ 1.94 (d, 1H, CH_2), 2.57 (d, 1H, CH_2), 2.47 (d, 1H, CH_2), 2.84 (d, 1H, CH_2), 4.34 (d, 1H, CH_2), 5.01 (d, 1H, CH_2), 6.24 (d, 1H, Py), 6.40 (d, 1H, Ar), 6.59 (t, 1H, Py), 6.69 (t, 1H, Py), 6.79 (d, 1H, Ar), 7.00 (d, 1H, Ar), 7.26 (d, 1H, Ar), 10.2 (d, 1H, Py).). ^{13}C{^{1}H} NMR (125 MHz, C_6D_6, only few peaks identified): δ 59.0 (CH_2 C14), 62.0 (CH_2 C7), 65.2 (CH_2 C6), 120.1 (Py C4), 122.1 (Py C2), 127.4 (Ar C16), 128.1 (Ar C9), 128.8 (Ar C18), 129.4 (Ar C11), 137.4 (Py C3), 149.5 (Py C1).

Lactide polymerization. In a glove box, the desired amount of *rac*-lactide was placed into a J.-Young tube and dissolved in C_6D_6. If required, a stock solution of an additive (EtOH, etc.) was added, followed by a stock solution of the catalyst (≈20 mM in C_6D_6). The reaction was followed by ^{1}H NMR. The reaction was quenched by addition of ≈5 equiv of a $CDCl_3$ solution of acetic acid (5 mM). The volatiles were immediately evaporated and solid polymer samples were stored at –80 °C for further analysis. Conversion was

determined from ^{1}H NMR by comparison to remaining lactide. P_m values were determined from homodecoupled ^{1}H NMR spectra and calculated from $P_m = 1 - 2 \cdot I_1/(I_1+I_2)$, with I_1 = 5.15 – 5.21 ppm (*rmr, mmr/rmm*), I_2 = 5.21 – 5.25 ppm (*mmr/rmm, mmm, mrm*).

DFT calculations were performed with Gaussian16[59] using the M06 functional.[60] In geometry optimization and frequency calculation (ZPE and thermal correction to 298 K), a 6-31+G(d,p) basis set was used for all light atoms and a LANL2DZ effective-core potential basis set for zinc and silicon. All optimized geometries showed real frequencies only. Single-point energies on the optimized geometries were obtained with the Def2TZVPP basis set. NMR spectra were calculated from single-point calculations using the optimized gas-phase geometries. NMR calculations (GIAO) used a benzene solvent model (SMD), the mPW1PW91 functional[61] and a 6-311+G(2d,p) basis set on all atoms. (Using a geometry optimized with the benzene solvent model instead of gas phase geometry caused chemical shift differences of less than 0.03 ppm.)

X-ray diffraction. Diffraction data were collected on a Bruker APEXII with a Cu microsource/Quazar MX using the APEX2 software package.[62] Data reduction was performed with SAINT,[63] absorption corrections with SADABS.[64] Structures were solved by dual-space refinement (SHELXT).[65] All non-hydrogen atoms were refined anisotropic using full-matrix least-squares on F^2 and hydrogen atoms refined with fixed isotropic U using a riding model (SHELXL97).[66] Further experimental details can be found in Table 3 and in the supporting information (CIF).

Table 3.3. Details of the X-ray diffraction studies

	2	**3**
Formula	2 $C_{40}H_{28}Cl_8N_4O_4Zr$, 1.5 C_7H_8	$C_{42}H_{64}N_2O_4Zr$
M_w (g/mol); $d_{calcd.}$ (g/cm^3)	2145.17	752.2; 1.17
T (K); F(000)	100; 2166	200; 1608
Crystal System	triclinic	monoclinic
Space Group	P–1	$P2_1/c$

Unit Cell:	a (Å)	14.3402(3)	11.1841(2)
	b (Å)	15.2460(3)	20.5710(3)
	c (Å)	20.7979(5)	18.7032(3)
	α (°)	82.944(1)	
	β (°)	75.794(1)	96.892(1)
	γ (°)	82.845(1)	
V (Å^3); Z		4353.51(16); 2	4271.92(12); 4
μ (mm^{-1}); Abs. Corr.		7.003; multi-scan	2.405; multi-scan
θ range (°); completeness		2.2 – 67.7; 0.98	3.2 – 67.7; 1.00
collected reflections; R_σ		108371; 0.026	58658; 0.018
unique reflections; R_{int}		16574; 0.047	8367; 0.033
R1(F) (I > 2σ(I))		0.031	0.033
wR(F^2) (all data)		0.082	0.094
GoF(F^2)		1.03	1.12
Residual electron density		0.91; –0.69	0.54; –0.51

Funding was supplied by the NSERC discovery program (RGPIN-2016-04953) and the Centre for Green Chemistry and Catalysis (FQRNT). DFT calculations were enabled by support provided by Calcul Québec (www.calculquebec.ca) and Compute Canada (www.computecanada.ca). We thank Dr. Daniel Chartrand for support with X-ray crystallography.

References chapter 3

1. Abdelmoez, W.; Dahab, I.; Ragab, E. M.; Abdelsalam, O. A.; Mustafa, A., Bio- and oxo-degradable plastics: Insights on facts and challenges. *Polym. Adv. Technol.* **2021,** *32* (5), 1981-1996.
2. Filiciotto, L.; Rothenberg, G., Biodegradable Plastics: Standards, Policies, and Impacts. *ChemSusChem* **2021,** *14* (1), 56-72.
3. Lyubov, D. M.; Tolpygin, A. O.; Trifonov, A. A., Rare-earth metal complexes as catalysts for ring-opening polymerization of cyclic esters. *Coord. Chem. Rev.* **2019,** *392*, 83-145.
4. Li, X.; Chen, C.; Wu, J., Lewis Pair Catalysts in the Polymerization of Lactide and Related Cyclic Esters. *Molecules* **2018,** *23* (1).
5. Kuroishi, P. K.; Dove, A. P., On like a light. *Nature Catalysis* **2018,** *1* (7), 486-487.
6. Redshaw, C., Use of Metal Catalysts Bearing Schiff Base Macrocycles for the Ring Opening Polymerization (ROP) of Cyclic Esters. *Catalysts* **2017,** *7* (5).
7. Osten, K. M.; Mehrkhodavandi, P., Indium Catalysts for Ring Opening Polymerization: Exploring the Importance of Catalyst Aggregation. *Acc. Chem. Res.* **2017,** *50* (11), 2861-2869.
8. Fuoco, T.; Pappalardo, D., Aluminum Alkyl Complexes Bearing Salicylaldiminato Ligands: Versatile Initiators in the Ring-Opening Polymerization of Cyclic Esters. *Catalysts* **2017,** *7* (2).
9. Paul, S.; Zhu, Y.; Romain, C.; Brooks, R.; Saini, P. K.; Williams, C. K., Ring-Opening Copolymerization (Rocop): Synthesis and Properties of Polyesters and Polycarbonates. *Chem. Commun. (Cambridge, U. K.)* **2015,** *51* (30), 6459-6479.
10. MacDonald, J. P.; Shaver, M. P., Aluminum Salen and Salan Polymerization Catalysts: From Monomer Scope to Macrostructure Control. In *Green Polymer Chemistry: Biobased Materials and Biocatalysis*, American Chemical Society: 2015; Vol. 1192, pp 147-167.
11. Guillaume, S. M.; Kirillov, E.; Sarazin, Y.; Carpentier, J.-F., Beyond Stereoselectivity, Switchable Catalysis: Some of the Last Frontier Challenges in Ring-Opening Polymerization of Cyclic Esters. *Chem.-Eur. J.* **2015,** *21* (22), 7988-8003.
12. Sauer, A.; Kapelski, A.; Fliedel, C.; Dagorne, S.; Kol, M.; Okuda, J., Structurally Well-Defined Group 4 Metal Complexes as Initiators for the Ring-Opening Polymerization of Lactide Monomers. *Dalton Trans.* **2013,** *42* (25), 9007-9023.
13. Dagorne, S.; Normand, M.; Kirillov, E.; Carpentier, J.-F., Gallium and Indium Complexes for Ring-Opening Polymerization of Cyclic Ethers, Esters and Carbonates. *Coord. Chem. Rev.* **2013,** *257* (11–12), 1869-1886.
14. Dagorne, S.; Fliedel, C., Organoaluminum Species in Homogeneous Polymerization Catalysis. In *Modern Organoaluminum Reagents: Preparation, Structure, Reactivity and Use*, Woodward, S.; Dagorne, S., Eds. Springer Berlin Heidelberg: Berlin, Heidelberg, 2013; pp 125-171.
15. Carpentier, J.-F.; Liu, B.; Sarazin, Y., Charge-Neutral and Cationic Complexes of Large Alkaline Earths for Ring-Opening Polymerization and Fine Chemicals Catalysis. In *Advances in Organometallic Chemistry and Catalysis*, John Wiley & Sons, Inc.: 2013; pp 359-378.
16. dos Santos Vieira, I.; Herres-Pawlis, S., Lactide Polymerisation with Complexes of Neutral N-Donors – New Strategies for Robust Catalysts. *Eur. J. Inorg. Chem.* **2012,** *2012* (5), 765-774.
17. Wheaton, C. A.; Hayes, P. G., Designing Cationic Zinc and Magnesium Catalysts for Coordination–Insertion Polymerization of Lactide. *Comments Inorg. Chem.* **2011,** *32* (3), 127-162.
18. Dutta, S.; Hung, W.-C.; Huang, B.-H.; Lin, C.-C., Recent Developments in Metal-Catalyzed Ring-Opening Polymerization of Lactides and Glycolides: Preparation of Polylactides,

Polyglycolide, and Poly(Lactide-Co-Glycolide). In *Synthetic Biodegradable Polymers*, Rieger, B.; Künkel, A.; Coates, G. W.; Reichardt, R.; Dinjus, E.; Zevaco, T. A., Eds. Springer-Verlag: Berlin, 2011; pp 219-284.
19. Dijkstra, P. J.; Du, H.; Feijen, J., Single Site Catalysts for Stereoselective Ring-Opening Polymerization of Lactides. *Polym. Chem.* **2011,** *2* (3), 520-527.
20. Thomas, C. M., Stereocontrolled Ring-Opening Polymerization of Cyclic Esters: Synthesis of New Polyester Microstructures. *Chem. Soc. Rev.* **2010,** *39* (1), 165.
21. Stanford, M. J.; Dove, A. P., Stereocontrolled Ring-Opening Polymerization of Lactide. *Chem. Soc. Rev.* **2010,** *39*, 486-494.
22. Jones, M. D., Heterogeneous Initiators for Sustainable Polymerization Processes. In *Heterogenized Homogeneous Catalysts for Fine Chemicals Production*, Barbaro, P.; Liguori, F., Eds. Springer Netherlands: 2010; Vol. 33, pp 385-412.
23. Wheaton, C. A.; Hayes, P. G.; Ireland, B. J., Complexes of Mg, Ca and Zn as Homogeneous Catalysts for Lactide Polymerization. *Dalton Trans.* **2009**, 4832 - 4846.
24. Williams, C. K.; Hillmyer, M. A., Polymers from Renewable Resources: A Perspective for a Special Issue of Polymer Reviews. *Polym. Rev.* **2008,** *48* (1), 1-10.
25. Platel, R. H.; Hodgson, L. M.; Williams, C. K., Biocompatible Initiators for Lactide Polymerization. *Polym. Rev.* **2008,** *48* (1), 11 - 63.
26. Amgoune, A.; Thomas, C. M.; Carpentier, J.-F., Controlled Ring-Opening Polymerization of Lactide by Group 3 Metal Complexes. *Pure Appl. Chem.* **2007,** *79* (11), 2013-2030.
27. Dechy-Cabaret, O.; Martin-Vaca, B.; Bourissou, D., Controlled Ring-Opening Polymerization of Lactide and Glycolide. *Chem. Rev.* **2004,** *104* (12), 6147-6176.
28. O'Keefe, B. J.; Hillmyer, M. A.; Tolman, W. B., Polymerization of Lactide and Related Cyclic Esters by Discrete Metal Complexes. *J. Chem. Soc., Dalton Trans.* **2001,** (15), 2215-2224.
29. Daneshmand, P.; Michalsky, I.; Aguiar, P. M.; Schaper, F., Configurationally flexible zinc complexes as catalysts for rac-lactide polymerisation. *Dalton Trans.* **2018,** *47*, 16279 - 16291.
30. Daneshmand, P.; van der Est, A.; Schaper, F., Mechanism and Stereocontrol in Isotactic *rac*-Lactide Polymerization with Copper(II) Complexes. *ACS Catal.* **2017,** *7*, 6289-6301.
31. Fortun, S.; Daneshmand, P.; Schaper, F., Isotactic Rac-Lactide Polymerization with Copper Complexes: The Influence of Complex Nuclearity. *Angew. Chem., Int. Ed.* **2015,** *54* (46), 13669-13672.
32. Whitehorne, T. J. J.; Vabre, B.; Schaper, F., Lactide Polymerization Catalyzed by Mg and Zn Diketiminate Complexes with Flexible Ligand Frameworks. *Dalton Trans.* **2014,** *43* (17), 6339-6352.
33. Whitehorne, T. J. J.; Schaper, F., Square-Planar Cu(Ii) Diketiminate Complexes in Lactide Polymerization. *Inorg. Chem.* **2013,** *52*, 13612-13622.
34. El-Zoghbi, I.; Whitehorne, T. J. J.; Schaper, F., Exceptionally High Lactide Polymerization Activity of Zirconium Complexes with Bridged Diketiminate Ligands. *Dalton Trans.* **2013,** *42*, 9376 - 9387.
35. Whitehorne, T. J. J.; Schaper, F., *Nacnac*^{Bn}CuO*i*Pr: A Strained Geometry Resulting in Very High Lactide Polymerization Activity. *Chem. Commun. (Cambridge, U. K.)* **2012,** *48*, 10334-10336.
36. Drouin, F.; Oguadinma, P. O.; Whitehorne, T. J. J.; Prud'homme, R. E.; Schaper, F., Lactide Polymerization with Chiral Beta-Diketiminate Zinc Complexes. *Organometallics* **2010,** *29* (9), 2139-2147.

37. Orhan, B.; Tschan, M. J. L.; Wirotius, A.-L.; Dove, A. P.; Coulembier, O.; Taton, D., Isoselective Ring-Opening Polymerization of rac-Lactide from Chiral Takemoto's Organocatalysts: Elucidation of Stereocontrol. *ACS Macro Lett.* **2018,** *7* (12), 1413-1419.
38. Normand, M.; Dorcet, V.; Kirillov, E.; Carpentier, J.-F., {Phenoxy-imine}aluminum versus -indium Complexes for the Immortal ROP of Lactide: Different Stereocontrol, Different Mechanisms. *Organometallics* **2013,** *32* (6), 1694-1709.
39. Calvo, B.; Davidson, M. G.; Garcia-Vivo, D., Polyamine-Stabilized Sodium Aryloxides: Simple Initiators for the Ring-Opening Polymerization of Rac-Lactide. *Inorg. Chem.* **2011,** *50* (Copyright (C) 2012 American Chemical Society (ACS). All Rights Reserved.), 3589-3595.
40. Liu, B.; Roisnel, T.; Maron, L.; Carpentier, J.-F.; Sarazin, Y., Discrete Divalent Rare-Earth Cationic Rop Catalysts: Ligand-Dependent Redox Behavior and Discrepancies with Alkaline-Earth Analogues in a Ligand-Assisted Activated Monomer Mechanism. *Chem.-Eur. J.* **2013,** *19* (12), 3986-3994.
41. Zhang, J.; Xiong, J.; Sun, Y.; Tang, N.; Wu, J., Highly Iso-Selective and Active Catalysts of Sodium and Potassium Monophenoxides Capped by a Crown Ether for the Ring-Opening Polymerization of Rac-Lactide. *Macromolecules* **2014,** *47* (22), 7789-7796.
42. Dai, Z.; Sun, Y.; Xiong, J.; Pan, X.; Wu, J., Alkali-Metal Monophenolates with a Sandwich-Type Catalytic Center as Catalysts for Highly Isoselective Polymerization of Rac-Lactide. *ACS Macro Lett.* **2015,** *4* (5), 556-560.
43. Xiong, J.; Zhang, J.; Sun, Y.; Dai, Z.; Pan, X.; Wu, J., Iso-Selective Ring-Opening Polymerization of Rac-Lactide Catalyzed by Crown Ether Complexes of Sodium and Potassium Naphthalenolates. *Inorg. Chem.* **2015,** *54* (4), 1737-1743.
44. Dai, Z.; Sun, Y.; Xiong, J.; Pan, X.; Tang, N.; Wu, J., Simple Sodium and Potassium Phenolates as Catalysts for Highly Isoselective Polymerization of Rac-Lactide. *Catalysis Science & Technology* **2016,** *6* (2), 515-520.
45. Sun, Y.; Xiong, J.; Dai, Z.; Pan, X.; Tang, N.; Wu, J., Stereoselective Alkali-Metal Catalysts for Highly Isotactic Poly(Rac-Lactide) Synthesis. *Inorg. Chem.* **2016,** *55* (1), 136-143.
46. Chen, C.; Cui, Y.; Mao, X.; Pan, X.; Wu, J., Suppressing Cyclic Polymerization for Isoselective Synthesis of High-Molecular-Weight Linear Polylactide Catalyzed by Sodium/Potassium Sulfonamidate Complexes. *Macromolecules* **2017,** *50* (1), 83-96.
47. Cui, Y.; Chen, C.; Sun, Y.; Wu, J.; Pan, X., Isoselective mechanism of the ring-opening polymerization of rac-lactide catalyzed by chiral potassium binolates. *Inorg. Chem. Front.* **2017,** *4* (2), 261-269.
48. Chen, C.; Jiang, J.; Mao, X.; Cong, Y.; Cui, Y.; Pan, X.; Wu, J., Isoselective Polymerization of rac-Lactide Catalyzed by Ion-Paired Potassium Amidinate Complexes. *Inorg. Chem.* **2018,** *57* (6), 3158-3168.
49. Xiong, J.; Sun, Y.; Jiang, J.; Chen, C.; Pan, X.; Wang, C.; Wu, J., Metal-size influence of alkali metal complexes for polymerization of rac-lactide. *Polyhedron* **2018,** *141*, 118-124.
50. Cui, Y.; Jiang, J.; Mao, X.; Wu, J., Mononuclear Salen–Sodium Ion Pairs as Catalysts for Isoselective Polymerization of rac-Lactide. *Inorganic Chemistry* **2019,** *58* (1), 218-227.
51. Hu, M.; Han, F.; Zhang, W.; Ma, W.; Deng, Q.; Song, W.; Yan, H.; Dong, G., Preparation of zirconium and hafnium complexes containing chiral N atoms from asymmetric tertiary amine ligands, and their catalytic properties for polymerization of rac-lactide. *Catalysis Science & Technology* **2017,** *7* (6), 1394-1403.
52. Wang, B.; Zhao, H.; Wang, L.; Sun, J.; Zhang, Y.; Cao, Z., Immortal ring-opening polymerization of lactides with super high monomer to catalyst ratios initiated by zirconium and

titanium complexes containing multidentate amino-bis(phenolate) ligands. *New J. Chem.* **2017,** *41* (13), 5669-5677.
53. Fu, L.-Z.; Zhou, L.-L.; Tang, L.-Z.; Zhang, Y.-X.; Zhan, S.-Z., A molecular iron(III) electrocatalyst supported by amine-bis(phenolate) ligand for water reduction. *Int. J. Hydrogen Energy* **2015,** *40* (28), 8688-8694.
54. Kerton, F. M.; Holloway, S.; Power, A.; Soper, R. G.; Sheridan, K.; Lynam, J. M.; Whitwood, A. C.; Willans, C. E., Accelerated Syntheses of Amine-Bis(Phenol) Ligands in Polyethylene Glycol or "on Water" under Microwave Irradiation. *Can. J. Chem.* **2008,** *86*, 435–443.
55. Heidari, S.; Safaei, E.; Wojtczak, A.; Cotič, P.; Kozakiewicz, A., Iron(III) complexes of pyridine-based tetradentate aminophenol ligands as structural model complexes for the catechol-bound intermediate of catechol dioxygenases. *Polyhedron* **2013,** *55*, 109-116.
56. Toupance, T.; Dubberley, S. R.; Rees, N. H.; Tyrrell, B. R.; Mountford, P., Zirconium Complexes of Diamine−Bis(phenolate) Ligands: Synthesis, Structures, and Solution Dynamics. *Organometallics* **2002,** *21* (7), 1367-1382.
57. Chmura, A. J.; Davidson, M. G.; Jones, M. D.; Lunn, M. D.; Mahon, M. F.; Johnson, A. F.; Khunkamchoo, P.; Roberts, S. L.; Wong, S. S. F., Group 4 Complexes with Aminebisphenolate Ligands and Their Application for the Ring Opening Polymerization of Cyclic Esters. *Macromolecules* **2006,** *39* (21), 7250-7257.
58. Gendler, S.; Segal, S.; Goldberg, I.; Goldschmidt, Z.; Kol, M., Titanium and Zirconium Complexes of Dianionic and Trianionic Amine−Phenolate-Type Ligands in Catalysis of Lactide Polymerization. *Inorg. Chem.* **2006,** *45* (12), 4783-4790.
59. Frisch, M. J.; Trucks, G. W.; Schlegel, H. B.; Scuseria, G. E.; Robb, M. A.; Cheeseman, J. R.; Scalmani, G.; Barone, V.; Petersson, G. A.; Nakatsuji, H.; Li, X.; Caricato, M.; Marenich, A. V.; Bloino, J.; Janesko, B. G.; Gomperts, R.; Mennucci, B.; Hratchian, H. P.; Ortiz, J. V.; Izmaylov, A. F.; Sonnenberg, J. L.; Williams; Ding, F.; Lipparini, F.; Egidi, F.; Goings, J.; Peng, B.; Petrone, A.; Henderson, T.; Ranasinghe, D.; Zakrzewski, V. G.; Gao, J.; Rega, N.; Zheng, G.; Liang, W.; Hada, M.; Ehara, M.; Toyota, K.; Fukuda, R.; Hasegawa, J.; Ishida, M.; Nakajima, T.; Honda, Y.; Kitao, O.; Nakai, H.; Vreven, T.; Throssell, K.; Montgomery Jr., J. A.; Peralta, J. E.; Ogliaro, F.; Bearpark, M. J.; Heyd, J. J.; Brothers, E. N.; Kudin, K. N.; Staroverov, V. N.; Keith, T. A.; Kobayashi, R.; Normand, J.; Raghavachari, K.; Rendell, A. P.; Burant, J. C.; Iyengar, S. S.; Tomasi, J.; Cossi, M.; Millam, J. M.; Klene, M.; Adamo, C.; Cammi, R.; Ochterski, J. W.; Martin, R. L.; Morokuma, K.; Farkas, O.; Foresman, J. B.; Fox, D. J. *Gaussian 16 Rev. C.01*, Wallingford, CT, 2016.
60. Zhao, Y.; Truhlar, D. G., The M06 suite of density functionals for main group thermochemistry, thermochemical kinetics, noncovalent interactions, excited states, and transition elements: two new functionals and systematic testing of four M06-class functionals and 12 other functionals. *Theor. Chem. Acc.* **2008,** *120* (1), 215-241.
61. Adamo, C.; Barone, V., Exchange functionals with improved long-range behavior and adiabatic connection methods without adjustable parameters: The mPW and mPW1PW models. **1998,** *108* (2), 664-675.
62. *Apex2*, Release 2.1-0; Bruker AXS Inc.: Madison, USA, 2006.
63. *Saint*, Release 7.34A; Bruker AXS Inc.: Madison, USA, 2006.
64. Sheldrick, G. M. *Sadabs*, Bruker AXS Inc.: Madison, USA, 1996 & 2004.
65. Sheldrick, G., Shelxt - Integrated Space-Group and Crystal-Structure Determination. *Acta Crystallogr., Sect. A: Found. Adv.* **2015,** *71* (1), 3-8.

66. Sheldrick, G. M., A Short History of Shelx. *Acta Crystallogr.* **2008,** *A64*, 112-122.

Supporting Information

Lactide polymerization with 8-coordinated Zirconium complexes

Fatemeh Dordahan, Frank Schaper*

Centre in Green Chemistry and Catalysis, Université de Montréal, Department of Chemistry, Montréal, Canada

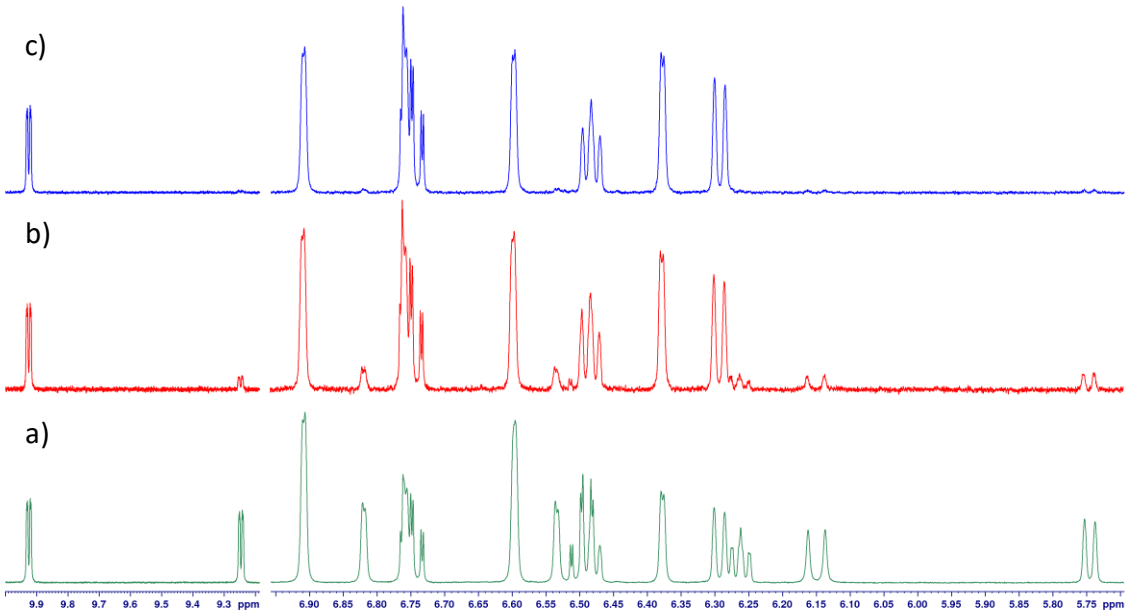

Figure S3.1. Aromatic regions of ^{1}H NMR spectra of **1** in C_6D_6. a) Crude reaction mixture containing **1** and **1b**. b) Precipitate obtained at –80 °C in toluene. c) Supernatant toluene solution at –80 °C containing only **1**.

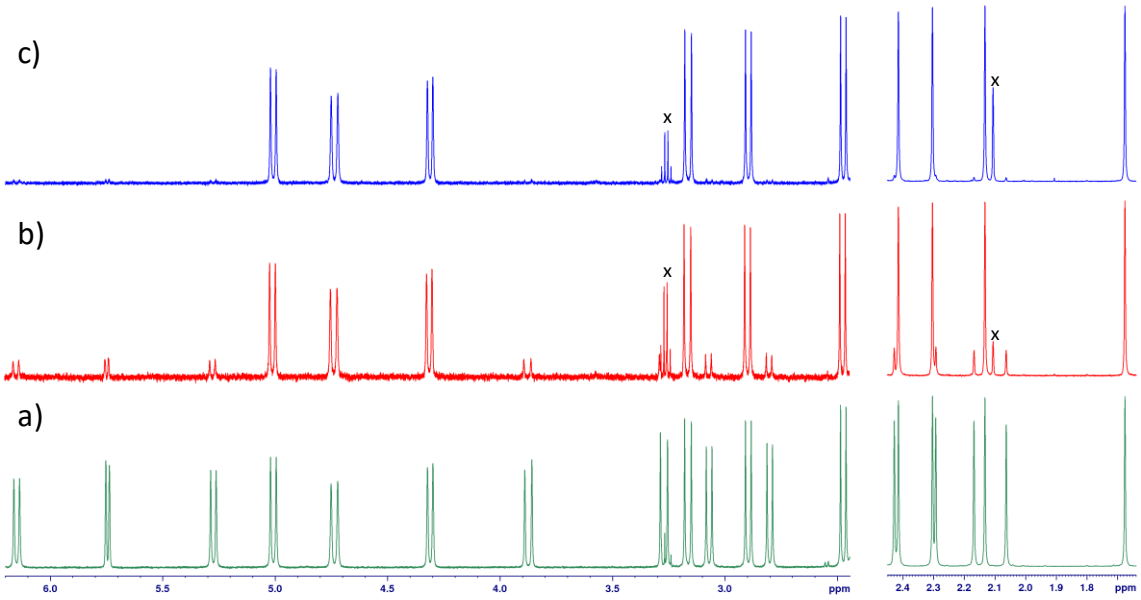

Figure S3.2. Aliphatic regions of ^{1}H NMR spectra of **1** in C_6D_6 (left: methylene groups, right: methyl groups) a) Crude reaction mixture containing **1** and **1b**. b) Precipitate obtained at –80 °C in toluene. c) Supernatant toluene solution at –80 °C containing only **1**. The "x" marks some toluene and ether contamination.

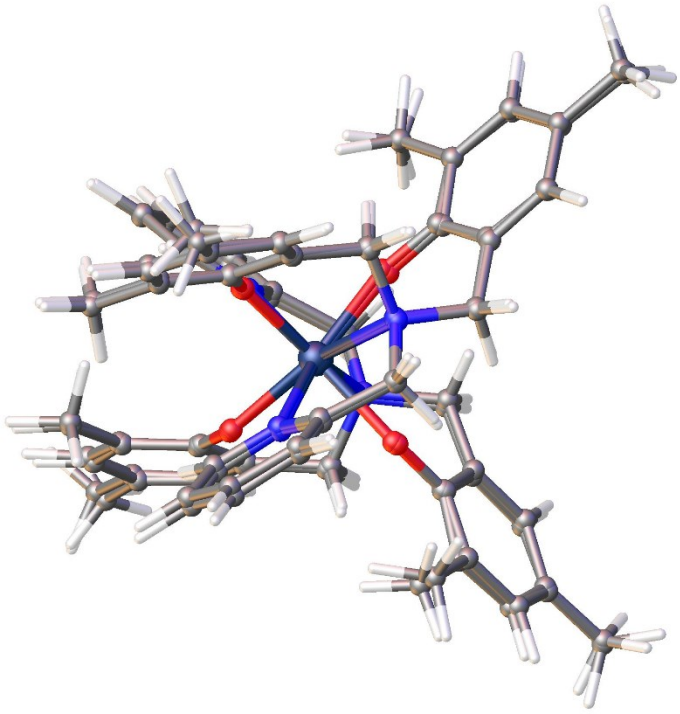

Figure S3.3. Overlay of the DFT-optimized structures of 1 with the X-ray structure obtained from Toupance, T.; Dubberley, S. R.; Rees, N. H.; Tyrrell, B. R.; Mountford, P. *Organometallics* **2002**, *21*, 1367.

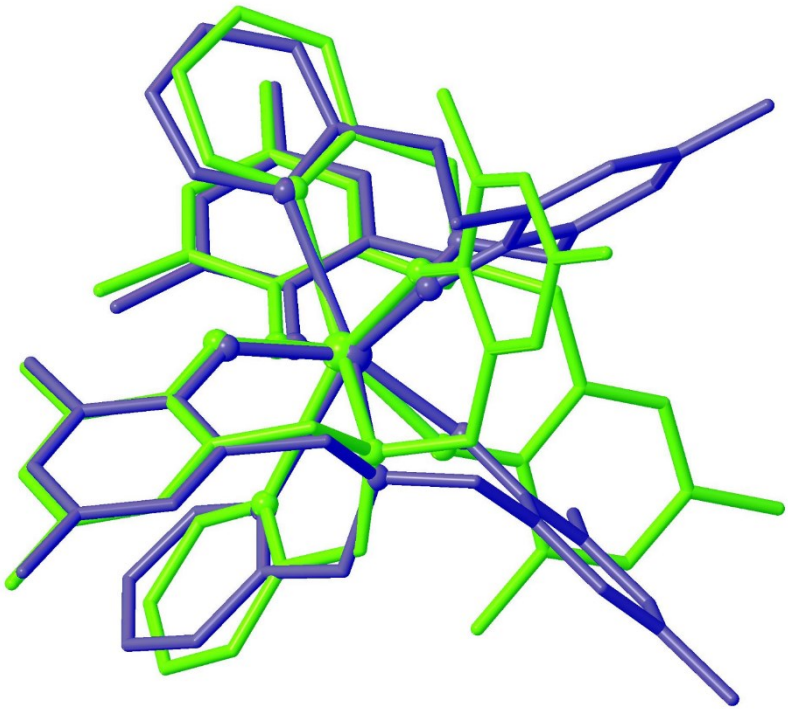

Figure S3.4. Overlay of the DFT-optimized structures of *cis,cis*-**1** (green)and *trans,trans*-**1b** (blue).

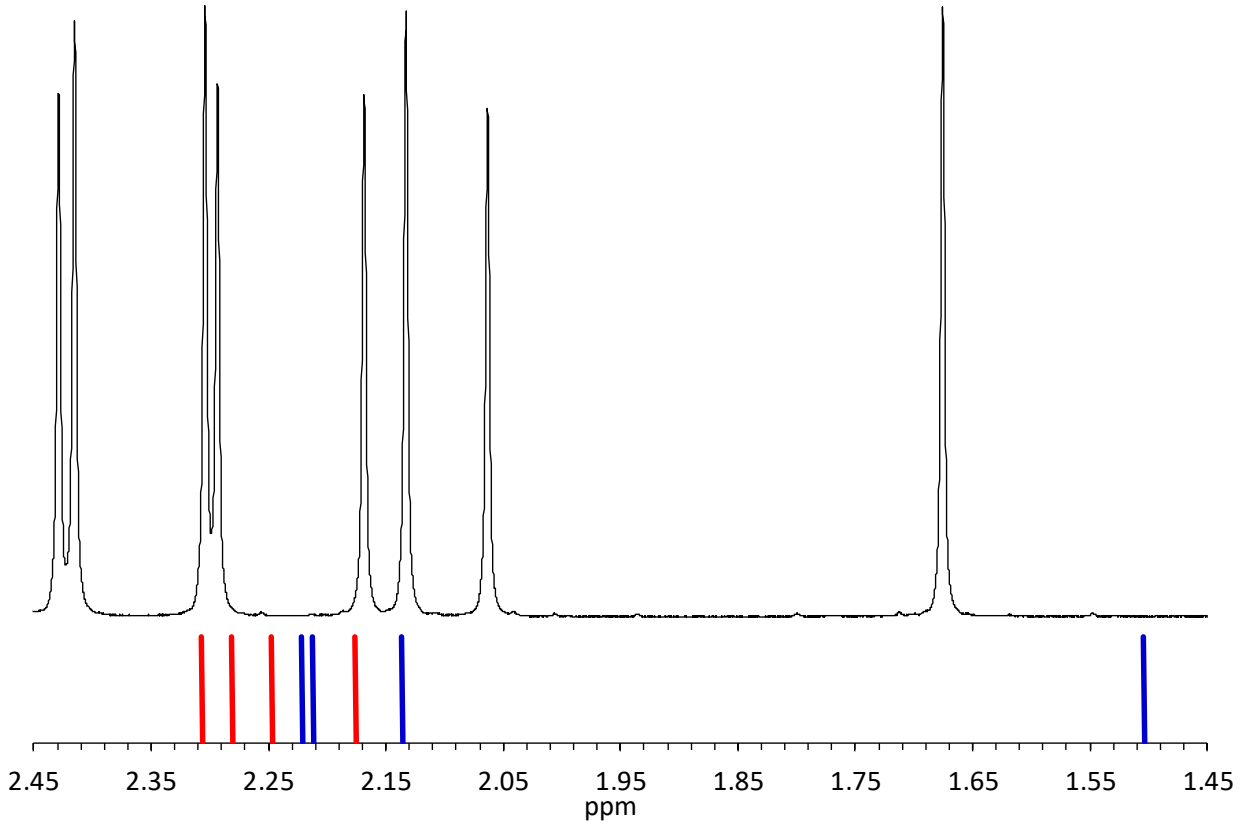

Figure S3.5. Methyl region of the ^{1}H NMR of **1** and **1b** and the calculated NMR shifts of DFT-calculated structures (blue : *cis,cis*-**1**, red : *trans,trans*-**1b**).

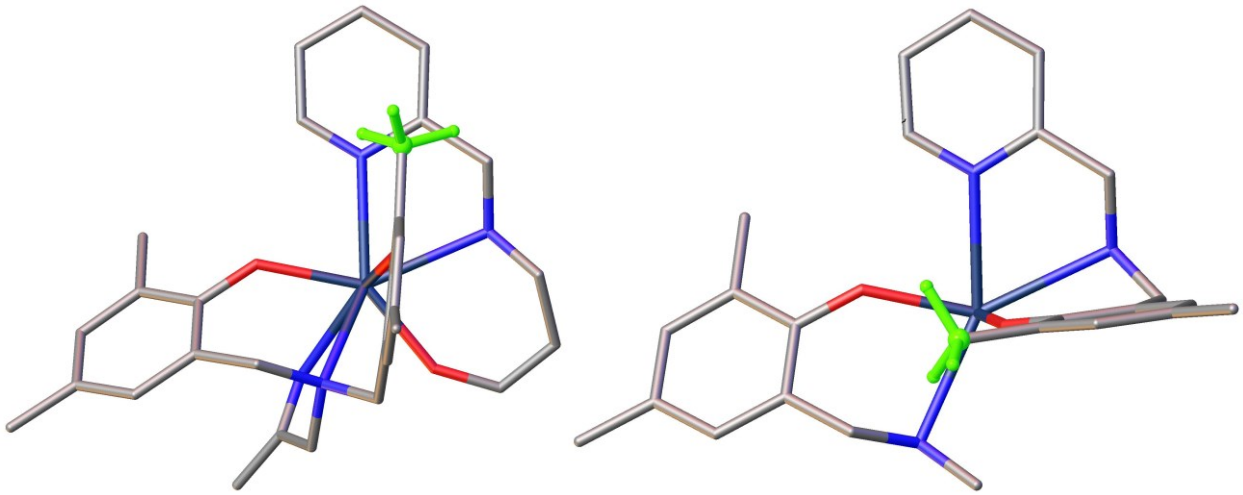

Figure S3.6. Orientation of the *ortho* methyl group in the non-π-stacked phenolate ligand in *cis,cis*-**1** (left) and *trans,trans*-**1b** (right).

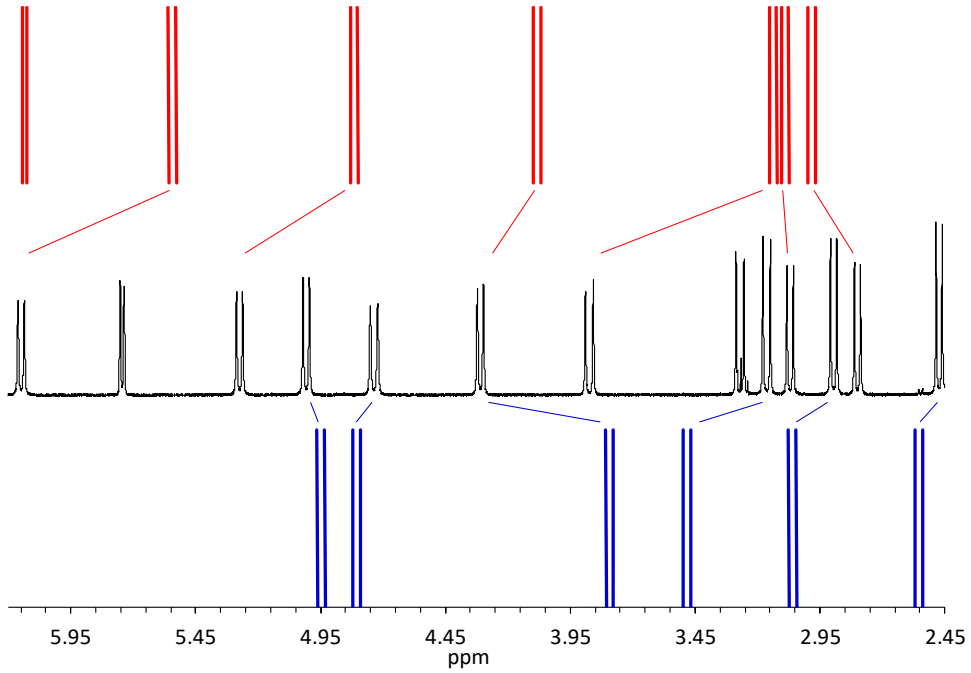

Figure S3.7. Methylene region of the ^{1}H NMR of **1** and **1b** and the calculated NMR shifts of DFT-calculated structures (bottom, blue : *cis,cis*-**1**, top, red: *trans,trans*-**1b**).

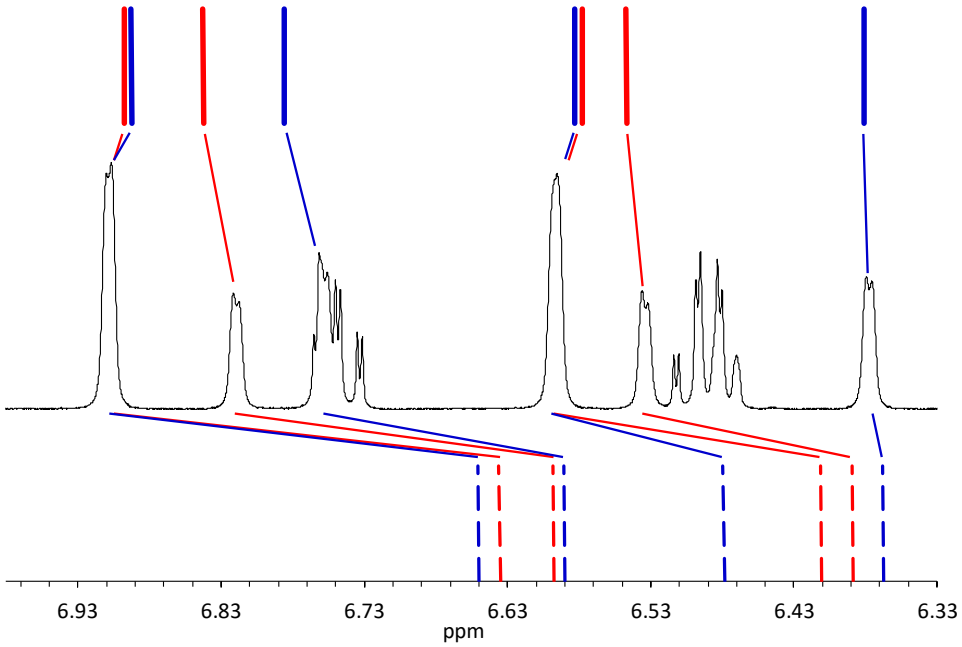

Figure S3.8. Aromatic region of the ^{1}H NMR of **1** and **1b** and the calculated NMR shifts of the phenolate hydrogen atoms in the DFT-calculated structures (blue : *cis,cis*-**1**, red: *trans,trans*-**1b**, bottom, dashed lines: scaling using all chemicals shifts; top: scaling calculated using the respective signals only).

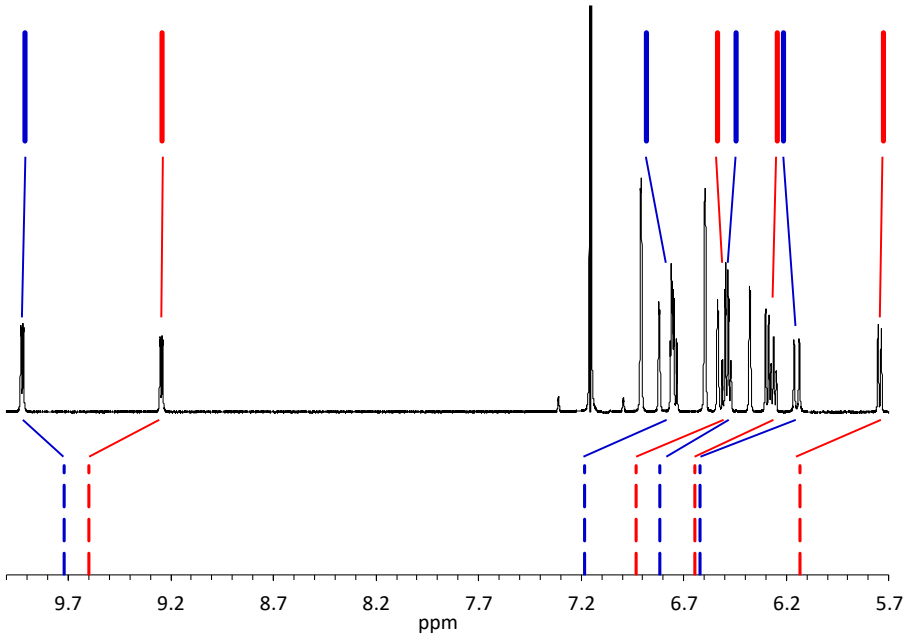

Figure S3.9. Aromatic region of the ^{1}H NMR of **1** and **1b** and the calculated NMR shifts of the pyridine hydrogen atoms in the DFT-calculated structures (blue : *cis,cis*-**1**, red: *trans,trans*-**1b**, bottom, dashed lines: scaling using all chemicals shifts, top, thick lines: scaling calculated using respective signals only).

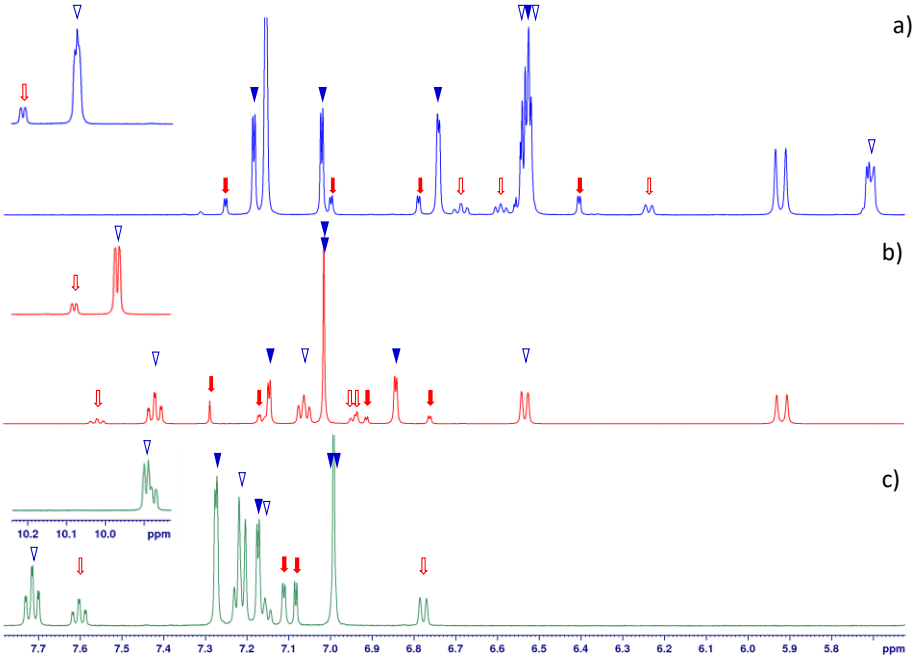

Figure S3.10. Aromatic region of ^{1}H NMR spectra of **2** in C_6D_6 (a), $CDCl_3$ (b), and *d*$_6$-DMSO (c) and showing the major species **2** (blue triangles, filled: phenolate signals, hollow: pyridine signals) and the minor species **2b** (red arrows, filled: phenolate signals, hollow: pyridine signals) in different ratios.

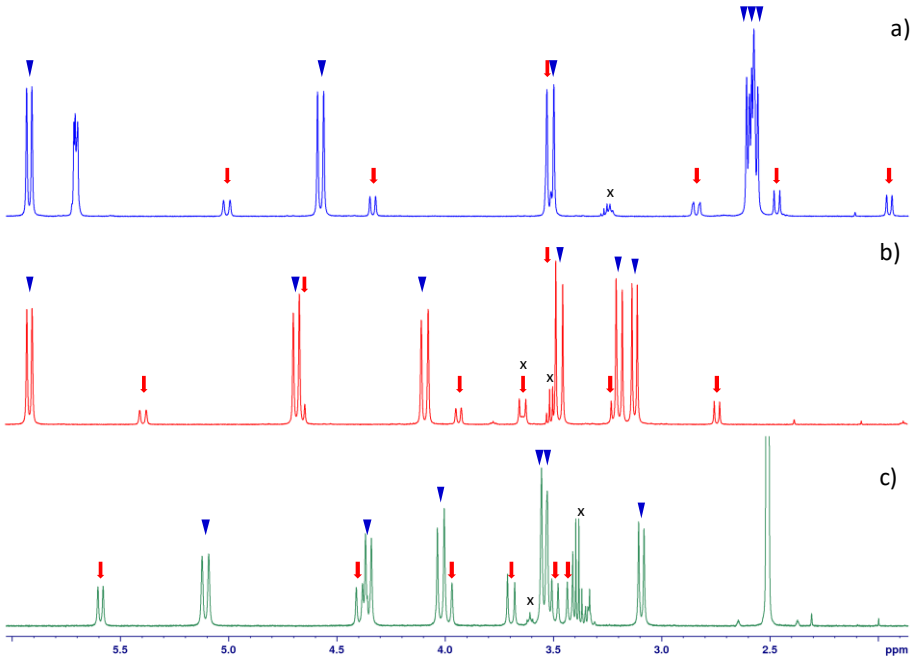

Figure S3.11. Aliphatic region of ^{1}H NMR spectra of #3# in C_6D_6 (a), $CDCl_3$ (b), and d_6-DMSO (c) and showing the major species **2** (blue triangles) and the minor species **2b** (red arrows) in different ratios.

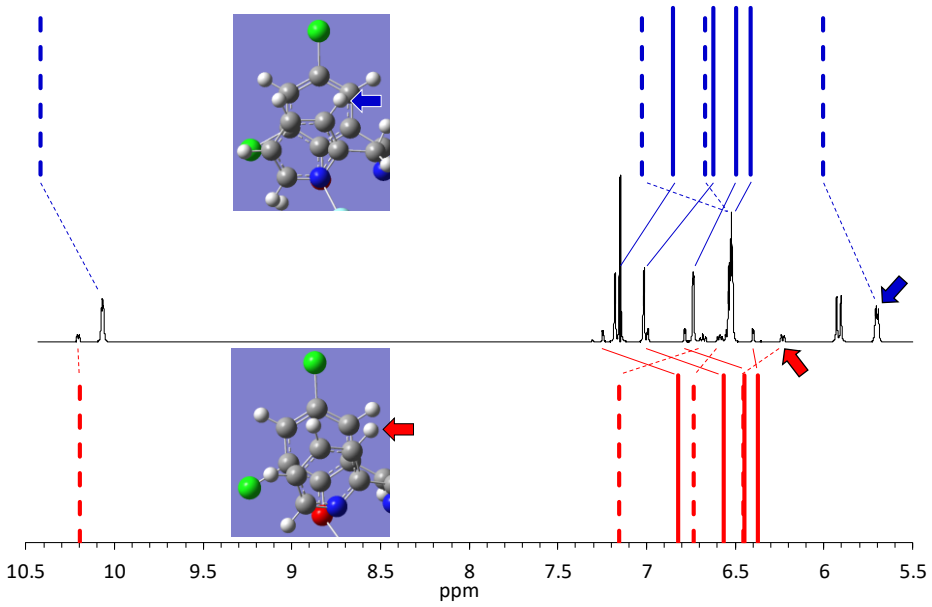

Figure S3.12. Comparison of calculated ^{1}H NMR spectra of *cis,cis*-**2** (red, bottom) and *trans,trans*-**2b** (blue, top) with the experimental spectrum of the equilibrium mixture. Chemical shift for the hydrogen atoms on the pyridine indicated with dashed lines. The arrows indicate the hydrogen in the 3-position, which shows the most notable displacement.

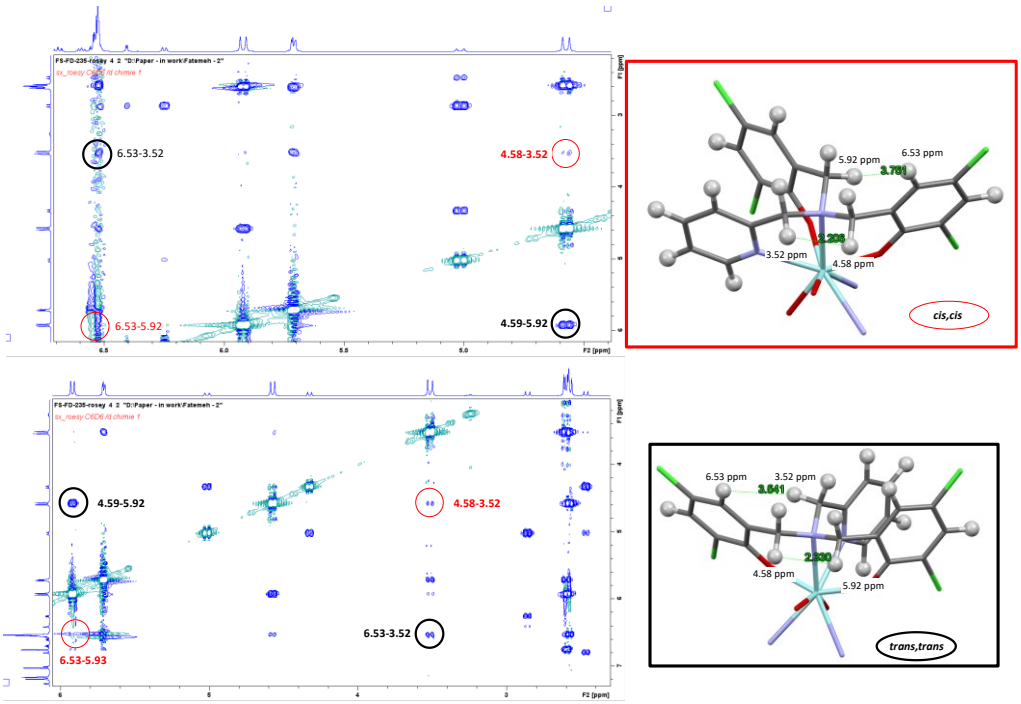

Figure S3.13. ROESY NMR spectra of **2**. Crosspeaks indicate that the major species is the *trans,trans*-isomer (black) rather than the *cis,cis*-isomer (red). Both crosspeak sections are shown, since t1 noise obscures some crosspeaks.

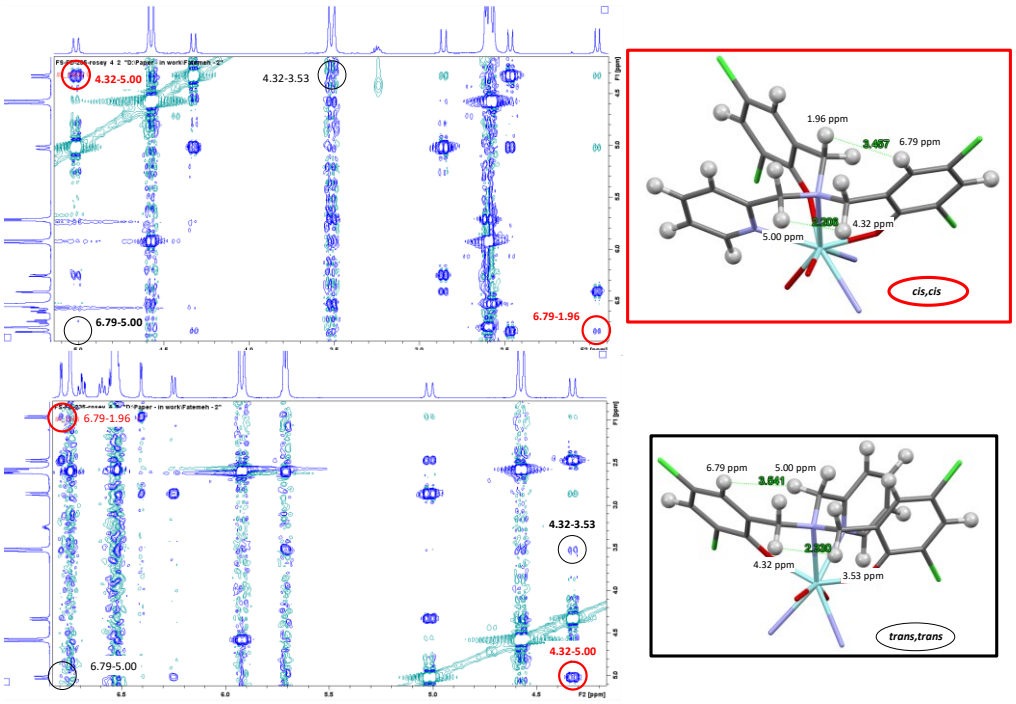

Figure S3.14. ROESY NMR spectra of **2**. Crosspeaks indicate that the minor species is the *cis,cis*-isomer (red) rather than the *trans,trans*-isomer (black). Both crosspeak sections are shown, since t1 noise obscures some crosspeaks.

Table S3.1. Calculated and experimental bond distances and calculated energies for isomers of complexes **1** and **2**. [a]

	cis,cis-**1**	X-ray *cis,cis*-**1**[b]	*trans,trans*-**1b**	*cis,trans*-**1c**	*trans,trans*-**2**	X-ray *trans,trans*-**2**	*cis,cis*-**2b**
Zr-$O_{\pi\text{-stacked}}$ [Å]	2.12	2.07(1), 2.10(1)	2.10	2.11, 2.12	2.09	2.06-2.07	2.12
Zr-$O_{\text{non-}\pi\text{-stacked}}$ [Å]	2.09	2.05(1), 2.06(1)	2.07	2.05, 2.10	2.08	2.05-2.08	2.10
Zr-N_{pyridine} [Å]	2.47	2.45(1), 2.46(1)	2.57	2.45, 2.67	2.54	2.51-2.53	2.45
Zr-N_{amine} [Å]	2.58	2.52(1), 2.55(1)	2.62	2.56, 2.63	2.61	2.55-2.56	2.58
E (small basis) [c]	-2425.61782		-2425.612716	-2425.59002	-2225.941551		-2225.949562
ZPE [c]	0.898925		0.899085	0.897911	0.605197		0.605417
Thermal correction to Gibbs energy [c]	0.813696		0.812639	0.809999	0.522264		0.523014
E (large basis) [d]	-2426.88455		-2426.880504	-2426.85836	-5789.258435		-5789.265329
E +ZPE [e]	-2425.98562		-2425.981419	-2425.96045	-2225.336354		-2225.344145
$G_{298\ K}$ [e]	-2426.07085		-2426.067865	-2426.04836	-5788.736171		-5788.742315
$\Delta G_{298\ K}$ [kJ/mol] [e]	0		7.8	59.0	16.1		0

[a] All energies given in Hartree. [b] Taken from Toupance, T.; Dubberley, S. R.; Rees, N. H.; Tyrrell, B. R.; Mountford, P. *Organometallics* **2002**, *21*, 1367. [c] Small basis set: 6-31+G(d,p) for light atoms and LANL2DZ for Cl and Zr used for geometry optimization and frequency calculations. [d] Large basis set: Def2TZVPP on all atoms. [e] Electronic energy using large basis set, thermal corrections from frequency calculations with the small basis set.

Table S3.2. Comparison of electronic energies (without thermal corrections) with different basis sets/solvent models.

Model	**#1**	**#2**	**#3**	**#4**	**#5**	**#6**	**#7**
Geometry	optimized	from #1	from #1	from #1	from #1	optimized	from #6
Functional	M06	M06	M06	M06	mPW1PW91	M06	M06
Basis set	6-31+G(d,p) /LANL2DZ	Def2TZVPP	Def2TZVPP	Def2TZVPP	6-311+G(2d,p)	6-31+G(d,p)/ LANL2DZ	Def2TZVPP
Solvent model	none	none	benzene	DMSO	benzene	benzene	benzene
cis,cis-(**L1**)$_2$Zr, **1** [Hartree]	-2425.617823	-2426.884545	-2426.925645		-2428.09822	-2425.660341	-2426.925645
trans,trans-(**L1**)$_2$Zr, **1b** [Hartree]	-2425.612716	-2426.880504	-2426.920845		-2428.095525	-2425.654732	-2426.920845
ΔE(*trans*)- ΔE(*cis*) [kJ/mol]	13.4	10.6	12.6		7.1	14.7	12.6
cis,cis-(**L2**)$_2$Zr, **2b** [Hartree]	-2225.949562	-5789.265329	-5789.31191	-5789.306049	-5790.603344		
trans,trans-(**L2**)$_2$Zr, **2** [Hartree]	-2225.941551	-5789.258435	-5789.304569	-5789.299006	-5790.596091		
ΔE(*cis*-*trans*) [kJ/mol]	21.0	18.1	19.2	18.5	19.0		

Table S3.3. *rac*-Lactide polymerizations with **1-3**.

#	Catalyst	*c*(catalyst) [mM]	*c*(BnOH)/ *c*(catalyst)	Time [h]	Conversion	P_m	M_n (theo.)	M_n (obs)	M_w/M_n
1	**1**	12	1	2	97%	0.47	TBD	TBD	TBD
2	**2**	12	1	4	44%	0.46			
				24	82%	0.44	TBD	TBD	TBD
3	**2**	38	0	1	0%	-			
				2	17%	-			
				20	86%	0.40	TBD	TBD	TBD
4	**2**	38	1	1	17%	-			
				2	20%	-			
				20	85%	0.46	TBD	TBD	TBD
5	**2**	38	5	1	48%	0.47			
				2	72%	0.48			
				20	93%	0.50	TBD	TBD	TBD
6	**2**	83 (neat monomer)	0	4	33%	0.47			
				24	83%	0.47	TBD	TBD	TBD
7	**2**	3	0	2462%	no reaction	-			
8	**2**	3	1	24	no reaction	-			
9	**2**	3	5	2	72%	0.47			
				4	83%	0.46			
				24	92%	0.47	TBD	TBD	TBD
10	3	2	0	1	24%	-			
				2	43%	0.57			
				4	61%	0.58			
				24	62% [a]		TBD	TBD	TBD

Conditions : [lactide]:[catalyst] = 100 :1, C_6D_6 or none, T = 140 °C. [a] Polymerization did not reach completion, likely due to contamination or decomposition.

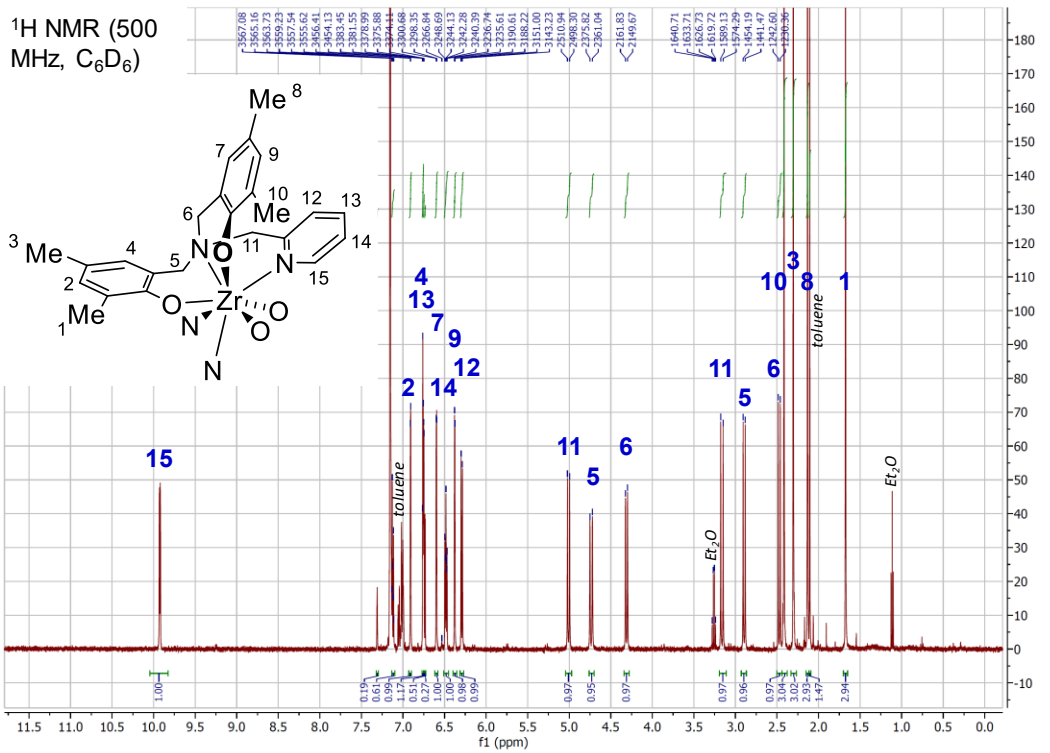

Figure S3.15. ^{1}H NMR spectrum (C_6D_6, 500 MHz) of **1**.

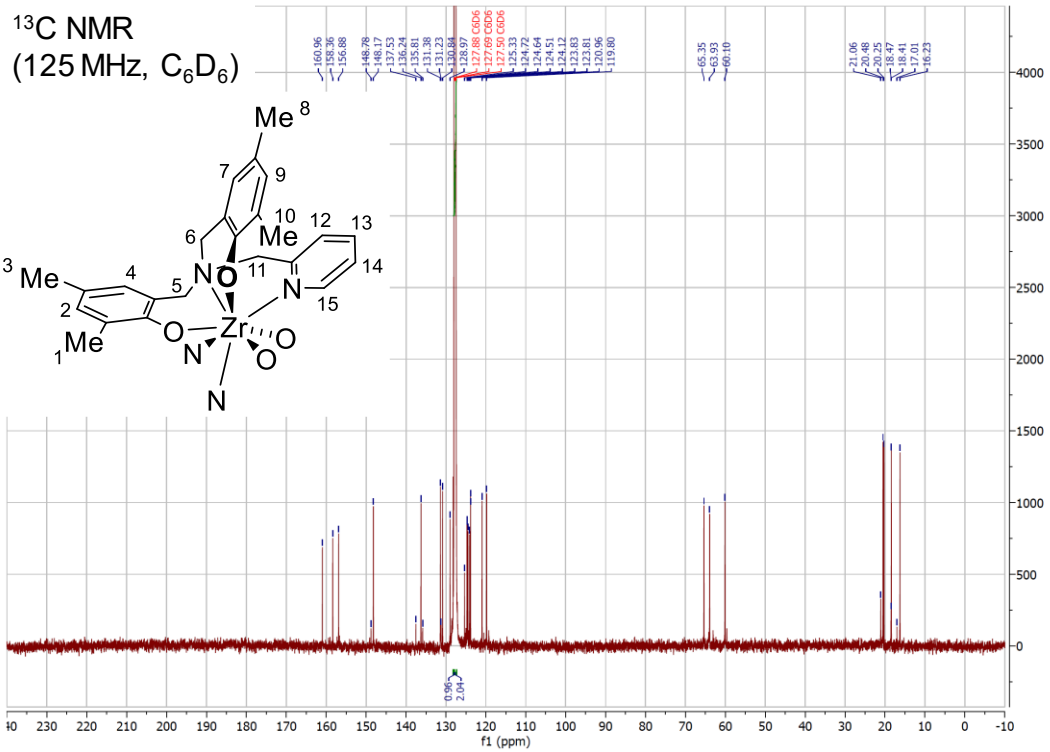

Figure S3.16. $^{13}C\{^{1}H\}$ NMR spectrum (C_6D_6, 125 MHz) of **1**.

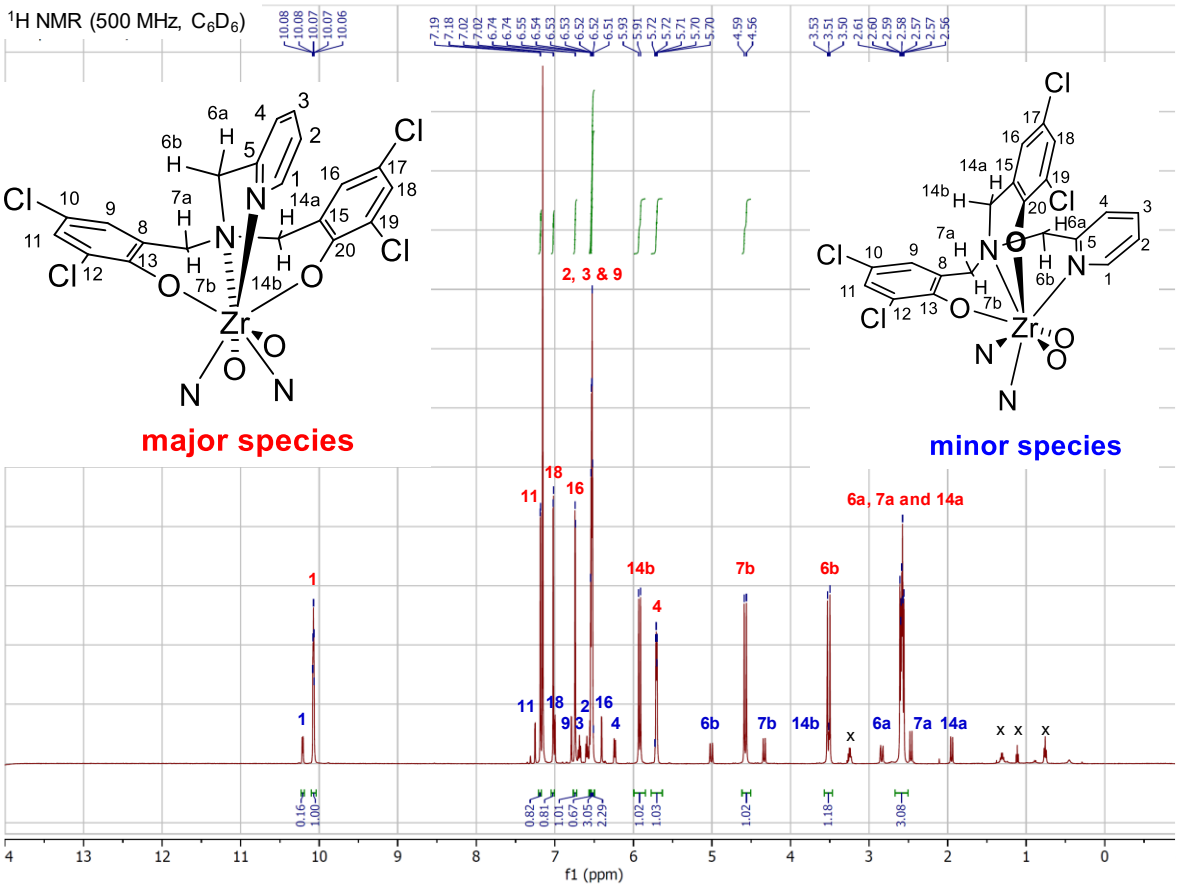

Figure S3.17. ^{1}H NMR spectrum (C_6D_6, 500 MHz) of the equilibrium mixture of **2** and **2b**.

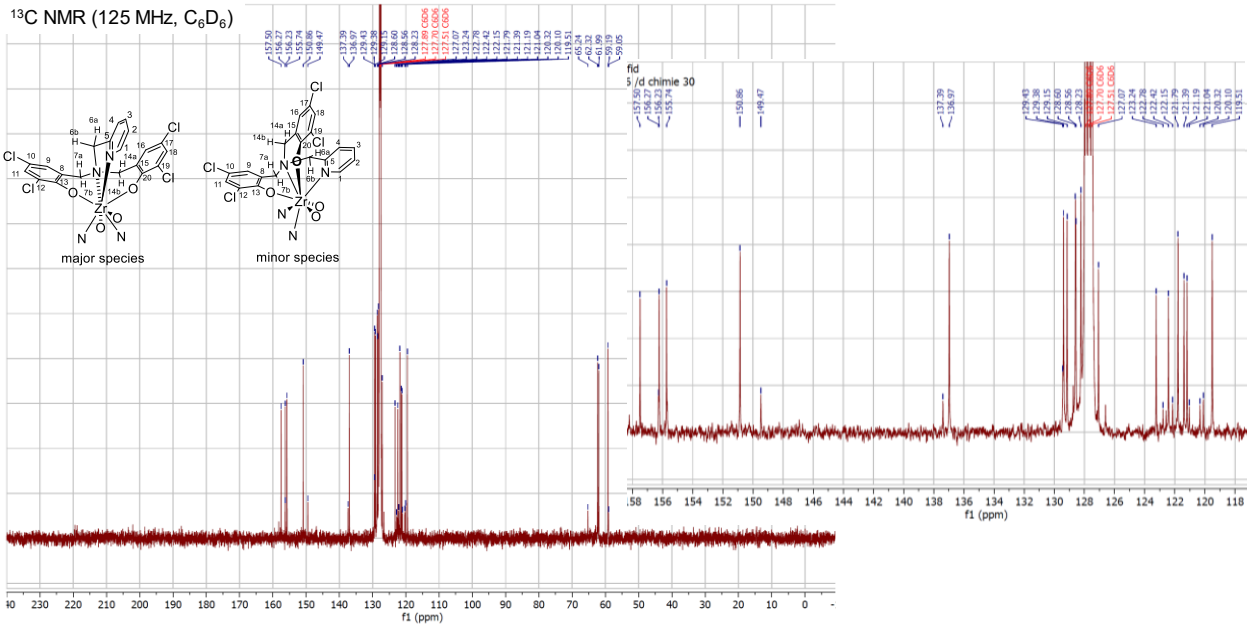

Figure S3.18. $^{13}C\{^{1}H\}$ NMR spectrum (C_6D_6, 125 MHz) of the equilibrium mixture of **2** and **2b**.

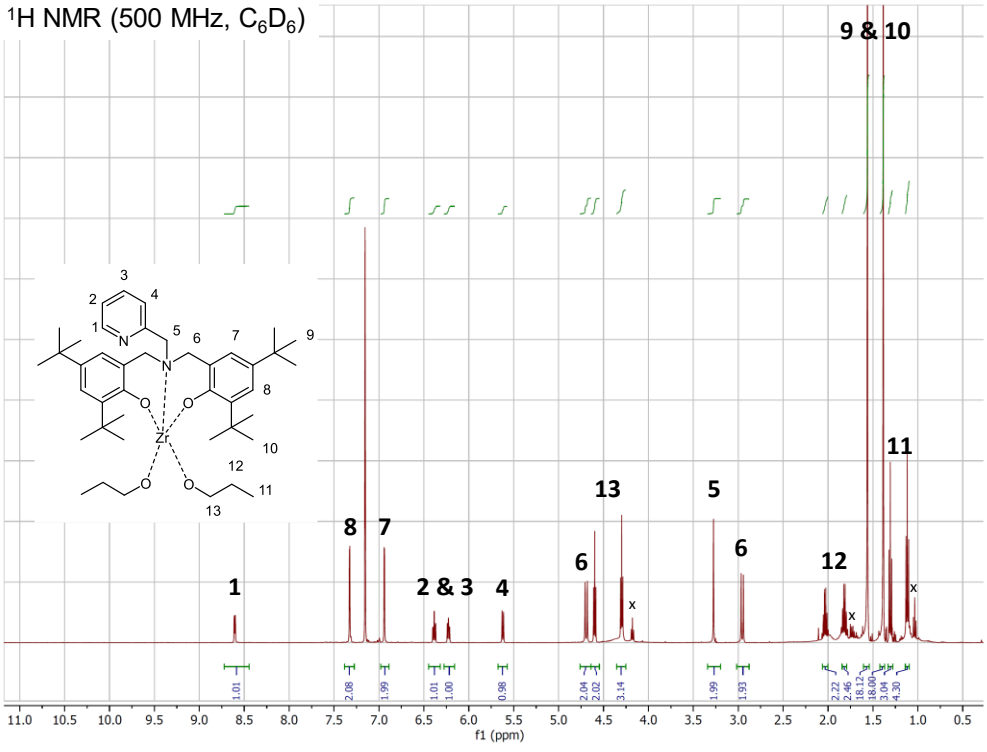

Figure S3.19. ^{1}H NMR spectrum (C_6D_6, 500 MHz) of **3**.

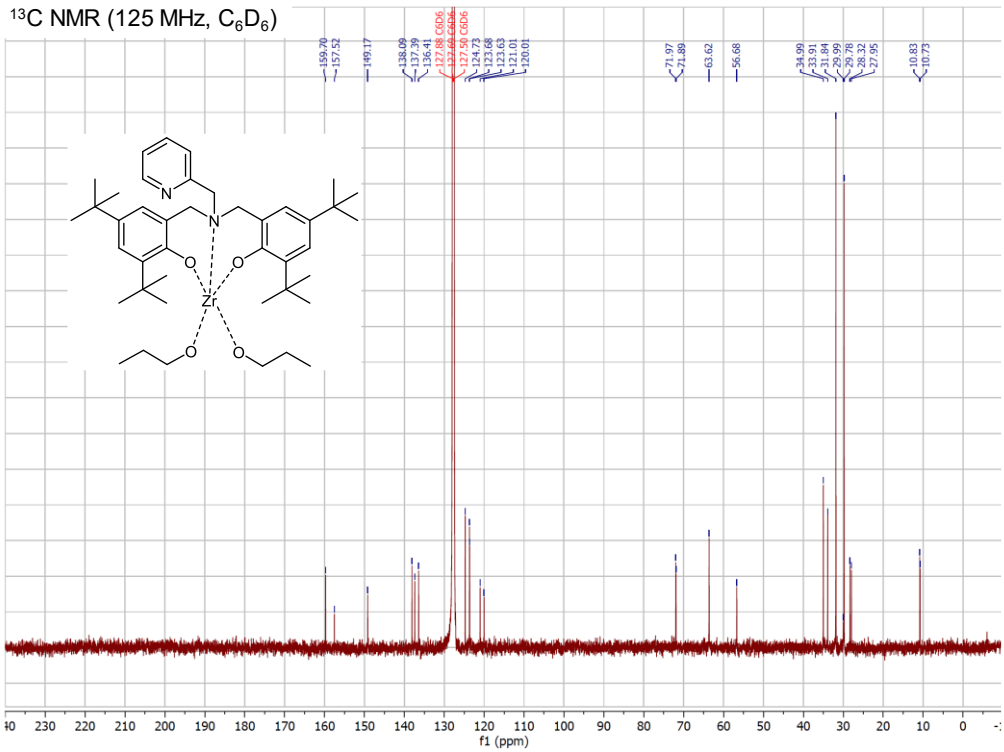

Figure S3.20. $^{13}C\{^{1}H\}$ NMR spectrum (C_6D_6, 125 MHz) of **3**.

Chapter 4. Conclusions

The synthesis of the zinc complex in Chapter 2 was straightforward via condensation of paraformaldehyde, 4-(*tert*-butyl)-2-tritylphenol and di-(2-picolyl)amine, followed by the addition of $Zn(N(SiMe_3)_2)_2$, thus forming the desired complex. $LZnN(SiMe_3)_2$ proved to provide very poor molecular weight control and did not produce isotactic polymer. In contrast to previous examples, increasing the steric bulk at the *ortho*-position (*tert*-butyl) did not cause an increase in stereoselectivity, atactic PLA was obtained instead. The proposed mechanism was catalytic-site mediated chain-end control for polymerization.

The eight-coordinated zirconium complexes L_2Zr found in Chapter 3 were synthesized in a one step, utilizing $Zr(O\textit{n}Pr)_4$ as the starting material. Lactide polymerization with these catalysts required benzyl alcohol as co-initiator. These complexes were moderately active in *rac*-lactide polymerization in the melt and no stereoselectivity was observed in this reaction. The activated-monomer mechanism was proposed based on the polymerization data.

The aim of my work was to use unusual mechanisms to allow more rational catalyst development. Unfortunately, we were not able to achieved this goal for the zinc complex. Although the desired stereocontrol mechanism was successfully included into the catalyst, it did not allow more rational catalyst improvement. Even a simple increase in steric bulk of the catalyst led to a decrease in stability and loss of stereocontrol.

My work showed that replacing *tert*-butyl with triphenyl methyl increases the steric bulk too much and destabilizes the compound. If I still want to increase stereocontrol by increasing steric bulk, another option would be using a group which has close to the metal center the same steric, but is more bulky further away (Scheme 4.1.a). Or, instead of increasing steric bulk at the *ortho* position it can increase on at the coordinating amine, e.

g. by using propylamine (Scheme 4.1.b). A third alternative, would be to avoid changing the steric bulk, but try to tighten the transition state by reducing the electron donation from the ligand (Scheme 4.1.c).

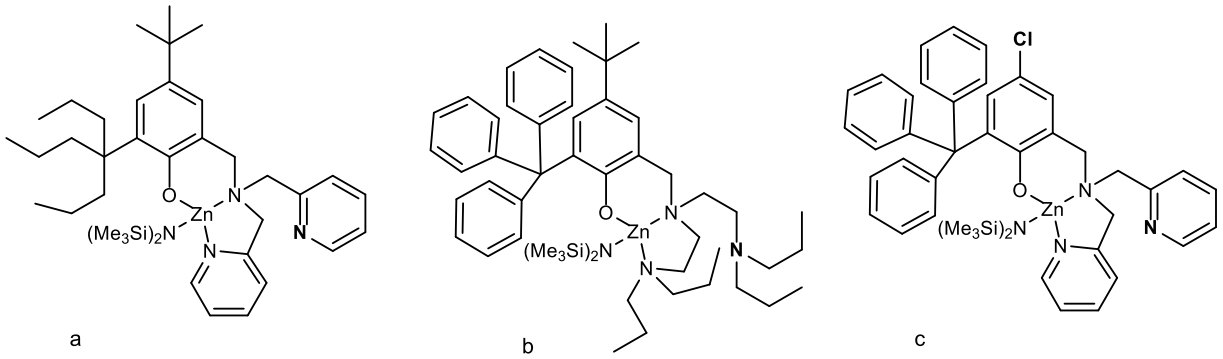

Scheme 4.1. Proposed zinc complexes for *rac*-lactide polymerization

For the zirconium complexes, the problem was that we cannot be sure if the mechanism we wanted to employ was actually followed. The presence of a basic site on the ligand was expected to incorporate stereocontrol into the activated monomer mechanism. In the absence of stereocontrol, it is uncertain whether we observed a ligand-assisted activated monomer mechanism or simply a traditional activated monomer mechanism. It would be interesting to check the mechanism with a ligand using phenyl instead of pyridine (thus without a basic site). Since the complex is less saturated (6 coordination instead of 8 coordination), it would be expected to be more active. If it shows lower activity, this would be an indication that the basic site helps in alcohol activation (Scheme 4.2.a). One problem of achieving stereocontrol might be the low activity of the complex, since pyridine dissociation was relatively difficult. Thus, it could be worthwhile to substitute pyridine with weaker donors, such as morpholine or dimethyl amine (Scheme 4.2.b).

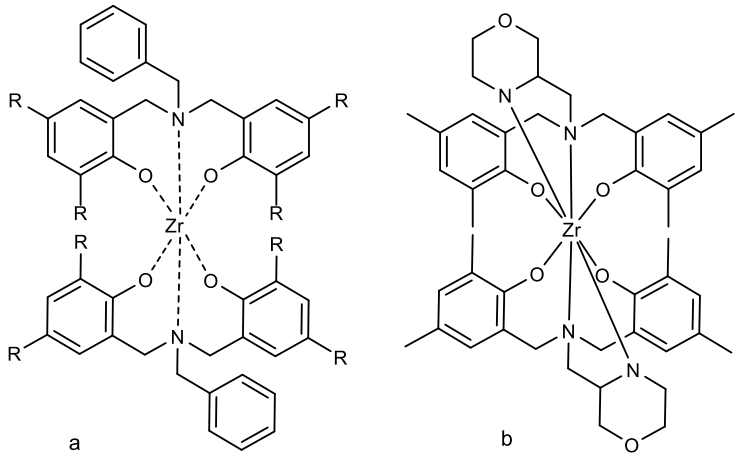

Scheme 4.2. Proposed zirconium complexes for *rac*-lactide polymerization

As a final conclusion, however, we have to admit that rational catalyst development might not be possible for lactide polymerization, and it might be more fruitful to concentrate on testing as many ligands/catalysts as possible. This means it might be more important to develop methods for parallel synthesis of catalysts than to take a rational design approach for this kind of polymerization.